UNIVERSITY OF CALIFORNIA SAN DIEGO

Triple-Alpha Process and the General Relativistic Instability in Super-Massive Stars

A dissertation submitted in partial satisfaction of the
requirements for the degree
Doctor of Philosophy

in

Physics

by

Sébastien Zein Tawa

Committee in charge:

Professor George Fuller, Chair
Professor Farhat Beg
Professor Patrick Diamond
Professor Michael Holst
Professor Mark Thiemens

2020

The dissertation of Sébastien Zein Tawa is approved, and it is acceptable in quality and form for publication on microfilm and electronically:

_____

_____

_____

_____

_____

Chair

University of California San Diego

2020

TABLE OF CONTENTS

LIST OF FIGURES

VITA

2011	B. A. in Physics, University of Colorado, Boulder
2012-2005	Graduate Teaching Assistant, University of California, San Diego
2014	M. S. in Physics, University of California, San Diego
2014	Graduate Research Assistant, University of California, San Diego
2015-2019	Physics Tutorial Center Manager, University of California, San Diego
2019	Graduate Research Assistant, University of California, San Diego
2020	Ph. D. in Physics, University of California, San Diego

FIELDS OF STUDY

Major Field: Physics
Studies in Astrophysics
Professor George Fuller
Studies in Neuro-physics
Professor Tatyana Sharpee

ABSTRACT OF THE DISSERTATION

Triple-Alpha Process and the General Relativistic Instability in Super-Massive Stars

by

Sébastien Zein Tawa

Doctor of Philosophy in Physics

University of California San Diego, 2020

Professor George Fuller, Chair

The existence of super-massive ($> 10^4 M_\odot$) Pop III stars has been theorized, but never observed. If such stars were to have existed during early galaxy formation, it has long been thought that in absence of heavy metals ($A > 4$), they would have collapsed due to instabilities caused by general relativity. Such a collapse would have resulted in the creation of a super-massive black hole, possibly emitting gravitational waves if accompanied by an anisotropic neutrino burst. Super-massive black holes have been detected very early on in galaxy formation (red shift: $z \approx 7$), and their origin remains unknown. Gravitational waves created by such a collapse may be detectable by next generation gravitational wave detectors.

Recent simulations have suggested that a narrow range of super-massive stars with masses

around $5 \times 10^4 M_\odot$ may have exploded due to simultaneously reaching the general relativistic instability and the ignition of triple-α fusion. If such explosions were to have occurred, depending on their frequency of occurrence, they may have left behind a measurable elemental signature of heavy elements in an otherwise primordial elemental composition during early galaxy formation.

This dissertation details the investigation of post-instability energetics, both from a theoretical stand point as well as via simulations using the KEPLER stellar evolution code. Previous research has found that for a small range of stars with masses around $5 \times 10^4 M_\odot$, due to the extreme temperature sensitivity of the triple-α process at its ignition point ($\sim 2 \times 10^8$ K), there is a theoretical basis for accelerated nuclear energy production to possibly reverse the collapse before too much energy is lost in electron-positron pair annihilation neutrinos combined with in-falling kinetic energy. However, complimentary findings via simulations were not found to be satisfactory. Future three dimensional simulations with high precision accounting of nuclear energy production as well as energy losses and kinematics would be necessary to definitively conclude whether such explosions are energetically possible.

Chapter 1

Introduction

1.1 Pop III Stars and Super-Massive Black Holes

Pop III stars are theorized to have been the first generation of stars to form in the universe. Consequently, they should have primordial chemical abundances, i.e. zero metallicity ($A > 4$). It is possible, however, for some younger or longer lived, i.e. smaller Pop III stars to have gained metallicity, if they were sprayed by heavy metals due to another larger/older Pop III star having gone supernova nearby. Although stellar evolution models suggest that Pop III stars would have had typical masses around $10^2 M_\odot$ [1–4], it has been theorized that in the absence of heavy metals, combined with the relatively warmer temperature of the universe at that epoch, these stars may have had masses of up to $\approx 10^8 M_\odot$ [5–7]. Although originally proposed as a possible source of strong radio emissions, it was quickly noticed that if such stars existed, they could have been progenitors of SMBH's [5, 8–11]. It should be noted, that Pop III stars are a hypothetical stellar population, and have never been directly observed; however, possible indirect evidence for them has been proposed via gravitational lensing [12].

On the other hand, super-massive black holes (SMBH) with mass ranges of, $10^5 M_\odot \longrightarrow 10^9 M_\odot$, have been observed less than 1Gyr after the Big Bang, $z = 7$ [13–17]. It remains a

mystery however, how such large black holes could have formed so soon after the Big Bang. Broadly speaking, two possible pathways have been proposed: via primordial black holes [18–20] and via collapsing gravitationally bound clouds or stars. In the latter case, there are multiple routes starting from a primordial gas cloud [21–26] or dense star cluster [27–30] and ending in a SMBH [31, 32], some of which involve the collapsing of super-massive Pop III stars [33, 34](see fig. 1.1). If such a collapse were to have occured in an asymmetric fashion, it could have emitted gravitational waves detectable by next generation gravitational wave detectors [35, 36], resulting from large neutrino bursts near the black hole formation [37–39]. However, as mentioned earlier, Pop III stars are not thought to have masses of $10^9 M_\odot$, and any blackhole resulting from one would still have to undergo rapid accretion to explain early SMBH's. It is nevertheless advantageous for such a process to begin with as large of a seed back hole as possible.

Pop III stars are the only candidates for such massive stars, as previous research has shown that for stars to reach such large masses ($\gtrsim 10^4 M_\odot$) they must have zero metallicity to avoid thermonuclear explosion [40], (see fig. 1.3).

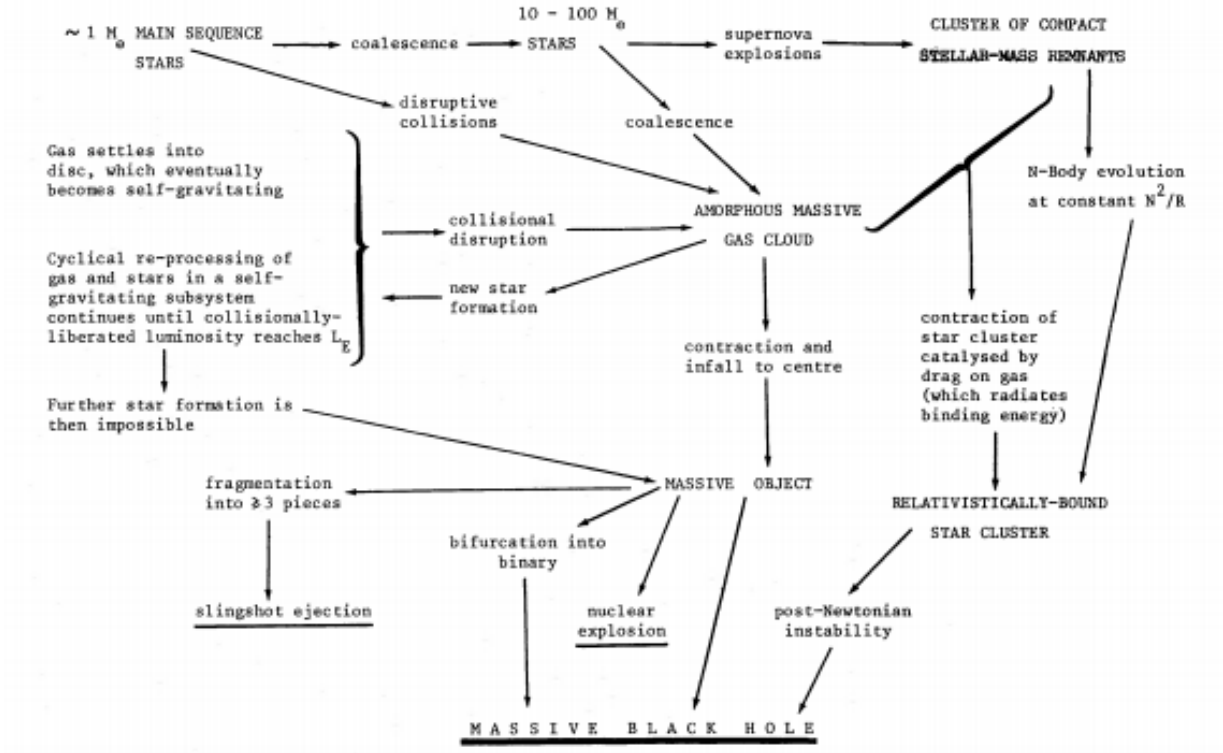

Figure 1.1: Pathways to SMBH.
Begelman and Rees flow chart hypothesizing the various paths to creating a SMBH [31], some of which involve the creation of a SMS (referred to as a 'Massive Object').

1.2 Very Massive Stars

Very massive stars (VMS), have a total mass-energy dominated by baryon rest-mass, but are primarily supported by radiation pressure, and are characterized by the electron-positron pair instability (EPPI). The EPPI is an effective loss of pressure support due to high energy photons creating non-relativistic electron-positron pairs. This dissertation will not delve into a detailed analysis of this effect, but a basic overview will be described in sect. 4.2. Their ultimate fate is dependent on their mass and metallicity [41]. Assuming Pop III stars with zero metallicity, lower mass VMS's as well as higher mass VMS's are predicted via stellar evolution models to collapse to black holes; while VMS's of intermediate masses ($\sim 140 - 260 M_{\odot}$), will become pair-instability supernovae, leaving behind no remnants [41] (see fig. 1.2).

We can increase the mass of a VMO to maximize the mass of the seed for a SMBH, however, above a certain mass, due to non-linear general relativistic gravitational corrections, the star will go unstable via the Feynman-Chandrasekhar General Relativistic Instability (GRI) [42, 43] prior to experiencing the EPPI (see sect. 4.2). This boundary between the GRI and the EPPI will loosely define the difference between a Very Massive Star and a Super-Massive Star (SMS). The details of this boundary will be explored in sect. 4.2.

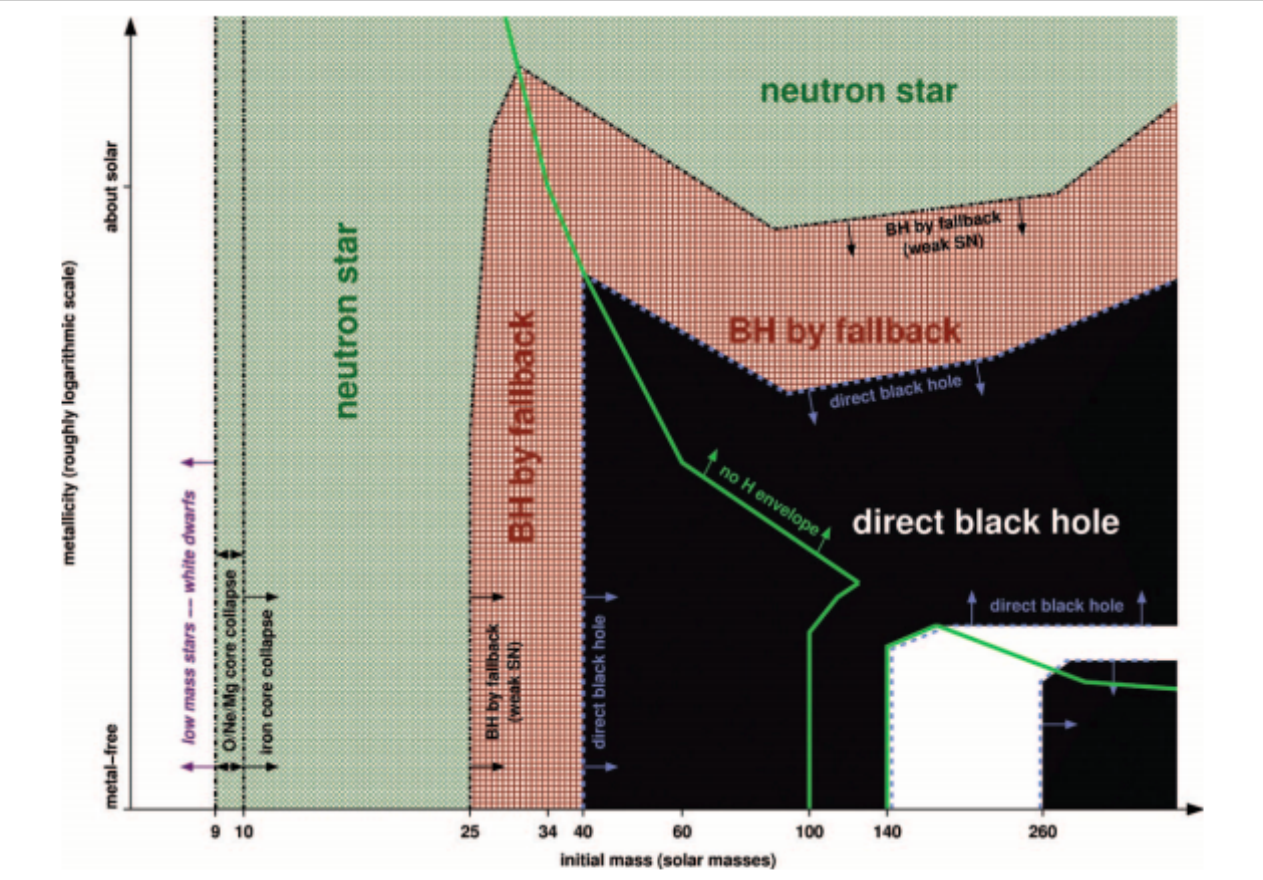

Figure 1.2: Fate of VMS's.
Simulated fates of VMS's depending on stellar mass (horizontal axis) and metallicity (vertical axis). The white region in the bottom right corner represents pair-instability supernovae. Figure source: [41]

1.3 Super-Massive Stars

As will be shown in sect. 4.2, adhering to our definition of a SMS versus a VMS, SMS's are characterized by masses greater than $\sim 10^4 M_\odot$. Like VMS's, these stars' mass-energy is predominately baryon rest-mass, but they are even more radiation dominated than VMS's due to having larger masses. Consequently they have lower densities, higher temperatures, and reach the GRI prior to the EPPI.

The details of the internal structure of SMS's will be discussed in chapt. 2. Past theoretical research on SMS's has found that, similarly to VMS's, the ultimate fate of an SMS depends on its mass and metallicity (see fig. 1.3) [40].

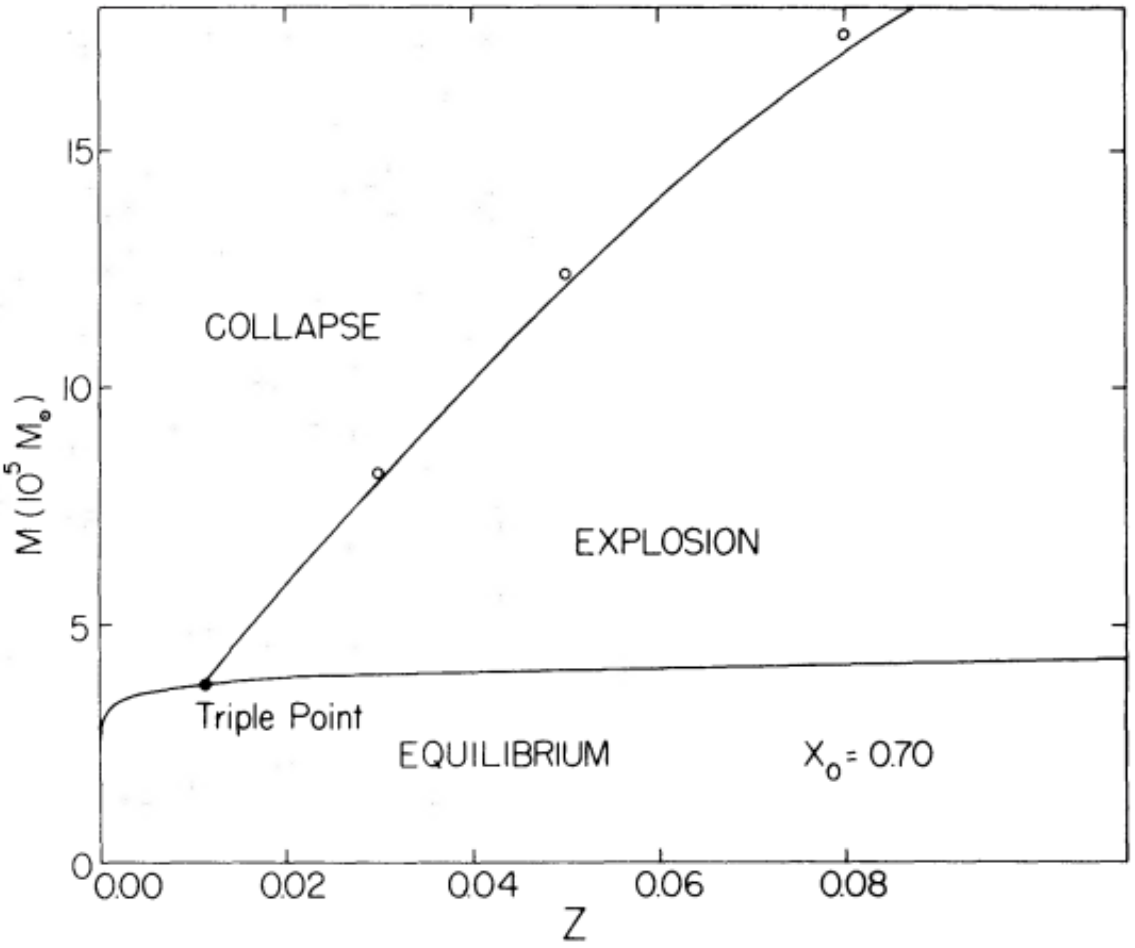

Figure 1.3: Regions of Stability in Super-Massive Stars vs. Metallicity.
Theoretical fate of SMS' depending on stellar mass (vertical axis) and metallicity (horizontal axis). $X_0 = {}^1H$ mass abundance, $Z =$ metal ($A > 4$) mass abundance. The 'equilibrium' region signifies that the star will reach hydrostatic equilibrium and continue along its main sequence phase. Figure source: [40].

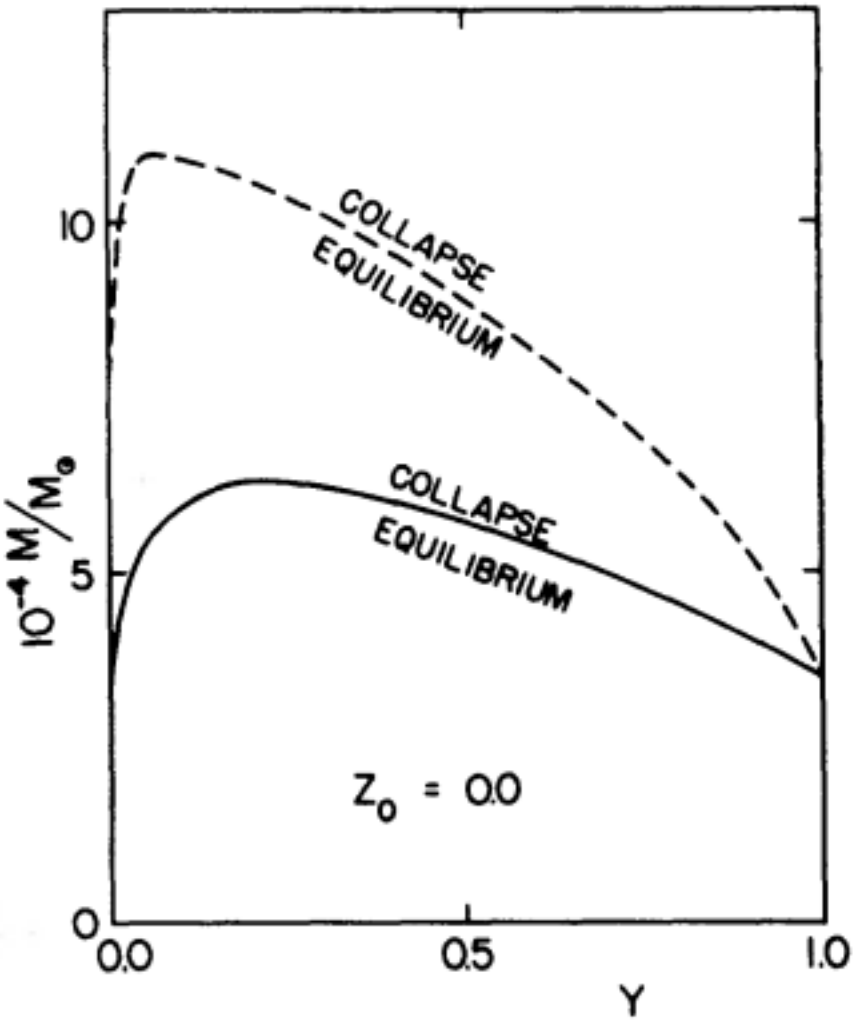

Figure 1.4: Regions of Stability in Super-Massive Stars vs. ^4He Content.
Theoretical fate of zero metallicity ($Z_0 = 0$) SMS' depending on stellar mass (vertical axis) and ^4He mass fraction, Y, (horizontal axis). The dashed line allows for quasi-static contraction, while the solid line doesn't. A SMS with mass less than $\sim 4-5\times 10^4 M_\odot$ will burn ^4He stably. Figure source: [40].

As per fig. 1.3, it was previously thought that zero-metallicity SMS, should all eventually collapse to a black hole [40], but recent computer simulations have found that there may exist a small mass range ($\sim 5.5\times 10^4 M_\odot$), for which a SMS will go unstable only upon completing its main sequence phase and beginning to fuse helium into carbon via the triple-α process; that may explode rather than collapse [44]. This result was found using both 1-D (KEPLER) and 2-D

(CASTRO) stellar evolution codes (KEPLER for the lifetime of the star and CASTRO to model the collapse and explosion). It is uncertain, however, whether this result is due to numerical effects, or real physical processes. If the effect is real, the physics leading to the explosion has not been fully explored.

If there existed Pop III SMS' that exploded, the explosion would have blown heavy elements into the universe, possibly leaving a measurable signature on the chemical abundances of heavy elements in early galaxies [45–47]. If the SMS was near other SMS', the explosion would have sprayed them with metals, possibly triggering other explosions (see fig. 1.3. Such explosions could also be marked by a pulse of gravitational waves, akin to those emanating from core collapse and pair-instability supernovae [48–53]. This dissertation will investigate the nuclear evolution and energy budget of a post-main sequence SMS near the GRI, and compare to stellar evolution simulations using KEPLER to determine what possible theoretical mechanisms could lead to the explosions found in [44].

This dissertation is organized as follows: Chapters 2 - 4 overview the theoretical framework for the physics of SMS', the GRI, and the EPPI. Chapters 5-7 present a theoretical model describing the energetics and nuclear physics determining the future of an SMS once the GRI has been reached. Chapters 8-9 discuss the results of KEPLER simulations of SMS's; and how they compare to the expectations of the theory laid out in the previous chapters. Throughout this dissertation, natural units will be used: $G = \hbar = c = K_B = 1$.

Chapter 2

Overview of Stellar Physics

2.1 Stellar Structure

Consider a spherically symmetric star of mass M, pressure P, density ρ, and entropy per baryon S; all functions of the radial distance, r. Given an equation of state, $P(\rho, S)$, the star's structure must satisfy the following equations:

$$\frac{dM(r)}{dr} = 4\pi r^2 \rho \text{ (mass continuity)} \tag{2.1}$$

$$\nabla P = \frac{dP}{dr} = -\frac{m(r)\rho}{r^2} \text{ (hydrostatic equilibrium)} \tag{2.2}$$

Combining eqs. 2.1 and 2.2 yields:

$$\frac{d}{dr}\left(\frac{r^2}{\rho}\frac{dP}{dr}\right) = -4\pi\rho r^2 \tag{2.3}$$

The theoretical model used in this dissertation we will assume a polytrope relation with index n: $r = r_0\xi$, $\rho = \rho_c\theta^n$ and $P = K\rho^\Gamma$, where ρ_c = the central density, K = constant, $r_0 = \left[\frac{(n+1)K}{4\pi}\right]^{1/2} \rho_c^{(1-n)/(2n)}$, and $\Gamma = 1 + 1/n$. This results in the Lane-Emden Equation [54]:

$$\frac{d}{d\xi}\left(\xi^2\frac{d\theta}{d\xi}\right) = -\xi^2\theta^n \tag{2.4}$$

with boundary conditions: $\theta(0) = 1$ and $\left.\frac{d\theta}{d\xi}\right|_{\xi=0} = 0$. The radius of the star, R, is determined by setting the pressure to 0: $\theta(\xi_1) = 0$, such that $R = r_0\xi_1$. It should be noted that in actuality the boundary of a real star is ill-defined, and so the polytrope radius, R, is a somewhat coarse-grained quantity. Consequentially, one should expect the polytrope model to break down in the outer regions of the star. This is generally not a problem, as most of the mass and important physics is concentrated in the star's central regions. Issues related to the radius of the star are discussed in 8.3.

The mass of the star is given by:

$$M = \int_0^R 4\pi r^2\rho dr = 4\pi r_0^3\rho_c\int_0^{\xi_1}\xi^2\theta^n d\xi \tag{2.5}$$

Using the Lane-Emden equation (eq. 2.4) we have:

$$M = -4\pi r_0^3\rho_c\int_0^{\xi_1}\frac{d}{d\xi}\left(\xi^2\frac{d\theta}{d\xi}\right)d\xi = 4\pi r_0^3\rho_c\xi_1^2\left|\theta'(\xi_1)\right| = 4\pi\left[\frac{(n+1)K}{4\pi}\right]^{3/2}\rho_c^{\frac{3-n}{2n}}\xi_1^2\left|\theta'(\xi_1)\right| \tag{2.6}$$

Consequentially:

$$r_0 = \left[\frac{M}{4\pi\xi_1^2\left|\theta'\right|}\right]^{1/3}\rho_c^{-\frac{n-1}{2n}} \tag{2.7}$$

and

$$R = r_0\xi_1 = \left[\frac{M}{4\pi\xi_1^2\left|\theta'\right|}\right]^{1/3}\rho_c^{-\frac{n-1}{2n}}\xi_1 \tag{2.8}$$

The mass can then be related to the radius by:

$$M = 4\pi \left(\frac{R}{\xi_1}\right)^{\frac{3-n}{1-n}} \left[\frac{(n+1)K}{4\pi}\right]^{\frac{n}{n-1}} \xi_1^2 \left|\theta'(\xi_1)\right| \tag{2.9}$$

Notice that for $n = 3$, the radius of the star is independent of its mass. The mean density of the star is:

$$\overline{\rho} = \frac{M}{V} = \frac{3\left|\theta'(\xi_1)\right|}{\xi_1}\rho_c \tag{2.10}$$

Pressure support for the star will be provided in part by radiation pressure, and in part by gas pressure. Defining $\beta \equiv P_{gas}/P$ for a some volume, V, we have:

$$P_{gas} = \beta P = \frac{N}{V}T = \frac{\rho}{\mu m_b}T \tag{2.11}$$

where $m_b =$ mass of a baryon (1.67×10^{-24}g), and $\mu =$ the mean particle mass in units of m_b as defined by eq. 2.12.

$$\mu \equiv \frac{m}{m_b \cdot \sum_i N_i} \tag{2.12}$$

where N_i is the number of particles of the i^{th} non-relativistic species within a volume with total mass m. The radiation pressure is:

$$P_{rad} = (1-\beta)P = \frac{a}{3}T^4 \tag{2.13}$$

where a is a constant that depends on the particle species making up the radiation. If only photons are relativistic, then $a = \frac{\pi^2}{15}$. Solving for pressure and temperature gives:

$$T = \left(\frac{3(1-\beta)}{a m_b \mu \beta}\right)^{1/3} \rho^{1/3} = T_c\theta, \;\; P = \left[\left(\frac{1}{m_b\mu}\right)^4 \frac{3}{a}\frac{1-\beta}{\beta^4}\right]^{1/3} \rho^{4/3} = P_c\theta^4 \tag{2.14}$$

Hence,

$$K = \left[\left(\frac{1}{m_b \mu}\right)^4 \frac{3}{a}\frac{(1-\beta)}{\beta^4}\right]^{1/3}, \Gamma = \frac{4}{3}, \text{ and } n = 3 \tag{2.15}$$

For the polytrope assumption to hold, β must be constant throughout the star. This condition is known as the 'standard' or 'Eddington' model of stellar structure; and it turns out that for typical stars, i.e. $\sim 1M_\odot$ the energy generation rate and opacity vary with radius inversely to one another as to keep β constant throughout the star [54, 55]. In the case of a SMS however, despite the bulk of the star being radiation dominated the envelope of the star is dominated by gas pressure, causing star to progressively shed its envelope [54]. Consequently β must change in the star's outer regions, and we should expect the polytrope model break down in the outer regions of the star. This is not an issue as the important physical processes are concentrated in the interior of the star; and the mass lost in the envelope accounts for a negligible fraction of the the total mass of the star [44, 56–59]. Consequently, the constant β assumption, and hence the polytrope model, should hold for the bulk of the star. The mass of the star is:

$$M = 4\left(\frac{3}{\pi a}\right)^{1/2} \frac{1}{m_b^2}\xi_1^2 \left|\theta'(\xi_1)\right| \frac{\sqrt{1-\beta}}{\mu^2\beta^2} \approx 18M_\odot \frac{\sqrt{1-\beta}}{\mu^2\beta^2} \tag{2.16}$$

If β is small, we have:

$$\beta \approx \sqrt{\frac{18M_\odot}{M}}\left(\frac{1}{\mu}\right) \tag{2.17}$$

Plugging back into eqs. 2.15 and 2.7 gives:

$$K = \left[\pi\left(\frac{M}{4\xi_1^2\left|\theta'(\xi_1)\right|}\right)^2\right]^{1/3} \text{and } r_0 = \left[\frac{M}{4\pi\xi_1^2\left|\theta'\right|\rho_c}\right]^{1/3} \tag{2.18}$$

For stars with $M >> 20M_\odot$, we get:

$$\beta \approx \sqrt{\frac{18M_\odot}{M}}\frac{1}{\mu} \ll 1 \tag{2.19}$$

and

$$T \approx \left(\frac{1500}{\sqrt{2}\pi^2 m_b}\sqrt{M_4}\right)^{1/3} \rho^{1/3} \tag{2.20}$$

where $M_4 =$ the mass of the star in units of $10^4 M_\odot$. Note that β, should be interpreted as the fraction of gas pressure a star *requires* in order to remain in hydrostatic equilibrium. If β drops below this fraction, then the luminosity is too high and the star will expand. Conversely, if β is too high, then the star will contract.

2.2 Newtonian Energy Balance

From the First Law of Thermodynamics, we have the change in internal energy:

$$dU = -PdV + TdS + T\sum_i (\eta_i dN_i) \tag{2.21}$$

Let us assume all processes to be adiabatic, i.e. there is no heat flow,

$$dQ = TdS + T\sum_i (\eta_i dN_i) = 0 \tag{2.22}$$

where η_i and N_i are the degeneracy parameter (chemical potential over temperature) and particle number for the i^{th} species, respectively. For a fixed number of particles, the second term on the right-hand side of eq. 2.22 can be dropped. The first term on the right-hand side of eq. 2.22 will be close to zero as for radiation dominated regimes the entropy per baryon is constant throughout the star (see appendix A.7.2). This does not hold in the envelope of the star,

which is gas dominated. Because the entropy is constant, despite the temperature decreasing with increased radius, the star tends to be convectively unstable and therefore the entire star is convective up to the envelope. This causes the star to shed its envelope [54, 55], as mentioned in sect. 2.1. Furthermore, this causes the material in the star to be continuously mixed keeping, the mean particle mass, μ, more or less constant throughout most of the star (although it will increase in time from nuclear fusion, see chapt. 6). Since for adiabatic processes we have $dQ = 0$, the First Law of thermodynamics (eq. 2.21) will reduce to $dU = -PdV$.

From the n=3 polytrope relation ($\Gamma = \frac{4}{3}$), we have:

$$\frac{dP(\rho,S)}{d\rho} = \left.\frac{\partial P}{\partial \rho}\right|_S + \left.\frac{\partial P}{\partial S}\right|_\rho \frac{dS}{d\rho} = \Gamma \cdot \frac{P(\rho,S)}{\rho} = \frac{4}{3} \cdot \frac{P(\rho,S)}{\rho} \tag{2.23}$$

We shall now define the adiabatic index, Γ_1, such that:

$$\left.\frac{\partial P}{\partial \rho}\right|_S \equiv \Gamma_1 \frac{P}{\rho} \Longrightarrow \Gamma_1 \equiv \left.\frac{\partial ln(P)}{\partial ln(\rho)}\right|_S \tag{2.24}$$

whereas,

$$\Gamma \equiv \frac{d\,ln(P)}{d\,ln(\rho)} \tag{2.25}$$

Plugging back into eq. 2.23 we have:

$$\frac{dP(\rho,S)}{d\rho} = \Gamma \frac{P}{\rho} = \Gamma_1 \frac{P}{\rho} + \left.\frac{\partial P}{\partial S}\right|_\rho \frac{dS}{d\rho} \tag{2.26}$$

or, rearranging:

$$\Gamma_1 = \Gamma - \frac{\rho}{P} \cdot \left.\frac{\partial P}{\partial S}\right|_\rho \frac{dS}{d\rho} \tag{2.27}$$

Note that $\Gamma_1 = \Gamma$ only if the entropy is constant (e.g. no gas pressure), and hence for a SMS, $\Gamma_1 \approx \Gamma$. Physically speaking, Γ_1 quantifies an answer to the following question: If a lump

of matter is quickly squeezed such that no heat has time to flow, how does the pressure respond? In a sense, Γ_1 is akin to a spring constant for the material under adiabatic compression/expansion. For a given mass element, the density is inversely proportional to the volume, so we can rewrite eq. 2.24 as:

$$\left.\frac{dP}{P}\right|_S + \Gamma_1 \frac{dV}{V} = 0 \tag{2.28}$$

.

We shall now find Γ_1. For the radiation field the internal energy is $U_{rad} = 3P_{rad}V = aT^4V$. For an ionized gas of N particles, the internal energy is $U_{gas} = \frac{3}{2}NT = \frac{3}{2} \cdot \frac{P_{gas}}{V}$. Hence we have:

$$U = aT^4V + \frac{3}{2}NT \tag{2.29}$$

$$P = \frac{1}{3}aT^4 + \frac{NT}{V} \tag{2.30}$$

Differentiating eqs. 2.29 and 2.30, and applying the 1^{st} Law of Thermodynamics (eq. 2.21), gives:

$$dU = -PdV = 3(1-\beta)PV\left(4\frac{dT}{T} + \frac{dV}{V}\right) + \frac{3}{2}\beta PV \cdot \frac{dT}{T} \tag{2.31}$$

$$dP = 4(1-\beta)P \cdot \frac{dT}{T} + \beta\left(\frac{dT}{T} - \frac{dV}{V}\right) \tag{2.32}$$

Eliminating $\frac{dT}{T}$ gives:

$$\frac{dP}{P} + \frac{32 - 24\beta - 3\beta^2}{3(8-7\beta)}\frac{dV}{V} = 0 \tag{2.33}$$

Hence, from eq. 2.28:

$$\Gamma_1 = \frac{32 - 24\beta - 3\beta^2}{3(8 - 7\beta)} \tag{2.34}$$

As β goes from $0 \to 1$, Γ_1 goes from $\frac{4}{3} \to \frac{5}{3}$. For radiation dominated stars, Γ_1 can be approximated to first order in β:

$$\Gamma_1 \approx \frac{4}{3} + \frac{\beta}{6} \quad (\text{if } \beta << 1) \tag{2.35}$$

It should be noted that eq. 2.34 does not take into consideration shifts in the equilibrium ratio of the number photons to electron-positron pairs, and as a result is not valid in a regime where pair creation is significant, i.e. it does not hold when considering the EPPI.

Since we are only considering adiabatic processes, we shall take $\Gamma = \Gamma_1$ for the remainder of this dissertation, unless stated otherwise. The total internal energy of the star, U will be $\int u dm$, where $u \equiv \frac{dU}{dm}$ (the internal energy per unit mass. Taking a mass element, Δm, we have:

$$dU = -PdV = -Pd\left(\frac{1}{\rho}\right) \cdot \Delta m. \text{ Hence: } du = \frac{P}{\rho^2} d\rho \tag{2.36}$$

Therefore,

$$u = \int K\rho^{\Gamma_1 - 2} d\rho = \frac{K\rho^{\Gamma_1 - 1}}{\Gamma_1 - 1} + \text{const.} \tag{2.37}$$

The constant term corresponds to the rest-mass energy density (ρ_x), which can be subtracted off. The gravitational potential energy of the star is:

$$-\int \frac{m(r)}{r} dm \tag{2.38}$$

So the total Newtonian binding energy of the star will be

$$E = E_{int} + E_{grav} = \int_0^M u dm - \int_0^M \frac{m(r)}{r} dm \tag{2.39}$$

Integrating over an $n = 3$ polytrope gives:

$$E = \alpha_1 K M \rho_c^{\Gamma_1 - 1} - \alpha_2 M^{5/3} \rho_c^{1/3} \tag{2.40}$$

where α_1 and α_2 are constants of order 1 resulting from integrating over the polytrope profile. In order to find the equilibrium central density and corresponding energy, we must find the stationary point(s) of E, by differentiating eq. 2.40 with respect to ρ_c (the only free parameter):

$$\frac{dE}{d\rho_c} = 0 = (\Gamma_1 - 1)\alpha_1 K M \rho_c^{\Gamma_1 - 2} - \frac{1}{3} \cdot \alpha_2 M^{5/3} \rho_c^{-2/3} \Rightarrow \alpha_1 K M \rho_c^{\Gamma_1 - 1} = \frac{\alpha_2 M^{5/3} \rho_c^{1/3}}{3(\Gamma_1 - 1)} \tag{2.41}$$

Plugging back into the eq. 2.40, we find the equilibrium energy of the star:

$$E_{eq} = -\frac{\alpha_2 M^{5/3} \rho_c^{1/3}}{\Gamma_1 - 1} \left(\Gamma_1 - \frac{4}{3} \right) \tag{2.42}$$

For a star that is entirely radiation dominated ($\Gamma_1 = \frac{4}{3}$) everywhere, the total binding energy is 0. We can now expand the energy about E_{eq} to get:

$$E = E_{eq} + E'_{eq} \Delta\rho_c + \frac{1}{2} \cdot E''_{eq} (\Delta\rho_c)^2 + ... \approx E_{eq} + 0 + \frac{1}{2} \cdot E''_{eq} (\Delta\rho_c)^2 \tag{2.43}$$

The star will be unstable to perturbations about E_{eq} when $E''_{eq} < 0$. Solving for E''_{eq} gives:

$$E''_{eq} = \frac{1}{3} \cdot \alpha_2 M^{5/3} \rho_c^{-5/3} \left(\Gamma_1 - \frac{4}{3} \right) \tag{2.44}$$

The star will therefore be unstable when $\Gamma_1 < \frac{4}{3}$. Under "normal" thermodynamic conditions Γ_1 ranges from $\frac{4}{3} \longrightarrow \frac{5}{3}$, and hence E''_{eq} is always greater than 0, therefore from a Newtonian perspective, stars in hydrodynamic equilibrium are always stable under adiabatic processes, unless some atypical process takes place in the star, that makes eq. 2.34 invalid and drives Γ_1 below $\frac{4}{3}$, i.e. the EPPI. Physically speaking, barring atypical processes such as the EPPI

(discussed in 4.2), if a star is slightly contracted, the changes pressure will always be sufficient to counteract the changes in gravitational forces (and similarly when the star is expanded). Alternatively, we can say that the net force (gravitation + pressure) under expansion/contraction will always be restoring. If $Gamma_1$ is exactly $\frac{4}{3}$, then the pressure scales exactly as gravity ($\sim \frac{1}{r^2}$), and contracting or expanding the star costs zero energy, resulting in equilibrium at any radius/density.

There are two important points to note here. Firstly, recall that we are considering adiabatic processes, and Γ_1 is adiabatic index $\Gamma_1 = \left.\frac{\partial \ln(P)}{\partial \ln(\rho)}\right|_S$, not the polytrope index, $1 + \frac{1}{n} = \frac{4}{3}$. Secondly, since Γ_1 is not necessarily constant throughout the star, a more rigorous and general analysis of perturbative deviations about the polytrope profile, yields that in fact the relevant quantity in eq. 2.44 is not Γ_1, which is ill-defined for the entire star if not constant, but the pressure weighted average of Γ_1 [10, 60]:

$$\widetilde{\Gamma}_1 \equiv \frac{\int P\Gamma_1 dV}{\int P dV} \tag{2.45}$$

A full analysis of perturbations about the polytrope profile will not be covered in this dissertation, but this is a well known result in the physics of stellar stability. A full derivation of this result is the subject of chapter 6 of [60].

Chapter 3

General Relativistic Energy Corrections

For a massive, radiation dominated star, since the total energy is nearly 0, the first order correction to the energy due to general relativity (GR) will become important, and must be considered. The Newtonian binding energy was defined as $E_{therm} + E_{grav}$, which can be interpreted as the total amount of energy needed to unbind the star (disperse the matter to infinity). From a GR perspective, an unbound gas at zero-temperature will have a total energy simply equal to its total rest-mass, i.e. Nm_b, where N is the number of baryons in the gas. Hence the binding energy will be the energy difference between the stars' total gravitational mass/energy, and Nm_b. If the star is is static and spherically symmetric, it will be described by Schwarzschild geometry. In this case we have:

$$E = M - Nm_b = M - \int \frac{dm}{(1+u)\sqrt{1-\frac{2m(r)}{r}}} = \int (1+u)\sqrt{1-\frac{2m(r)}{r}}\, dm_x - M_x \tag{3.1}$$

where x-subscripts indicate proper quantities, i.e. as measured by a local Minkowski observer. The factors of $\frac{1}{\sqrt{1-\frac{2m(r)}{r}}}$ are typically interpreted as accounting for the curvature of space when integrating over proper-space, and are the g_{rr} components of the Schwarzschild metric (see

appendix A.2 for further explanation).

The Newtonian energy (eq. 2.40) is of first order in $\frac{M_x}{R_x}$ and u. To get the first correction we expand eq. 3.1 to second order in $\frac{M_x}{R_x}$ and u to find a total binding energy of:

$$E = \alpha_1 K M \rho_c^{\Gamma_1 - 1} - \alpha_2 M^{5/3} \rho_c^{1/3} - \alpha_3 M^{7/3} \rho_c^{2/3} \tag{3.2}$$

where α_3 is again a constant of order 1, resulting from integrating over the polytrope profile of the star (see Appendix A.1 for full derivation of eq. 3.2). We can now find equilibrium and stability criteria as was done in the Newtonian case, yielding:

$$E_{eq} = -\frac{1}{\Gamma_1 - 1}\left[\alpha_2 M^{5/3} \rho_c^{1/3}\left(\Gamma_1 - \frac{4}{3}\right) - \alpha_3 M^{7/3} \rho_c^{2/3}\left(\frac{5}{3} - \Gamma_1\right)\right] \tag{3.3}$$

and

$$E''_{eq} = \frac{1}{3}\left[\alpha_2 M^{5/3} \rho_c^{-5/3}\left(\Gamma_1 - \frac{4}{3}\right) - 2\alpha_3 M^{7/3} \rho_c^{-4/3}\left(\frac{5}{3} - \Gamma_1\right)\right] \tag{3.4}$$

Instability sets in when when the central density, ρ_c, exceeds a critical density, ρ_{crit}:

$$\rho_{crit} = \left[\left(\frac{\alpha_2}{2\alpha_3}\right)\left(\frac{\Gamma_1 - \frac{4}{3}}{\frac{5}{3} - \Gamma_1}\right)\right]^3 \frac{1}{M^2} \tag{3.5}$$

Substituting eq. 3.5 back into eq. 3.3, we find the energy at instability to be:

$$E_{crit} = -\frac{\alpha_2^2 \left(\Gamma_1 - \frac{4}{3}\right)^2}{2\alpha_3(\Gamma_1 - 1)\left(\frac{5}{3} - \Gamma_1\right)} M \tag{3.6}$$

Recall that the important quantity for perturbations about the polytrope profile is actually the pressure averaged $\widetilde{\Gamma}_1$ (see eq. 2.45). We can use eq. 2.8 and $\Gamma_1 \approx \frac{4}{3}$, to rearrange eq. 3.5 and find the instability criteria to be:

$$\widetilde{\Gamma}_1 - \frac{4}{3} < 1.124 \frac{2M}{R} \tag{3.7}$$

In the Newtonian case, we found that net forces were always restoring (excepting the EPPI). However, when including GR, if the star slightly contracts, the increase in the strength of gravity will be a bit more than for Newtonian gravity, but not the pressure. If the criteria in eq. 3.7 is met, where under Newtonian gravity the increased pressure would have been just enough to counteract the increased gravitational force, now gravity is a bit stronger and will win, and the star will contract a little more. Due to the non-linear nature of GR, this will increase the gravitational forces even further, and the star will go into runaway collapse.

When including GR corrections, a $\Gamma_1 = \frac{4}{3}$ everywhere (radiation only) self gravitating object, which would have been just on the edge of stability in Newtonian gravity, will now always be unstable. In the case of a star however, there is always some gas pressure, so terms of first order in β must be kept. Combining eqs. 2.35, 2.17, 3.5, and 3.6 gives:

$$\rho_{crit} = \left[\frac{\alpha_2}{4\alpha_3}\sqrt{18M_\odot}\right]^3 \cdot \frac{1}{M^{7/2}\mu^3} = \frac{\rho_0}{\mu^3}\left(\frac{M_\odot}{M}\right)^{7/2} \tag{3.8}$$

$$E_{crit} = -\alpha_3 M^{7/3}\rho_{crit}^{2/3} = -\frac{E_0}{\mu^2} \tag{3.9}$$

where, $\rho_0 \equiv 2.496(10^{17})$ g/cc, and $E_0 = 8.964(10^{53})\text{ergs} = 0.501M_\odot$. Therefore the energy at instability is independent of the stars' mass, and only depends of the mean particle mass, μ. We can find the corresponding critical central temperature to first order in β from eq. 2.14:

$$T_{crit} = \left(\frac{3\rho_{crit}}{am_b\mu\beta}\right)^{1/3} = \frac{T_0}{\mu}\left(\frac{M_\odot}{M}\right) \tag{3.10}$$

where $T_0 = 1.245(10^{13})K$. The mean particle mass, μ, is not necessarily constant throughout the star, and has turned up as a result of $\Gamma_1 - \frac{4}{3} \propto \frac{1}{\mu}$. As a result, it is the pressure averaged inverse of μ that is the relevant quantity. Plugging eqs. 2.17 and 2.35into eq. 2.45, and using $dV = \frac{dm}{\rho}$, we get:

$$\widetilde{\Gamma}_1 \approx \frac{4}{3} + \left(\frac{M_\odot}{2M}\right)^{1/2} \left(\widetilde{\frac{1}{\mu}}\right) \tag{3.11}$$

where:

$$\left(\widetilde{\frac{1}{\mu}}\right) \equiv \frac{\int P\frac{1}{\mu}dV}{\int PdV} = \frac{\int \frac{P}{\rho}\cdot\frac{1}{\mu}dm}{\int \frac{P}{\rho}dm} \tag{3.12}$$

For convenience $\widetilde{\Gamma}_1$ has been expressed in terms mass integrals, as the KEPLER stellar evolution code uses mass zones rather than radial zones. For radiation dominated stars, the dominant mechanism for heat transfer throughout the entire star is convection. As a result the material throughout the star is regularly mixed and μ is approximately constant throughout the star as mentioned in chapter 2.1.

There is another subtle point that we must consider. Clearly, eq. 3.7 only holds while $\frac{2M}{R} < 1$ (formation of a black hole). Furthermore, we have assumed that the metric deviation is small: $\frac{2M}{R} \ll 1$, and of order β. However, for an $n = 3$ polytrope, the maximum metric deviation occurs somewhere inside the star rather than at its surface. If a trapped surface were to occur, it would first be created *inside* the star. So for good measure we must verify that at no point in the star, the metric deviation exceeds unity. Using eq. 2.4 we have:

$$m(r) = 4\pi r_0^3 \rho_c \int_0^\xi \theta^3 \xi^2 d\xi = -4\pi r_0 \rho_c \xi^2 \theta'(\xi) \text{ and } r = r_0\xi \tag{3.13}$$

$$\frac{2m(r)}{r} = -8\pi r_0^2 \rho_c \theta'(\xi)\xi \tag{3.14}$$

Differentiating eq. 3.14 with respect to ξ yields that $\left[\frac{2m(r)}{r}\right]_{max}$ is reached when:

$$-\theta'(\xi)\xi = \theta^3(\xi)\xi^2 \text{ i.e. when: } \frac{m(r)}{r} = \frac{dm(r)}{dr} \tag{3.15}$$

Where the condition in eq. 3.15 is met can be found numerically, yielding:

$$\left[\frac{2m}{r}\right]_{max} = 1.935\frac{2M}{R} \tag{3.16}$$

and the enclosed mass when the metric deviation is largest is:

$$m\left(\left[\frac{2m}{r}\right]_{max}\right) = .731M \tag{3.17}$$

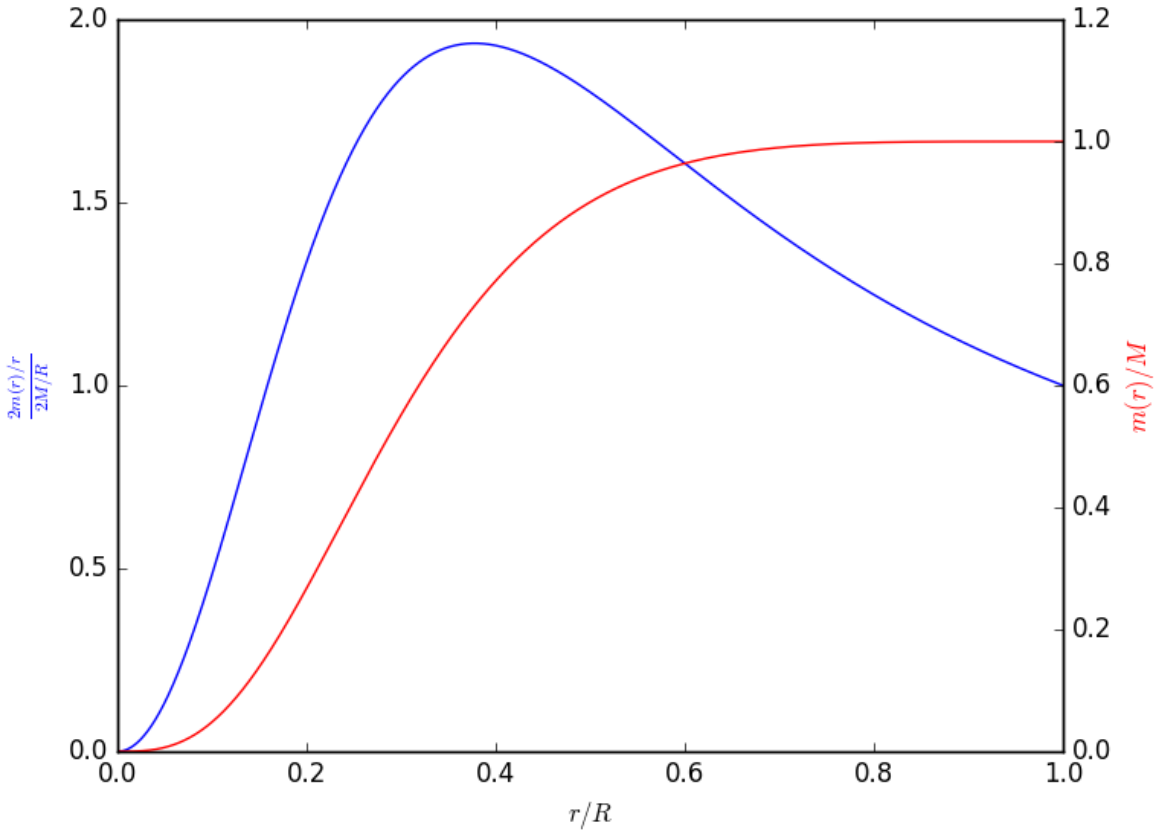

Figure 3.1: $\frac{2m(r)}{r}$ for $n = 3$ Polytrope.
Radial dependence of the metric deviation (in blue) normalized by the metric deviation at the star's surface for a $n = 3$ polytrope. The maximum metric deviation is inside the star and is equal to almost twice the metric deviation at the surface of the star. Enclosed mass as a function of radius (in red), normalized by the total stellar mass.

Setting $\left[\frac{2m}{r}\right]_{max} \ll 1$ at $\rho_c = \rho_{crit}$ (eq. 3.8),we find that for this analysis to be valid we

must have:

$$M \gg 1.48\,|E_{crit}| = \frac{.741 M_{\odot}}{\mu^2} \tag{3.18}$$

This condition is satisfied for a SMS. For notational simplicity we shall drop the tilde and use $\widetilde{\Gamma}_1 \longrightarrow \Gamma_1$, $\widetilde{\beta} \longrightarrow \beta$, and $\left(\widetilde{\frac{1}{\mu}}\right) \longrightarrow \frac{1}{\mu}$, with the understanding that these quantities are implied to be pressure averaged (labeled with tildes) quantities. Note that if μ is taken to be uniform throughout the star, then quantities with tildes don't differ from those without.

Chapter 4

Mass Ranges for the General Relativistic Instability

4.1 Upper Bound

We have derived the criteria for a star going unstable due to GR corrections. However, this effect is not valid for all star masses. In order for a star to remain in thermal equilibrium as it approaches the instability point, the material in the star must have time to quickly readjust to thermal changes. This means the hydrodynamic timescale must be shorter than the thermal evolution timescale. The thermal timescale, $t_{thermal}$ can be estimated as the magnitude of the star's energy divided by its photon luminosity, L_γ. While the hydrodynamic timescale, t_{hydro}, is approximately the star's free-fall time:

$$t_{thermal} \approx \frac{|E_{crit}|}{L_\gamma} \qquad\qquad t_{hydro} \approx (\overline{\rho})^{-1/2} \tag{4.1}$$

The luminosity of the a SMS will be very close to the Eddington luminosity (see appendix A.5). We can now use eq. 3.8 with $\mu \approx 1$ to get:

$$t_{hydro} < t_{thermal} \Longrightarrow \sqrt{\frac{\left(\frac{M}{M_\odot}\right)^{7/2}\xi_1}{3\rho_{crit}\,|\theta(\xi_1)|}} < \frac{E_0}{4\pi M m_b/\sigma_{thom}} \Longrightarrow M \lesssim 10^8 M_\odot \tag{4.2}$$

where σ_{Thom} is the Thomson cross section, equal to $6.65 \times 10^{-29}\ m^2$.

4.2 Lower Bound and the Electron-Positron Pair Instability

Although more massive stars require a higher central temperature to counteract the increased inward gravitational forces, the critical temperature decreases as the stellar mass increases (eq. 3.10). Lower mass SMS's, will therefore reach the GRI at temperatures where the electron-positron pair production will become important. At some point the critical temperature will be sufficiently high that the star will undergo the EPPI at the same time as the GRI.

As stated in sect. 1.2, the EPPI can be thought of as an effective pressure loss due to high energy photons converting into electron-positron pairs (eq. 4.3 and the first diagram in fig. 4.1). More precisely, the electron+positron number, $n_e = n_- + n_+$, will be in equilibrium (forward and reverse rates in eq. 4.3 are equal) with photon numbers, n_γ, numbers via:

$$2\gamma \rightleftharpoons e^- + e^+ \tag{4.3}$$

The ratio n_e/n_γ increases with temperature, which in turn decreases, Γ_1. Furthermore, as electrons and photons are transferred back and forth, occasionally an electron positron pair will annihilate to a neutrino anti-neutrino pair instead (bottom diagrams in fig. 4.1):

$$e^- + e^+ \longrightarrow \nu + \overline{\nu} \tag{4.4}$$

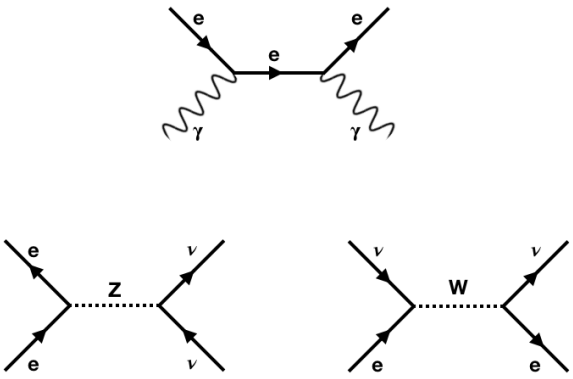

Figure 4.1: Feynman Diagrams for Electron-Positron Pair Creation/Annihilation

This process is a non-equilibrium process, as the neutrinos will then free-stream out of the star carrying away energy, further reducing the pressure. A basic overview is as follows.

For a pair of photons to annihilate to an electron-positron pair, the two photons must have a combined energy of at least $2m_e = 2 \times 511 MeV = 2 \cdot (6 \times 10^9) K$. The temperature in the core of stars is (typically) well below this temperature (hydrogen and helium fuse at around $10^7 K$ and $10^8 K$ respectively), consequently photons with sufficient energy to annihilate will only be found far in the high energy tail of the Planck distribution where the photon number decreases exponentially with energy, ε:

$$dn_\gamma(\varepsilon) \propto e^{-\varepsilon/T} \cdot \varepsilon^2 d\varepsilon \tag{4.5}$$

As a result, annihilations mostly take place closer to a total energy of $2m_e$. This means that radiation energy is mostly converted into rest mass, taking away pressure from the radiation field, and not compensating in gas pressure. Alternatively, the created pairs, will have to absorb energy from the surrounding heat bath to reach thermal equilibrium, resulting in a net pressure loss. From the point of view of Γ_1, if the material in the star is squeezed, some of the energy which would have gone into heat, increasing the pressure and pushing back against the increased gravity, now instead gets dumped into creating rest mass, and Γ_1 drops below $\frac{4}{3}$, i.e. there is no longer a restoring force. This effect holds even in absence of GR. At this point the star will begin

to collapse, as the more it contracts, the more photons are converted to pairs.

When including the effects of pair production, Γ_1 (eq. 2.35) will be modified [61]:

$$\Gamma_1 \approx \frac{4}{3} + \frac{\beta}{6} \cdot f(T, \eta) \tag{4.6}$$

with

$$f(T,\eta) = \frac{2\overline{Z}}{3(1+\overline{Z})} \left[\left(\frac{m_e}{T} \cdot \frac{\varepsilon - 3T}{m_e} \right)^2 \tanh(\eta) + \frac{m_e}{T} \left(3 \cdot \frac{\varepsilon - 3T}{m_e} - \frac{m_e}{T} \right) \coth(\eta) + \frac{3}{2\overline{Z}} \right] \tag{4.7}$$

where $\varepsilon =$ is the average energy of a single electron (including rest mass), $\eta =$ the electron degeneracy parameter, $\overline{Z} =$ the mean nuclear charge. The number densities and energy densities of electrons and positrons are:

$$n_{\mp} = \frac{T^3}{\pi^2} \int_0^{\infty} \frac{x^2}{e^{[q(x) \mp \eta]} + 1} dx \tag{4.8}$$

$$n_{\mp} = \frac{T^4}{\pi^2} \int_0^{\infty} \frac{x^2 \cdot q(x)}{e^{[q(x) \mp \eta]} + 1} dx \tag{4.9}$$

where the $q(x) \equiv \sqrt{x^2 + \left(\frac{m_e}{T}\right)^2} = \frac{\varepsilon}{T}$ (energy divided by temperature). Eqs. 4.8 and 4.9 cannot be integrated analytically in general, but analytical approximations for the number density and mean energy per particle [61, 62] (see appendix A.7.3) are:

$$n_{\mp} = \frac{m_e^3}{\pi^2} \cdot \left(\frac{T}{m_e} \right) \cdot K_2 \left(\frac{m_e}{T} \right) e^{\pm \eta} \tag{4.10}$$

where $K_i(x) =$ the i^{th} order modified Bessel function. It follows that the average energy of a single electron/positron is:

$$\varepsilon = 3T + m_e \frac{K_1\left(\frac{m_2}{T}\right)}{K_2\left(\frac{m_e}{T}\right)} \tag{4.11}$$

In the limiting cases of $T << m_e$ and $T >> m_e$, eq. 4.11 converges to:

$$\varepsilon \longrightarrow \begin{cases} m_e + \frac{3}{2}T & \text{for } T << m_e \\ 3T & \text{for } T >> m_e \end{cases} \tag{4.12}$$

Substituting eq. 4.11 into eq. 4.7 we have:

$$f(T,\eta) = \frac{2\overline{Z}}{3(1+\overline{Z})}\left[\left(\frac{m_e}{T}\cdot\frac{K_1\left(\frac{m_2}{T}\right)}{K_2\left(\frac{m_e}{T}\right)}\right)^2 \tanh(\eta) + \frac{m_e}{T}\left(3\cdot\frac{K_1\left(\frac{m_e}{T}\right)}{K_2\left(\frac{m_e}{T}\right)} - \frac{m_e}{T}\right)\coth(\eta) + \frac{3}{2\overline{Z}}\right] \tag{4.13}$$

At sufficiently high temperatures, $f(T,\eta)$ go negative, causing Γ_1 to drop below $\frac{4}{3}$, and the star will go unstable. In the limit where $T << m_e$ and $\tanh(\eta) \longrightarrow 1$, eq. 4.13 will reduce to:

$$f(T << m_e, \eta) \approx 1 - \frac{5\overline{Z}}{2(1+\overline{Z})}\cdot\left(\frac{T}{m_e}\right) \approx 1 - \frac{5\mu Y_e}{2}\cdot\left(\frac{T}{m_e}\right) \tag{4.14}$$

where $Y_e = \overline{Z}/\overline{A}$ and $\overline{A}$ is the average atomic number. Since Z is the number of protons per atomic nucleus, i.e. the number non-pair-created electrons per nucleus, we have:

$$n_p = n_- - n_+ = \frac{\rho Y_e}{m_b} \tag{4.15}$$

Substituting eqs. 4.10 and 2.20 into eq. 4.15 we find:

$$\sinh(\eta) = \left(\frac{\sqrt{2}\pi^4 Y_e}{3000\sqrt{M_4}}\right)\cdot\left[\frac{1}{\left(\frac{m_e}{T}\right)^2 K_2\left(\frac{m_e}{T}\right)}\right] \tag{4.16}$$

Now substituting eq. 4.16 into eq. 4.13, we can eliminate η to get:

$$f(T,\eta) \longrightarrow f(T,M) \tag{4.17}$$

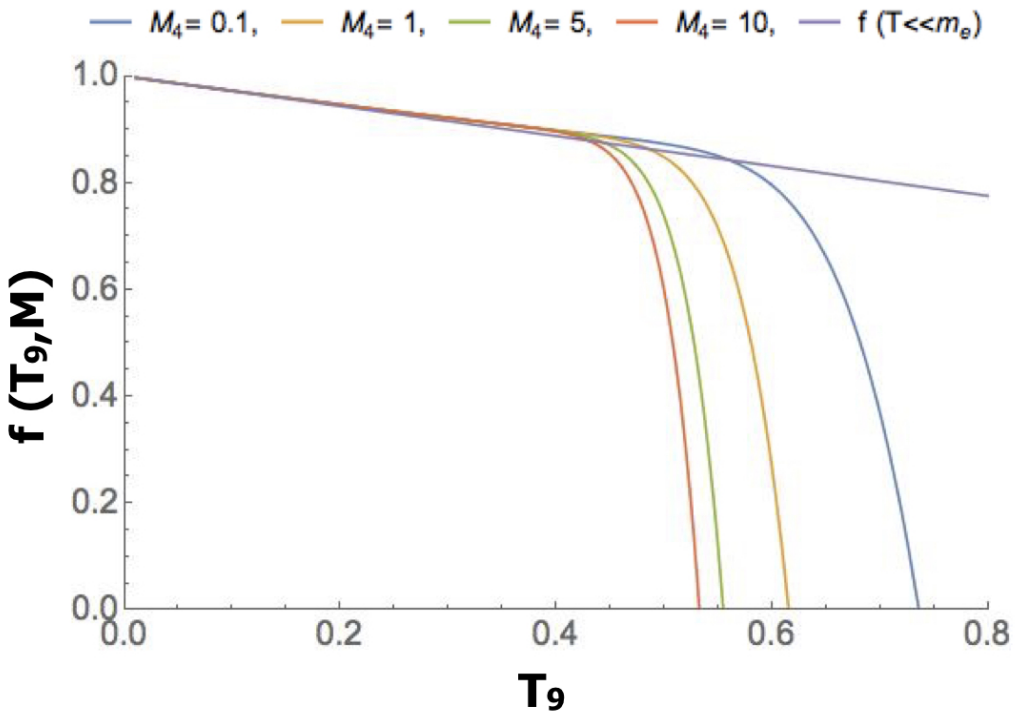

Figure 4.2: $f(T,M)$ vs. Temperature.

Plot of $f(T,M)$ vs. temperature for various masses, as derived by [61] (eq. 4.13). Plots are made for a ^4He composition: $Y_e = \frac{1}{2}$, $\mu = \frac{4}{3}$, $\overline{Z} = 2$. Note that for $M \widetilde{<} 3M_4$, μ will be greater than $\frac{4}{3}$, i.e. the star's composition will include significant amounts of elements heavier than ^4He (see fig. 8.11). When $f(T,M) < 0$, Γ_1 will drop below $\frac{4}{3}$, and the star will undergo the EPPI. Increasing the mass of the star pushes the EPPI to lower temperatures. The 'boundary' between a VMO and a SMS is loosely defined by the point where the EPPI and the GRI occur at the same central temperature or mass. The purple line is the low temperature approximation ($T << m_e$) of $f(T,M)$ (eq. 4.14), and is mass independent.

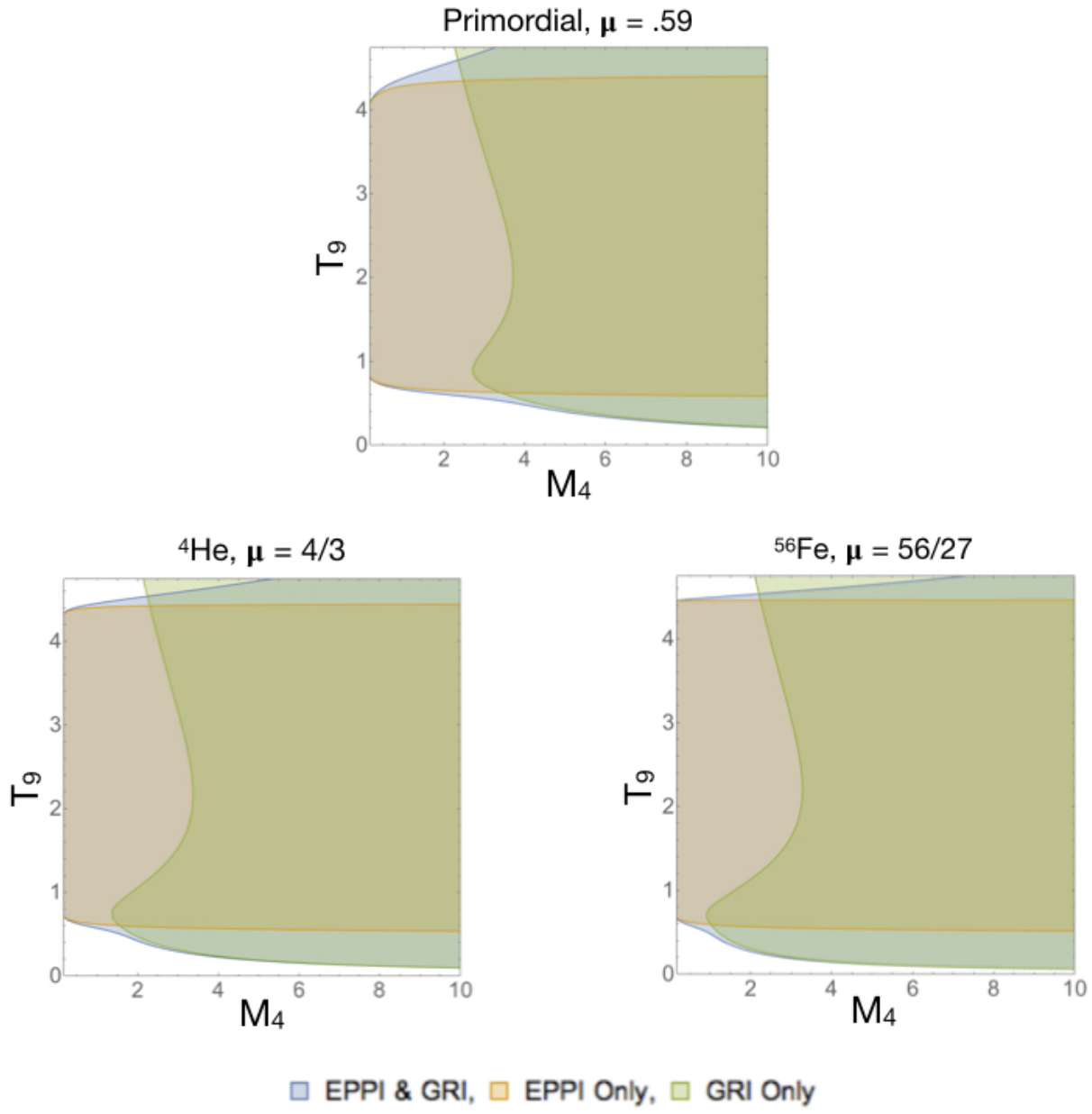

Figure 4.3: Regions of Instability for EPPI, GRI, and Elemental Composition.
The region of instability when considering both the EPPI and GRI (in blue) completely encloses the lower boundaries of instability when only considering the EPPI or GRI alone (in orange and green respectively). The EPPI alone has a lower threshold temperature of $T_9 > 0.6$, with almost no dependence on stellar mass and composition; as well as an upper limit of $T_9 < 5 \approx m_e$. Above this temperature the pairs are relativistic, and converting photons to electrons doesn't result in pressure loss, as both species contribute to radiation. The GRI alone is initially suppressed by the creation of non-relativistic electron-positron pairs, as they reduce the mean particle mass. As the temperature increases and the electrons become relativistic, they no longer contribute to the mean particle mass and $\mu \longrightarrow \overline{A}$.

As mentioned in sect. 1.2, traditionally the distinction between VMS's and SMS's has been defined by whether a star goes unstable due to the EPPI or the GRI, respectively. However, this definition is somewhat misleading, as in actuality a star will always go unstable due to both effects.

Ignoring the GRI, the instability criteria is:

$$\Gamma_1 < \frac{4}{3} \tag{4.18}$$

The EPPI is caused by a rise in electron-positron pair creation, leading to Γ_1 being driven down until it is below $\frac{4}{3}$, i.e. changes in the left-hand side of eq. 4.18. On the other hand, the GRI doesn't modify Γ_1, but instead increases the threshold for the minimum stable Γ_1 to give an instability criteria of:

$$\Gamma_1 < \frac{4}{3} + O\left(\frac{2M}{R}\right) \tag{4.19}$$

That is, a modification of the right-hand side of eq. 4.18. The two are not mutually exclusive however, and as Γ_1 is driven down, it will always reach $\frac{4}{3} + O\left(\frac{2M}{R}\right)$ before reaching $\frac{4}{3}$. Similarly, the effects of pair creation will always be present, even if small, eq. 4.6 will always push the star closer to instability, than if ignoring their effects. However, it is nonetheless possible to delineate ranges where one effect alone would still result in instability, separated by a region where neither effects of the EPPI nor those of the GRI alone will cause instability, but instability will set in only when both are considered. Hence the boundary between the two is somewhat fuzzy. These regions are shown in fig. 4.3. Luckily, the region where both effects are important is relatively small, and it can be loosely said that the lower bound on the GRI is roughly $M_4 \approx 1.8$, or, more accurately, when $T_{8,c} > 6$ (see fig. 4.3). For SMS with $M_4 \approx 5$ (depending on the value of μ),the effects of pair creation can be neglected.

Chapter 5

Behavior at the Critical Point

Let us define the dimensionless quantities $x \equiv \left(\frac{\rho}{\rho_M}\right)^{1/3} = \frac{T}{T_M}$, and $\varepsilon \equiv \frac{E}{E_0}$; with $\rho_M \equiv \rho_0 \cdot \left(\frac{M_\odot}{M}\right)^{7/2}$ and $T_M \equiv T_0 \cdot \frac{M_\odot}{M}$. Substituting into eq. 3.3 gives:

$$\varepsilon = x^2 - \frac{2x}{\mu},\ x_{crit} = \frac{1}{\mu}, \text{ and } \varepsilon_{crit} = -\frac{1}{\mu^2} \tag{5.1}$$

Alternatively, x_{crit} and ε_{crit} can also be found by setting $\left.\frac{\partial \varepsilon}{\partial x}\right|_\mu = 0$. If the curve $\varepsilon_{crit}(\mu) = -\frac{1}{\mu^2}$ is superimposed onto the graph of ε vs. x (the dashed magenta curve in fig. 5.1), we can see that as the star undergoes nuclear fusion, converting nuclei with atomic mass A_1 to heavier nuclei with atomic mass A_2 $(A_2 > A_1)$, μ will increase and the star will move upwards (closer to instability) in fig. 5.1. This means, that unless the star sufficiently expands/cools (corresponding to a leftward shift in fig. 5.1), it will eventually cross the curve $\varepsilon_{crit}(\mu) = -\frac{1}{\mu^2}$ and go unstable.

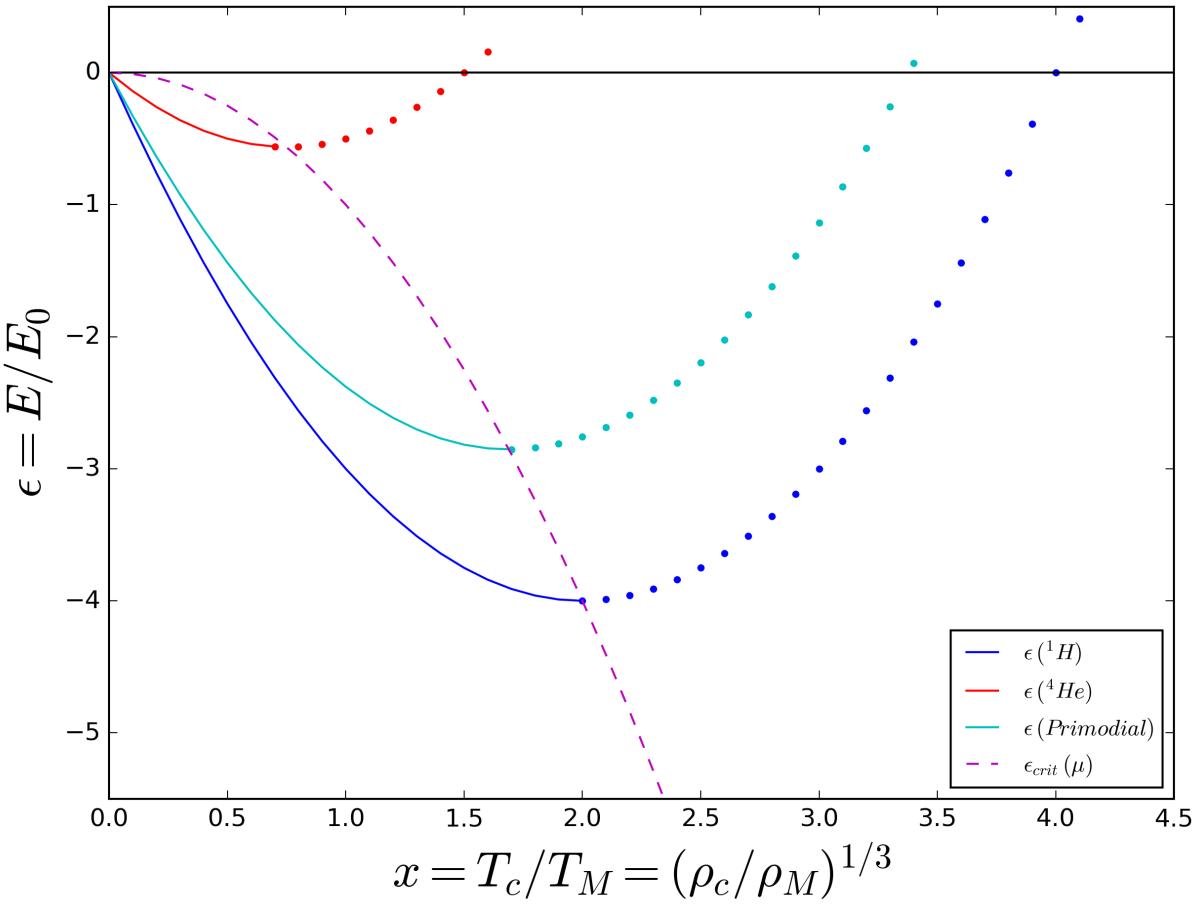

Figure 5.1: ε vs. x for Various Values of μ.
Dimensionless binding energy, ε vs. dimensionless proxy for central temperature or central density, x in a $n = 3$ polytrope star in hydrostatic equilibrium, for various values of the mean particle mass, μ. Solid lines represent stable regimes. Dotted lines represent unstable regimes. The magenta dashed line depicts the critical point energies vs. critical point densities/temperatures as a function of μ ($\varepsilon = -\frac{1}{\mu^2}$, $x = \frac{1}{\mu}$). As μ increases the star becomes less bound at the same value of x, and the instability density and temperature shift to lower values. As a result, as a star fuses nuclei to form heavier nuclei, the star will move up in this plot from from a given μ, to a higher μ. Unless the central density/temperature sufficiently decreases (in general it will increase), the star will inevitably reach the GRI (cross the dotted magenta line).

Now suppose a star has just reached its critical point. In a time dt, some amount of nuclear fuel with atomic mass A_1 will be converted through fusion to atomic mass A_2. This will result in a release of nuclear binding energy, dE, a corresponding change in mean particle mass, $d\mu$, and a change in x of dx. This will move the star from an equilibrium curve $\varepsilon(\mu, x)$ to a new curve

$\varepsilon(\mu + d\mu, \frac{1}{\mu} + dx)$. Hence we get:

$$[\varepsilon(\mu,x) + d\varepsilon]_{crit} = -\frac{1}{\mu} + \left.\frac{\partial \varepsilon}{\partial \mu}\right|_{\mu,\frac{1}{\mu}} \cdot d\mu + \left.\frac{\partial \varepsilon}{\partial x}\right|_{\mu,\frac{1}{\mu}} \cdot dx = -\frac{1}{\mu^2} + \frac{2}{\mu^3} \cdot d\mu + 0 \cdot dx \tag{5.2}$$

$$\implies d\varepsilon_{crit} = \frac{2d\mu}{\mu^3} \tag{5.3}$$

So at the critical point, an increase in μ will move the star vertically to the point $\left[\varepsilon(\mu + d\mu, \frac{1}{\mu}), \frac{1}{\mu}\right]$, which will necessarily be in an unstable regime, as it will have moved to the right of the $\varepsilon(\mu + d\mu, x)$ instability point. If the energy increase from nuclear fusion, dE, is greater than $E_0 d\varepsilon$ than the star will be too deep in the potential well, and will collapse, as it will sit below the $\varepsilon(\mu + d\mu, x)$ equilibrium curve. If, on the other hand, $dE > E_0 \cdot d\varepsilon$, then energy losses must be taken into account to determine the fate of the star. In other words, for a star to expand rather than collapse upon going unstable we must have:

$$dE > E_0 \cdot d\varepsilon_{crit} + dE_{loss} \tag{5.4}$$

It should be noted that if this condition is satisfied, this does not necessarily imply an explosion, simply a runaway expansion and unbinding of the star of some sort. In order to determine the fate of an SMS undergoing the GRI, we must first determine the nuclear energy generation and losses.

Chapter 6

Nuclear Rates and Energy Generation

6.1 Mean Particle Mass

The quantity μ has been defined to be the mean particle mass in units of m_b. This quantity will increase as lighter nuclei fuse to heavier nuclei. Consider a mass element, m, that is fusing helium to a heavier nuclei with atomic number, A. The mean particle mass in terms of the mass, the electron number, N_e, and number of particles of a given nuclear species, N_i, is: .

$$\mu \equiv \frac{m}{m_b\left(\sum_i N_i + N_e\right)} = \frac{M}{m_b}\frac{1}{N_\alpha + N_A + N_e + N_{other}} \tag{6.1}$$

$$\tag{6.2}$$

where N_α, N_A, and N_{other} are the numbers of ^4He, daughter nuclei with atomic mass, A, and any other nuclei, respectively. The electron fraction, Y_e is:

$$Y_e \equiv \frac{N_{protons}}{N_{baryons}} = \frac{N_{e^-} - N_{e^+}}{N_{baryons}} = \frac{\sum_i N_i Z_i}{\sum_i N_i A_i} == \left(\frac{\overline{Z}}{\overline{A}}\right) = \sum_i X_i \frac{Z_i}{A_i} \tag{6.3}$$

where X_i's are mass fractions $(X_i = N_i \cdot A_i \cdot m_n/m)$ and the 'barred' value is the average.

Using $dN_e = \sum_i dN_i Z_i$, and $dN_\alpha = -\frac{A}{A_\alpha} dN_A$ ($A_\alpha = 4$), we get:

$$d\mu = -\frac{m}{m_b} \frac{dN_\alpha(1+Z_\alpha) + dN_A(1+Z)}{(N_\alpha + N_A + N_e + N_{other})^2} = \frac{\mu^2 m_b}{A_\alpha m} \left[A(1+Z_\alpha) - A_\alpha(1+Z)\right] dN_A \tag{6.4}$$

or plugging in values for A_α and Z_α:

$$\dot{\mu} = \frac{3\mu^2 m_b}{4M} \left[A - \frac{4}{3}(1+Z)\right] \dot{N}_A \tag{6.5}$$

6.2 Nuclear Fusion via the Triple-α Process

For a star that has fused all or most of its hydrogen and left the Main Sequence, the next phase in nuclear burning is the triple-α process: $3 \times {}^4He \longrightarrow {}^{12}C$ via the two step process:

$${}^4He + {}^4He \rightleftharpoons {}^8Be - 0.1 \text{ MeV} \implies {}^8Be + {}^4He \longrightarrow {}^{12}C + 7.4 \text{ MeV} \tag{6.6}$$

The first reaction in eq. 6.6 is endothermic, and consequently less energetically favorable to $2 \times {}^4He$, and so ${}^8Be$ is not a stable nucleus, and most of the time it will split back into $2 \times {}^4He$. This reaction is also in nuclear statistical equilibrium (NSE), i.e. forward and reverse rates are equal. In order to make ${}^{12}C$, a third ${}^4He$ must be captured prior to the very short decay time of ${}^8Be$ (half-life $= 8.2 \times 10^{-17}$s [63]) for the second reaction in eq. 6.6 to take place, and ${}^{12}C$ to form. Because the reaction $2 \times {}^4He \rightleftharpoons {}^8Be$ is in NSE, there is a fixed net amount of ${}^8Be$ at any given time. The ${}^8Be$ mass fraction can be calculated via the Saha equation (see appendix A.8). Consequently, the number ratio of ${}^8Be$ to ${}^4He$ is found to be [55]:

$$\frac{N(^8Be)}{N(^4He)} \approx 2.8\times10^{-10}\cdot\left(\frac{\rho\cdot X(^4He)}{T_8^{3/2}}\right)\cdot10^{-4.64/T_8} \approx 3.6\times10^{-10}\cdot\left(\frac{T_8^{3/2}\cdot X(^4He)}{\sqrt{M_4}}\right)\cdot10^{-4.64/T_8} \tag{6.7}$$

where $N()$'s are particle numbers of a given species, $X()$'s are the mass fractions, ρ is in units of g/cc, and eq. 2.20 has been used in the expression on the right. Evaluating eq. 6.7 at the GRI gives:

$$\left.\frac{N(^8Be)}{N(^4He)}\right|_{crit} \approx 1.6\times10^{-8}\cdot\left(\frac{X(^4He)}{\mu^{3/2}M_4^2}\right)\cdot10^{-0.373\mu M_4} \tag{6.8}$$

As a result of the low numbers of ^8Be per ^4He ($\sim 10^{-12}$ around $M_4 = 5$), the formation of ^{12}C is very slow. The (non-NSE) reaction, $^4He + {}^8Be \longrightarrow {}^{12}C$, was found to be too slow to produce sufficient amounts ^{12}C to support a star [55, 64]. It was consequently predicted, and then discovered, that the $^4He + {}^8Be \longrightarrow {}^{12}C$ reaction must be amplified by the existence of a 0^+ excited state of ^{12}C, having a resonant energy with $^4He + {}^8Be$ at stellar temperatures [55, 64, 65], shown in fig. 6.1.

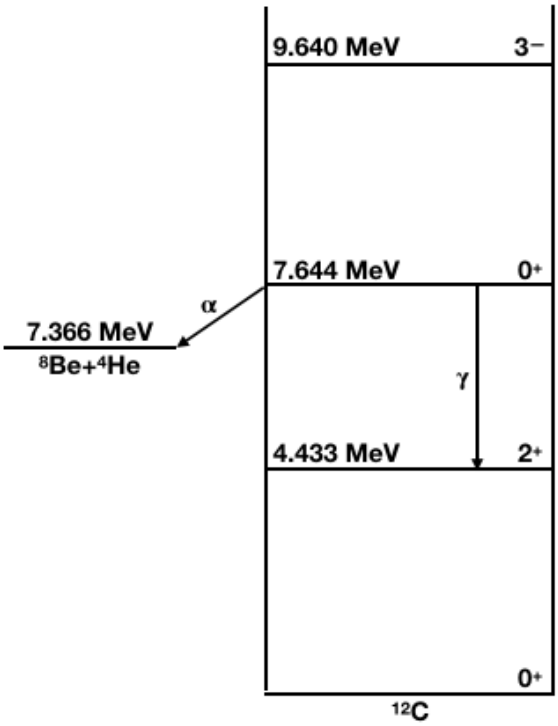

Figure 6.1: $^4He + {}^8Be \longrightarrow {}^{12}C$, 'Hoyle Level' Resonance
The 0^+ excited state of the ^{12}C nucleus, resonant with $^8Be + {}^4He$ (also 0^+) at stellar temperatures, was predicted by Fred Hoyle [64] and soon after discovered [65]. Its existence allows for accelerated production of ^{12}C in stellar interiors. Diagram adapted from [55].

The net triple-α energy production rate from combining

$$2 \times {}^4He \rightleftharpoons {}^8Be \text{ and } {}^4He + {}^8Be \longrightarrow {}^{12}C \tag{6.9}$$

can be calculated [55] to be:

$$\varepsilon_{3\alpha} \approx 3.9 \times 10^{11} \frac{\rho^2 X^3(^3He)}{T_8^3} \cdot e^{\left[-\frac{42.94}{T_8}\right]} \; ergs/g/s \tag{6.10}$$

From eq. 6.10 and effective triple-α nuclear rate, $\sigma_{3\alpha}$ can be backed out, via the differential equation:

$$\dot{n}_\alpha = -n_\alpha^3 \sigma_{3\alpha} \tag{6.11}$$

where n_α and $\dot{n}_\alpha$ are the helium number density and its time derivative, respectively. The comparison of eq. 6.10 to the experimental values from [66] is shown in fig. 6.2.

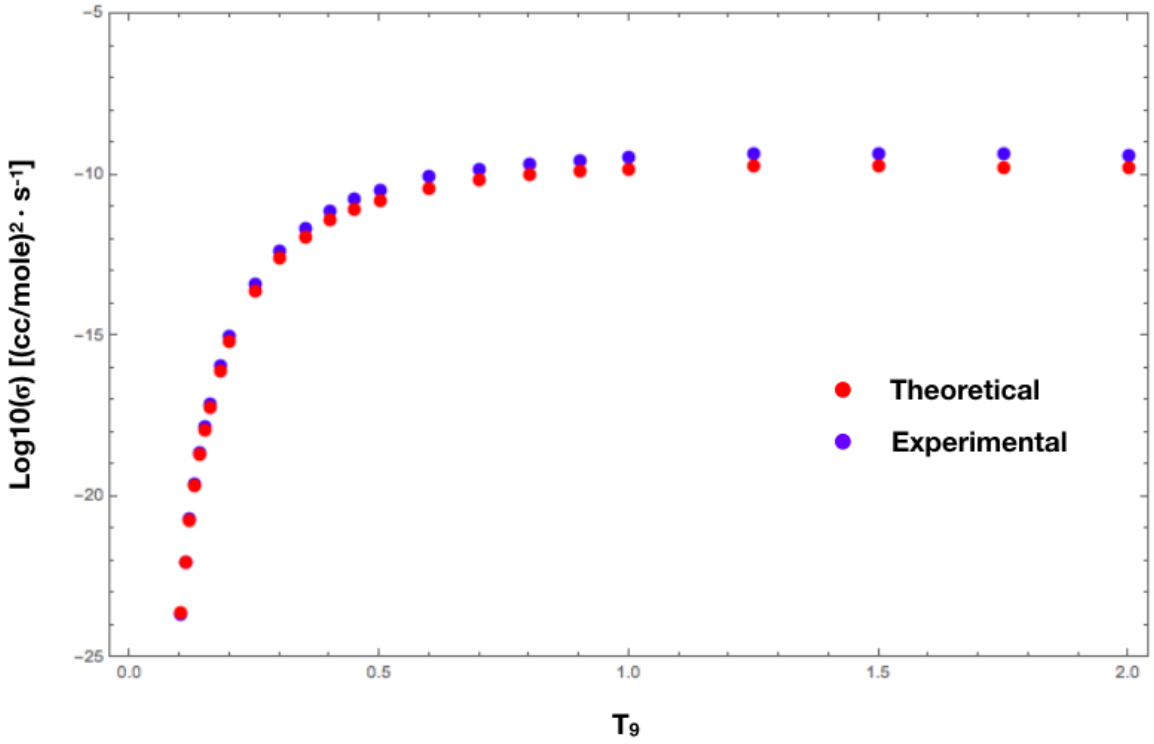

Figure 6.2: Triple-α Nuclear Rates

Triple-α nuclear capture rates as a function of temperature for the effective reaction: $3 \times {}^4He \longrightarrow {}^{12}C$ with the corresponding differential equation for the helium number density: $\dot{n}_\alpha = -n_\alpha^3 \sigma$. Theoretical rates derived from eq. 6.10 [55]. Experimental rates are taken form [66].

Despite being helped by the resonant 'Hoyle Level', the triple-α fusion rate is nonetheless relatively slow. Combined with the relatively small amount of nuclear binding energy released (0.6MeV/baryon), the net result is a relatively weak energy generation rate.

However, once a ${}^{12}C$ nucleus is made, it can fuse with another ${}^4He$ nucleus to form a ${}^{16}O$ nucleus, which can in turn capture another ${}^4He$ to make ${}^{20}Ne$, and so on. This is called the α-process, and in principle this chain reaction can continue (along with two e^--captures) up to ${}^{56}Fe$, so long as temperatures are sufficiently high to overcome Coulomb barriers. If the temperature is too low, then the process will be halted at some intermediate nucleus with atomic

mass, A_{max}. Therefore the set of differential equations that must be solved to determine the number densities of each species, n_i, is:

$$\begin{aligned}
\dot{n}_\alpha &= -\left(n_\alpha\right)^3 \sigma_{(3\alpha} - \textstyle\sum_{A_i=^{12}C}^{A_{max}-1} n_\alpha n_{A_i} \sigma_{(A_i,\alpha)} \\
\dot{n}_{^{12}C} &= \tfrac{1}{3}\left(n_\alpha\right)^3 \sigma_{(3\alpha,^{12}C)} - n_{^{12}C} n_\alpha \sigma_{(^{12}C,\alpha)} \\
\dot{n}_{^{16}O} &= n_{^{12}C} n_\alpha \sigma_{(^{12}C,\alpha)} - n_{^{16}O} n_{He_4} \sigma_{(^{16}O,\alpha)} \\
&\vdots \\
\dot{n}_{A_i} &= n_{A_{i-1}} n_\alpha \sigma_{(A_{i-1},\alpha)} - n_{A_i} n_\alpha \sigma_{(A_i,\alpha)} \\
&\vdots \\
\dot{n}_{A_{max}} &= n_{A_{max-1}} n_\alpha \sigma_{(A_{max-1},\alpha)}
\end{aligned} \tag{6.12}$$

where $\sigma_{(\,)}$'s = the temperature dependent capture rates between atomic species. The energy generation rate for a differential mass element with volume dV, will be the sum of the number generation rates times the binding energy released for each capture:

$$d\dot{E} = \sum_{^{12}C}^{A_{max}} A_i \Delta E_i \dot{n}_i dV \tag{6.13}$$

where ΔE_i binding energy per nucleon of the i^{th} species minus the binding energy per nucleon of ^4He. Unfortunately, because of the $\left(n_\alpha\right)^3$ terms in the triple-α process this set of equations is not solvable analytically. However, they can be constrained by looking at two limiting cases.

6.3 Instantaneous α-Process

Suppose that once a ^{12}C nucleus is made, it instantaneously captures α's up to some atomic species, A. A could range from $12 \longrightarrow 56$ in multiples of 4. If $A = 12$, then the process stops at ^{12}C and all we have is the triple-α process. And if $A = 56$, then ^4He is being converted straight to ^{56}Fe. In this way we can simply multiply the triple alpha rate by $\frac{A}{12}$ to account for the extra α's being captured. For convenience we will make the following change in notation: $\sigma_{(3\alpha)} \equiv \sigma$. This means we can reduce the set of equations 6.12 and 6.13 to the following equations:

$$\dot{n}_\alpha = -\frac{A}{12} n_\alpha^3 \sigma \tag{6.14}$$

$$\dot{n}_A = -\frac{4}{A} \dot{n}_\alpha \tag{6.15}$$

$$d\dot{E} = A\Delta E \dot{n}_A dV \tag{6.16}$$

where the ΔE will depend on which A is chosen. Solving with the initial condition that $n_\alpha = \frac{\rho}{4m_b}$ (the star is entirely ^4He) gives:

$$n_\alpha(t) = \frac{\rho}{4m_b \sqrt{1 + A\omega(\rho, T)t}} \tag{6.17}$$

$$n_A(t) = \frac{\rho}{Am_b} \left(1 - \frac{1}{\sqrt{1 + A\omega(\rho, T)t}} \right) \tag{6.18}$$

$$d\dot{E}(t, V) = A\Delta E dV \dot{n}_A(t) = \frac{A\Delta E \rho \omega(\rho, T) dV}{2m_b \left[1 + A\omega(\rho, T) \cdot t\right]^{3/2}} \tag{6.19}$$

where

$$\omega(\rho, T) \equiv \frac{\rho^2 \sigma(T)}{96 m_b^2} \tag{6.20}$$

If the star is not entirely composed of ^4He, from eq. 6.14, the energy generation will scale as three powers of the mass fraction: X_α^3. There are other nuclear fusion channels, but during helium burning phase, the α-process will be the dominant channel, and so we can safely say that the true energy generation rate will lie somewhere between the cases of $(A,Z) = (12,6)$ and $(A,Z) = (56,26)$. The width of this range is in fact relatively small (about a factor of 13), as the majority of the binding energy of a ^{56}Fe nucleus is lost during ^1H fusion. We can see this by comparing the two rates at $t = 0$:

$$\dot{E}(A,Z=12,6) < \dot{E}_{true} < \dot{E}(A,Z=56,26) \Longrightarrow \dot{E}(A,Z=12,6) < \dot{E}_{true} < 13\dot{E}(A,Z=12,6) \tag{6.21}$$

where we have used $\Delta E_{^{12}C} = .6$ MeV and $\Delta E_{^{56}Fe} = 1.7$ MeV. Using eqs. 5.3 and 6.19, eq. 5.4 can be rewritten in terms of $\dot{n}_A$ to give:

$$A\Delta E \dot{n}_A dV \left(1 - \frac{2E_0}{A\Delta E \mu^3} \frac{d\mu}{dN_A}\right) > \dot{E}_{loss} \tag{6.22}$$

Combining eqs. 6.19, 5.3, 5.4, and 6.5, and integrating over the entire volume of the star at the GRI we find that an SMS will unbind if:

$$A\Delta E \dot{N}_A \left[1 - \frac{m_b E_0 \left[3A - 4(1+Z)\right] T_{crit}}{2M_\odot A \Delta E T_0}\right] > \dot{E}_{loss} \tag{6.23}$$

In order to avoid the EPPI, we must have $T_{8,crit} < 6$ (see sect. 4.2) which limits the factor inside the large brackets in eq. 6.23 is greater than 0.98, and can therefore be set to 1. In order to evaluate $\dot{N}_A$ we need to know the triple-α ($3 \times {}^4He \longrightarrow {}^{12}C$) capture rate, σ. In this dissertation, the experimental capture rates from [66] were used; which are given per mole, rather than per particle. Hence we must divide σ by ${N_a}^2$ (Avogadro's Number), in order to use the values in these tables. At early times ($\omega t \approx 0$), we can integrate eq. 6.19 over an $n = 3$ polytrope at the

instability point to find the energy generated via triple-α to be:

$$\dot{E} = \frac{A\Delta E \rho_{crit}^3 r_0^3}{192 m_b^3 N_a^2} \int_0^{\xi_1} \sigma(T)\theta^9 \xi^2 d\xi \tag{6.24}$$

σ is highly sensitive to temperature. A two order of magnitude change in temperature from about $10^7 \longrightarrow 10^9\ K$ results in σ ranging from $10^{-47} \longrightarrow 10^{-10}\ cc^2/mole^2/s$ [66]. In order to numerically evaluate the integral in eq. 6.24, a continuous function, $\sigma(T)$ (recall that $T = T_c\theta$), can be approximated by interpolating the σ values found in the [66] tables, via a linear scheme in $\log\sigma$:

$$\log\left[\sigma(T_i \leq T \leq T_{i+1})\right] = \log(\sigma_i) + \frac{\log(\sigma_{i+1}) - \log(\sigma_i)}{T_{i+1} - T_i}(T - T_i) \tag{6.25}$$

where the i^{th} σ's and T's correspond to entries in the [66] tables.

6.4 Neutrino Emission and Energy Loss

As long as a star in hydrostatic equilibrium is not ejecting or accreting mass, i.e. baryons, the energy loss rate, $\dot{E}_{loss}$, is determined via only two mechanisms: photon emission from the surface and neutrino emission from the interior. The photon luminosity constitutes energy lost from the surface of the star, and is not relevant to the energy balance inside the star where thermonuclear reactions are taking place. However, while the star is in a stable regime the photon luminosity does indicate how much nuclear energy must be generated to support the star against gravity. Since a SMS is radiation dominated, it will radiate photons at nearly the Eddington luminosity (eq. 6.26). For a SMS to explode, it must at least produce enough energy to overcome gravitational forces plus the neutrino loss, that is, $\dot{E}nuc > L_{Edd} + L_\nu$.

$$L_{Edd} = \frac{4\pi M m_p}{\sigma_{Thom} Y_e} \quad \text{(see appendix A.5)} \tag{6.26}$$

Neutrinos, are primarily created in the center of the star, where the temperatures are higher, as their scattering cross sections are energy dependent. They then free stream their way out of the star, as they have mean free path of order 10^4 *AU* (see appendix A.6.3). Although, in a given regime, only one neutrino channel may be significant, in general there are numerous neutrino processes that need to be considered, while accounting for both neutral current (via a Z-Boson exchange) and charged current (via a W-Boson exchange) channels:

$L_{pair} \equiv$ Electron-positron annihilation (Pair Neutrino Process):

$$e^- + e^+ \longrightarrow \nu + \overline{\nu}$$

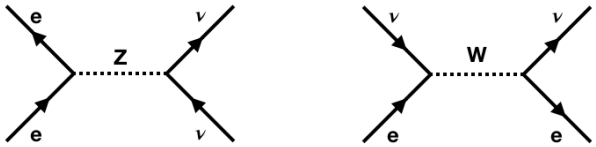

Figure 6.3: Pair Neutrino Process

$L_{photo} \equiv$ Inelastic electron-photon scattering (Photo-Neutrino Process):

$$e^- + \gamma \longrightarrow e^- + \nu + \overline{\nu}$$

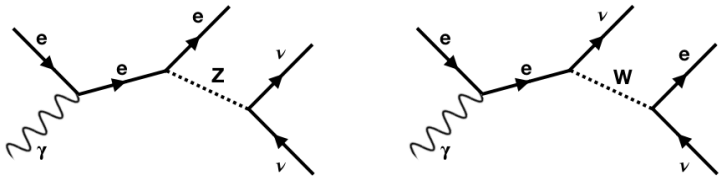

Figure 6.4: Photo-Neutrino Process

$L_{plasma} \equiv$ Plasmon scattering (Plasma Neutrino Process):

$$\gamma + \textit{plasmon} \longrightarrow \nu + \overline{\nu}$$

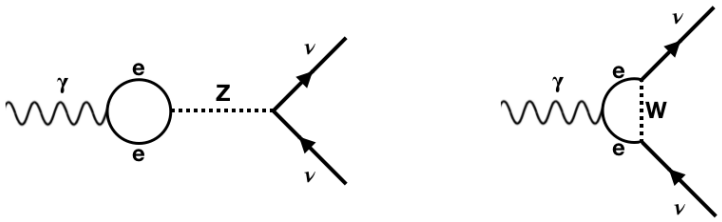

Figure 6.5: Plasma Neutrino Process

$L_{brems} \equiv$ Bremsstrahlung between weakly degenerate electrons and baryons (Bremsstrahlung Neutrino Process):

$$e^- + (A,Z) \longrightarrow e^- + (A,Z) + \nu + \overline{\nu}$$

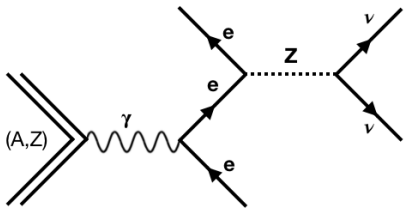

Figure 6.6: Bremsstrahlung Neutrino Process
*Note that the bold **Z** refers to the Z-boson, while the non-bold Z refers to the charge of the nucleus with atomic number A.

$L_{rec} \equiv$ Atomic capture of electrons (Recombination Neutrino Process):

$$(A,Z) + e^-_{free} \longrightarrow (A,Z) + e^-_{bound} + \nu + \overline{\nu}$$

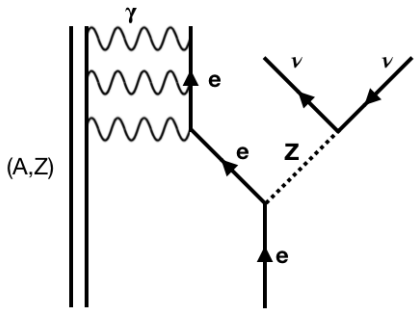

Figure 6.7: Recombination Neutrino Process
*Note that the bold **Z** refers to the Z-boson, while the non-bold *Z* refers to the charge of the nucleus with atomic number A.

Calculations of these neutrino loss processes were done using fitting formulas by [67] (see appendix A.3), which are also used in KEPLER. Fig. 6.8 shows the different neutrino loss rates for different star masses at instability.

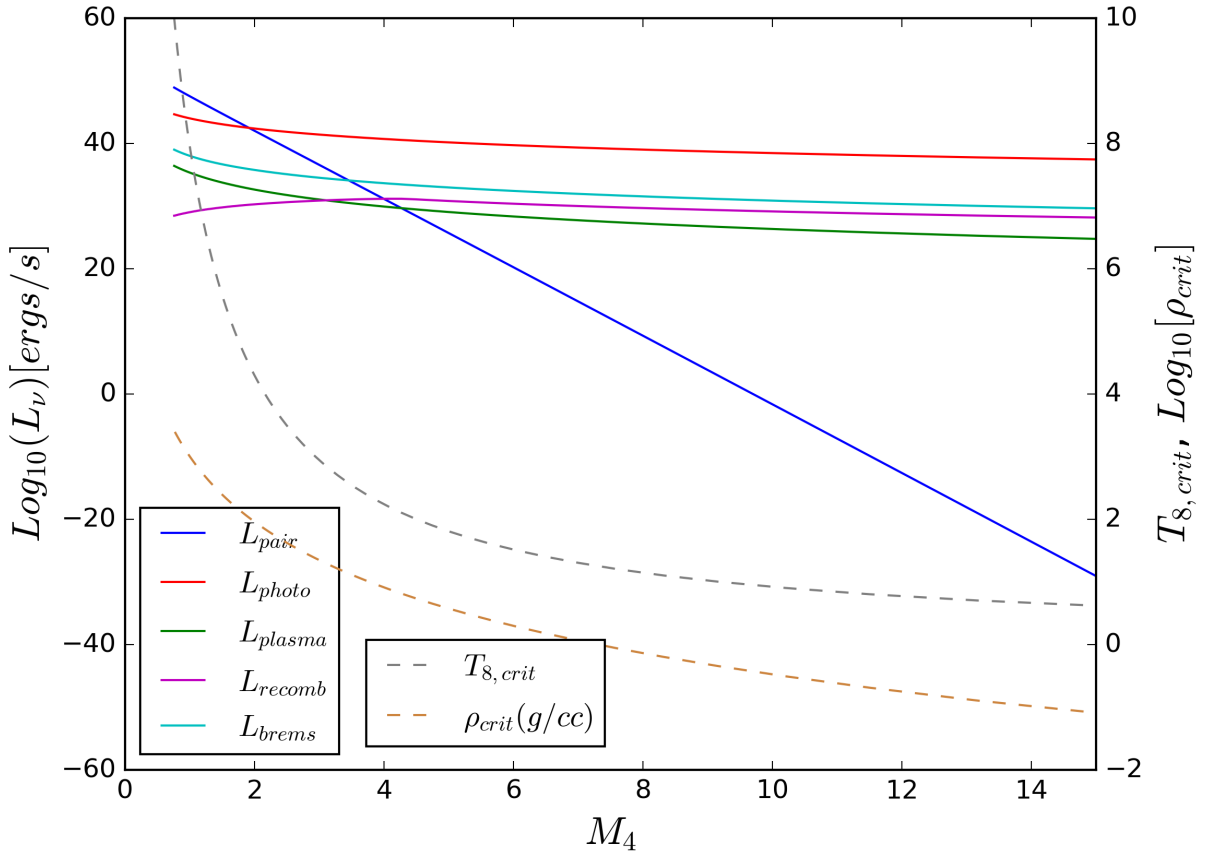

Figure 6.8: Luminosities of Neutrino Processes at the GRI.
Neutrino luminosities at the GRI (left vertical axis) as a function of stellar mass for various neutrino processes. Critical densities and temperatures at the GRI are on the right vertical axis. All neutrino processes are determined using the fits from [67] (also used in KEPLER). At lower temperatures, the photo-neutrino process (in red) accounts for most of the neutrino losses, while at higher temperatures ($T_8 \gtrsim 4$), the pair-neutrino process (in blue) dominates. Coincidentally, below this temperatures, neutrino losses are also small compared to photon emissions (see fig. 6.9), and hence only the pair-neutrinos need to be considered. All other neutrino processes can be neglected in energy calculations.

The lower mass limit on SMS's, as defined by undergoing the GRI rather than EPPI, can be well approximated by where L_{pair} becomes the dominant neutrino process. This will occur around $M_4 < 2$. Above this mass the dominant neutrino process is the photo-neutrino process (see fig. 6.8).

Neutrinos created through nuclear fusion/weak processes must also be accounted for, e.g., proton-proton chain. However in the processes being considered, weak interactions as a result of

fusing α's don't come into play until $A > 40$, at which point β-decay will convert some protons to neutrons in some unstable nuclei. Without β-decay, building up a heavier nuclei via the α-process, would lead to all nuclei having $Z = \frac{A}{2}$. Therefore, ΔE for the creation of elements with $A > 40$ will be slightly over estimated since a fraction of that energy produced will be lost to the neutrinos produced though β-decay.

Combining eqs. 6.24, 6.23, L_ν, L_{Edd}, and integrating over an $n = 3$ polytrope, the condition for an SMS to support itself via :

$$\frac{A\Delta E \rho_{crit}^3}{192 m_b^3 N_a^2} \cdot 4\pi r_0^3 \cdot \int_0^{\xi_1} \sigma(T)\theta^9 \xi^2 d\xi > 4\pi r_0^3 \cdot \int_0^{\xi_1} \sum_i Q_i(T)\xi^2 d\xi + L_{Edd} \tag{6.27}$$

or, in units of $\left[\frac{ergs}{sg}\right]$,

$$9.0 \times 10^{58} \left(\frac{A\Delta E}{MeV}\right) M_4^{-6} \int_0^{\xi_1} \sigma(T)\theta^9 \xi^2 d\xi > 1.2 \times 10^{33} M_4^{9/2} \cdot \int_0^{\xi_1} \sum_i Q_i(T)\xi^2 d\xi + 2.5 \times 10^{42} M_4 \tag{6.28}$$

where Q_i's are in units of $\left[\frac{ergs}{cc \cdot s}\right]$, μ has been set to $\frac{4}{3}$, $Y_e = \frac{1}{2}$, and the values of σ, in units of $\left[\frac{cc^2}{mole^2 \cdot s}\right]$ are those found in [66], interpolated via eq. 6.25.

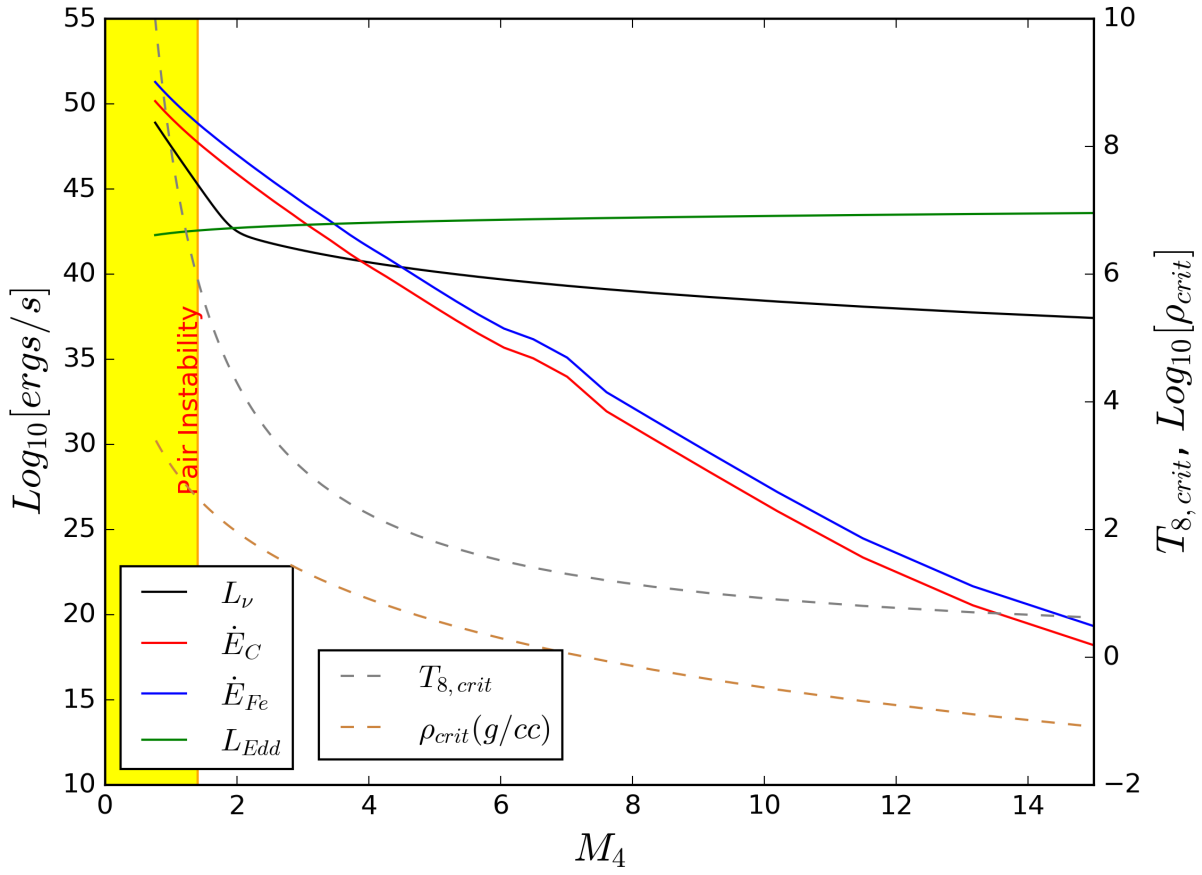

Figure 6.9: Nuclear Energy Generation and Neutrino Luminosity at the GRI.
Various energy generation/loss rates at the GRI (left vertical axis) as a function of stellar mass. $\dot{E}_C$ is the energy generation rate of a star only fusing $3\alpha \longrightarrow {}^{12}C$. $\dot{E}_{Fe}$ is the energy generation rate of a star fusing ${}^4He$ straight to ${}^{56}Fe$. The bump around $M_4 = 7$ is a numerical artifact of the interpolation scheme. Both assume $\mu = \frac{4}{3}$ (mass fraction of ${}^4He = 1$). Neutrino luminosities are calculated using the fits in [67]. The energy generation rate required to support the star against gravity is $L_{Edd} + L\nu$ (green + black) . A SMS with mass $\widetilde{<} 4M_4$, will produce enough energy through triple-α fusion to support the star against gravity. If the star is to explode, it must reach instability before this point, while still being hot enough to fuse ${}^4He$ ($T_8 \widetilde{>} 1 \longrightarrow M_4 \widetilde{<} 9$, see fig. 8.11), and while still containing enough ${}^1H$ for the star to be primarily supported by the CNO process. Note that EPPI boundary is a 'soft' boundary, and that the $L\nu$, $pair \approx L_{Edd}$ is a very good proxy for the location of the EPPI. If temperatures exceed $T_8 \approx 5$, the star won't be able to explode, as most of the energy generated will be lost in neutrinos.

From fig. 6.9, we see that a star with mass above $M_4 \approx 3.5$ will not produce enough energy via the triple-α process to support itself as it reaches the reaches the GRI. Above this mass, for a star to be in equilibrium, it must have some ${}^1H$ fusing to ${}^4He$ either partially or entirely

providing the pressure support against gravity if it is to be in hydrostatic equilibrium. Although a SMS will initially fuse ^1H to ^4He via the proton proton chain, by the time it gets close to the GRI it will be fusing ^1H via the CNO cycle, as only a small amount of heavier elements need to be produced to switch from the proton proton chain to the CNO cycle [55]. The CNO cycle has multiple channels for fusing ^1H, which are composition and temperature dependent. As a result, computing the energy output analytically is difficult. However, for temperatures below $T_8 \approx 2$ (cold CNO), the CN portion of the dominant loop , will account for most of the energy output, and the emissivity can be approximated [55] as:

$$7.4 \times 10^{24} \cdot \frac{\rho X_{^1H}^2}{T_8^{2/3}} \cdot e^{-32.814/T_8^{1/3}} \text{ ergs/g/s} \tag{6.29}$$

If the star has been powered by the CNO cycle for over $\sim 10^4$ years, then eq. 6.29 will be within be within $\sim 10\%$ of the total CNO emissivity [55]. Hence eq. 6.29 is a decent approximation for the cold CNO emissivity near the instability point.

For $T_8 > 2$, the hot CNO cycle will dominate. Coincidentally, for a SMS with $M_4 \approx 5$, the critical temperature will be about $2\,T_8$, right where hot and cold CNO channels are about equal. Hence, around this temperature, the total emissivity will be approximately $2\times$ eq. 6.29. Fig. 6.10 compares the emissivities of CNO vs triple-α at the GRI; where one can see that around $T_8 \approx 2$, even a small amount of hydrogen can result in super-Eddington emissivities.

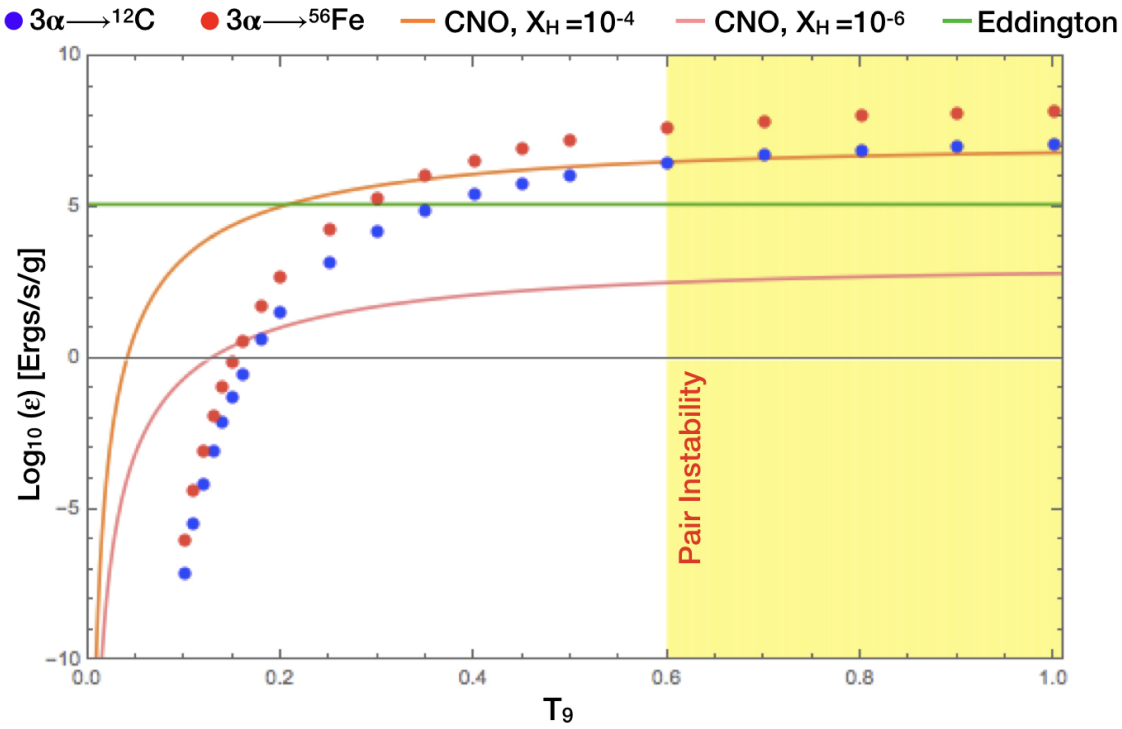

Figure 6.10: Triple-α vs. CNO at the GRI.
Emissivities vs. central temperature at the GRI assuming a ^4He mass fraction of 1. This assumption will not hold for masses less than $\approx 3M_4$ (see fig. 8.11). The CNO emissivity curves are only approximate, and will vary based on temperature, density, and composition. A SMS with $T_{8\,crit} \widetilde{<} 3$ ($M_4 \widetilde{>} 4$) will require $X_{1H} \widetilde{>} 10^{-6}$ to produce enough energy via CNO to support itself (Eddington). Note that for $T_8 \approx 1 \longrightarrow 4$, the triple-α emissivity has a very strong temperature dependence.

Chapter 7

Collapsing Super-Massive Stars

In order to determine the consequences of reaching the GRI, let us consider three regimes: low temperature, intermediate temperature, and high temperature; corresponding to high mass, intermediate mass, and low mass, respectively. The low temperature regime will corresponds to a T_{crit} below which triple-α emissivity is negligible. From fig. 6.10 this corresponds to $T_{8,crit} \lesssim 1$, or $M_4 \gtrsim 9$. The intermediate regime will correspond to where triple-α is highly temperature sensitive, but less than Eddington: $1 \lesssim T_{8,crit} \lesssim 3$, or $3 \lesssim M_4 \lesssim 9$. And the high temperature regime where the star burns triple-α stably at a relatively weaker temperature dependence; corresponding to $T_{8,crit} \gtrsim 3$ or $M_4 \lesssim 3$.

If the star is in the low temperature regime when it goes unstable, energy output will be dominated by CNO burning, and far from igniting significant triple-α. As it collapses, the increase in temperature will have little effect on the energy output, as the CNO cycle has a relatively weak temperature dependence. By the time the temperature has increased enough to ramp up triple-α burning, it will have picked up too much in-falling kinetic energy to overturn the collapse, and will collapse to a black hole.

If the star is in the high temperature regime, it will reach stable triple-α burning prior to the GRI. Consequently, it will fuse ^4He at a more or less fixed temperature until it begins to

run out of fuel, and only then will it continue to contract and heat up. As a result, by the time it reaches the GRI, it will be depleted of ^4He (the fusion rate is proportional to X_α^3). The star will already be struggling just to stay in equilibrium when it reaches the GRI, and as it collapses not only will the triple-α emissivity be weakened by the lack of fuel, but it will also be in a regime of comparably weaker temperature dependence. This will be further compounded by the fact that hitting the GRI at such high temperatures, and further increasing the temperature as the star contracts, will significantly increase the neutrino emissions, as the production of electron positron pairs ramps up. Having run out of ^4He fuel, the next stage in nuclear fusion is carbon fusion, which will become significant only after reaching the EPPI, and so the star will collapse to a black hole.

If the star is in the intermediate regime, then despite being essentially entirely made up of ^4He, it will be entirely or mostly supported by a small amount of hydrogen fusion. A mass fraction of $X_{_1H} \gtrsim 10^{-6}$ is enough support the star via CNO burning (see fig. 6.10). Furthermore, at these temperatures triple-α emissivity will be highly temperature dependent $\left(\sim T^{40} \text{ at } T_8 = 1 \text{ and } \sim T^{18} \text{ at } T_8 = 2\right)$ [55]. In this case, a small increase in temperature will quickly drive triple-α up to Eddington or super-Eddington emissions. All of this energy will go into unbinding the star, as on the one hand, CNO burning will already be producing enough energy to support the star, and on the other hand, neutrino emissions have not become important yet. As long as the initial temperature at collapse, is not too low, then the increased triple-α burning may kick in before the star has picked up too much in-falling kinetic energy, and it may be possible for the star to generate more nuclear energy than in-falling kinetic energy, without neutrino losses, and explode. The estimate on this narrow window is likely too wide, as at $T_8 = 1$ the triple-α rate is still very low; and at $T_8 = 3$ the rate is already approaching Eddington and most of the energy is going into maintaining equilibrium. If this window exists, the exact width can be better estimated via simulations. Note that the explosion found by [44] was for a $M_4 = 5.55,\ T_{8,crit} = 1.7$ star; which is in the middle of this window.

As the star collapses, it will accrue a debt of in-falling kinetic energy which it will have to be overcome, if it is to unbind, the new energy balance equation will be:

$$\Delta E_{nuc} > K.E. + \Delta E_{loss} \tag{7.1}$$

Having discovered a mechanism that may explain the narrow window of exploding SMS's numerous simulations were run using KEPLER to verify if the results of [44] could be replicated.

Chapter 8

KEPLER Simulations

8.1 Overview of KEPLER

KEPLER is a 1-D, implicit, Lagrangian, hydrodynamics stellar evolution code written in Fortran [68]. Despite being a Newtonian code, it has the ability to add 1st order general relativistic corrections to the kinematics and energy calculations [44, 68]. Because it can only deal with small corrections to Newtonian physics, these corrections can only be considered accurate for small metric deviations, $\frac{2m}{r} << 1$ and small velocities, $U << 1$. As $\frac{2m}{r} \longrightarrow 1$ and/or $U \longrightarrow 1$, the results of the code cannot be considered valid. A priori this is not a problem for the purposes of this dissertation, as SMS's are entirely Newtonian in structure (see chapt. 3), and the post-Newtonian correction is only important to determine the instability point. Details of the post-Newtonian correction are discussed in sect. 8.7.

Despite these limitations, KEPLER has the advantage of having a highly detailed network of nuclear processes, both weak and strong, including neutrino losses [44, 68, 69]. This is important, because as was found in chapt. 6, the existence of a narrow window in which a SMS may explode is largely dependent on comparing the nuclear energy generation to the neutrino energy losses. Contributions from electron-positron pair production as well as relativistic and

non-relativistic electrons and positrons, both degenerate and non-degenerate, are also computed by KEPLER [44, 68, 70].

Stars in KEPLER are divided up into a grid of mass zones. Each zone has a list of associated properties such as radius, temperature, density, etc. The equations of motion for the zone velocity, $U = \frac{dr}{dt}$, and the zone internal energy per gram, u, are solved in co-moving coordinates [68] and have the form:

$$\frac{dU}{dt} = -4\pi r^2 \frac{\partial P}{\partial m} - \frac{m}{r^2} + \frac{4\pi}{r}\frac{\partial Q}{\partial m} \tag{8.1}$$

$$\frac{du}{dt} = -4\pi P \frac{\partial}{\partial m}\left(U r^2\right) + 4\pi Q \frac{\partial}{\partial m}\left(\frac{U}{r}\right) - \frac{\partial L}{\partial m} + \varepsilon \tag{8.2}$$

where $r =$ the zone radius, $P =$ the zone pressure, $m =$ the enclosed mass (independent variable), $Q =$ zone dynamic viscosity, $L =$ the luminosity through the zone, and $\varepsilon =$ the zone energy emissivity (energy generation rate per gram). Eqs. 8.1 and 8.2 are solved implicitly by linearizing them in terms of the density, temperature, and luminosity and solving them over incremental time steps, assuming a fixed composition [68]. Changes in composition due to convective mixing and nuclear processes are then solved explicitly using the set of converged quantities [68]. As time evolves, physical processes and kinematics are calculated zone by zone, taking into consideration quantities that flow across zones. Zones can be created and added based on criteria involving thresholds in changes across a given zone or a pair of zones, e.g. if the difference in density across a zone is very large, the zone may be broken up into two zones, while keeping track of conserved quantities. KEPLER also has a range of artificial schemes to mimic processes the require higher spatial dimensions, i.e. rotation, torques, etc. The full nuclear network (ISEnet) was turned on for all simulations.

Initially runs were done to see if the results found by [44] could be reproduced, i.e. the existence of a narrow window around $5.55M_4$ where a SMS would explode. A number of runs

were done, with masses ranging from $1M_4 \longrightarrow 10M_4$. Runs began with primordial nuclear abundances, i.e. zero metallicity above ^4He. An example of a start file is found in A.9. The relevant parameters that were varied were:

Stellar mass

Temperatures and densities in initial grid

Initial nuclear abundances

Number of initial zones

Artificial rotation: 'rigidl'

Strength of the post-Newtonian correction (see eq. 8.8): p358

Nuclear burning networks: 'Approx', 'ISE', 'NSE', 'ISENET'

Time-steps and backups: p6, p7, p8, p9, p55

Rezoning and convergence precisions: p11, p12, p78, p79, p80, p81, p83, p84

Surface boundary pressure: p69

For details on the exact functions of these parameters see [71].

8.2 KEPLER and the Polytrope Profile

The first thing that needed to be verified was whether the polytrope model accurately describes stars in KEPLER. After all, the model is a simplified analytical approximation, and the true profile is determined numerically by KEPLER. While KEPLER initially assumes a polytrope profile, it is not constrained to maintaining it as time evolves. It was also important to verify if the predicted location of the instability point (see chapt. 3) agreed with the results from KEPLER. For the latter let us define, as a function of enclosed mass, m:

$$\gamma(m) \equiv \widetilde{\Gamma}_1(m) - \frac{4}{3} - \delta \cdot \left(\frac{2m}{r}\right) \tag{8.3}$$

(the $-\frac{2m}{r}$ term may or may not be included). δ is a structure dependent term of order unity. In the polytrope model it will vary with radial distance, being equal to 1.124 at the surface of the star, with a max value of 1.935 inside the star (see chapt. 3). As the polytrope is already an approximation, small changes in the value of δ are likely negligible; so in calculating $\gamma(m)$, δ has either been set to 1, when including the GRI, or 0 when ignoring it.

The star is predicted to go unstable when $\gamma < 0$, which should correspond to $\rho_c < \rho_{crit}$; however these two conditions were not met simultaneously in the simulations. The three rows in fig. 8.1, depict an example comparing the polytrope density, temperature, and pressure profiles with those generated by KEPLER at three different stages in the star's evolution: At the start of the simulation, when γ first drops below 0, and some time after collapse has commenced. The polytrope profile matches the KEPLER profiles very well, except in the very outer regions of the star. This is mostly due to the fact that, while the polytrope model has a clearly defined surface for the star (when $\theta = 0$), in actuality, as well as in KEPLER, stars do not have a clearly defined surface. This lack of precise stellar radius, is the cause of some discrepancies between the polytrope model and the simulations, as well as some computational challenges for KEPLER (see sect. 8.3 for more details). This discrepancy is further compounded by the constant β throughout the star assumption breaking down in the outer envelope of the star; which is predicted to be shed with time. As a result, the stellar radius computed by KEPLER tends to be about 10 times larger than that of the polytrope model (although only a very small fraction of the stellar mass is in this very low density region). The temperature profile has the largest discrepancy, because it is also dependent on the mean particle mass, μ, which does change a bit with radius as time evolves in KEPLER, but is also assumed to be constant in the polytrope model.

The majority of the mass, and consequently most important physical processes, however, are concentrated in the inner regions of the star, where KEPLER agrees very well with the

polytrope profile. Despite this general agreement, it is expected that there will be discrepancies between observed and predicted quantities that depend on stellar radius, e.g. the point in the star's evolution where $\gamma = 0$, i.e where $\rho_c = \rho_{crit}$. As a consequence one can see in fig. 8.1 that although the instability is clearly dominated by the GRI, at the surface of the star, the effects of the GRI disappear due to the much larger stellar radius, resulting in $\frac{2M}{R} \approx 0$).

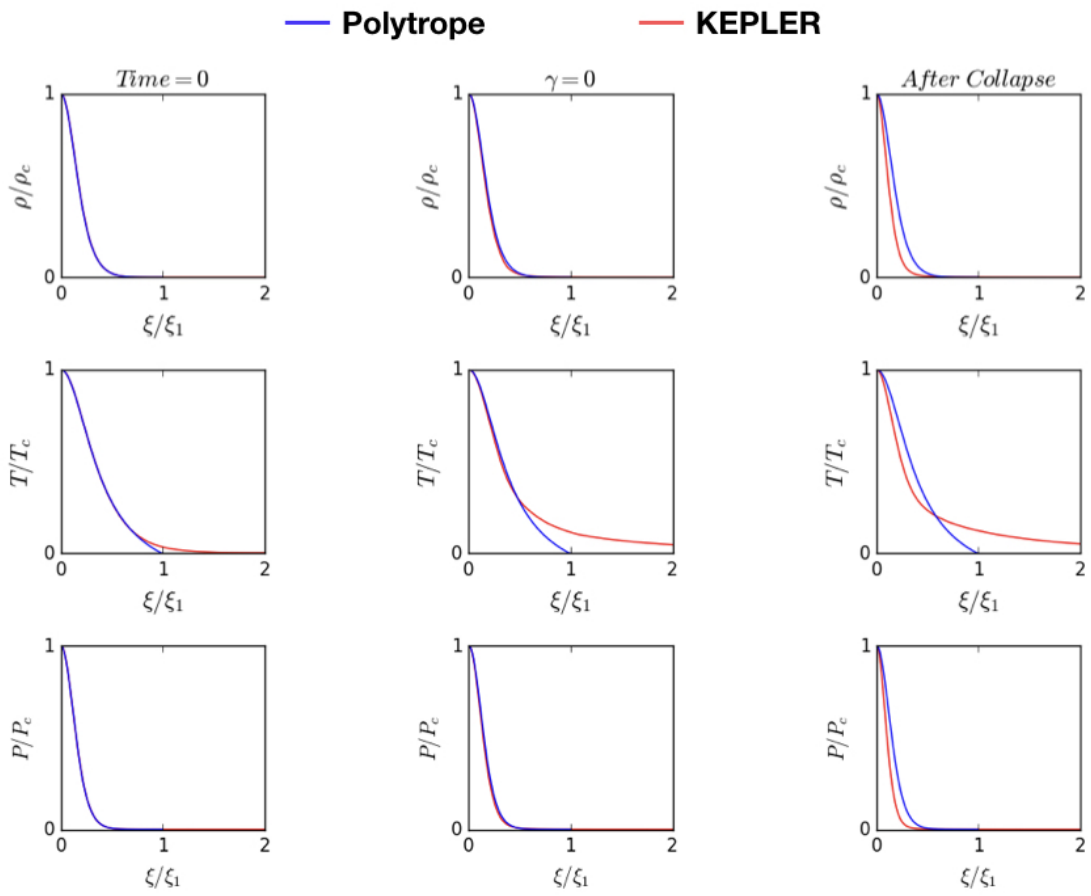

Figure 8.1: Comparison of the Polytrope Model with KEPLER.
Comparison of density, temperature and pressure profiles in KEPLER with the polytrope profile at three different times: initially, at the instability point ($\gamma = 0$), and after collapse has taken place. The polytrope model matches KEPLER closely except in the outer regions of the star, as the stellar radius is over twice as large as predicted by the polytrope model. This discrepancy in the envelope of the star was expected (see sect. 2.1, especially as time evolved. After collapse, the star goes out of hydrostatic equilibrium, deviating from the polytrope profile.

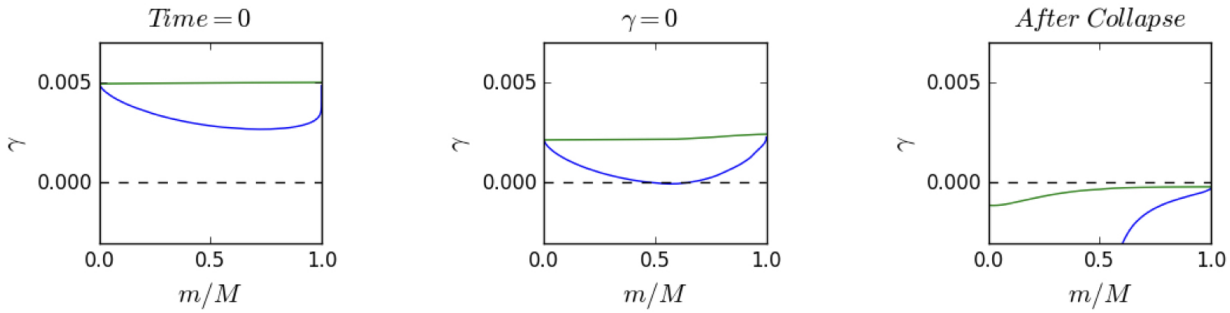

Figure 8.2: Determination of the Location of the GRI
Comparison of γ at three different times: initially, at instability ($\gamma = 0$), and after collapse has taken place. The blue curve includes GR effects, while the green curve doesn't. Due to the extended radius of the star in KEPLER, if γ were calculated only considering the metric deviation at the star's surface, the polytrope model would fail to accurately predict the location of the GRI.

8.3 Stellar Radius Issues

The polytrope model predicts the GRI to occur when $\widetilde{\Gamma}_1 < 1.124\left(\frac{2M}{R}\right)$ (see chapt. 3). However, as can be seen from fig. 8.1, the polytrope stellar radius is considerably smaller than the stellar radius determined by KEPLER. If the dominant cause of instability is the GRI, than large differences in R will cause large differences in the expected ρ_{crit}. As stated in sect. 8.2, the disagreement in stellar radius is caused by the the polytrope profile having a definite radius where $\rho = 0$. In reality though, there is no such radius, and in practice, stellar surfaces are generally defined as the radius of the photosphere, via the Stefan-Boltzmann Law. In KEPLER, the radius is also defined by $\rho = 0$; but zero density is reached more or less asymptotically, unlike in the polytrope profile. On top of the large disagreement in stellar radius, because of the asymptotic nature of the profile, as the density gets very low, numerical precision requirements become more difficult meet. In fact, when the density becomes very low, the very outer regions of the star

will tend to drift out to infinity (particularly for radiation dominated stars), and KEPLER will get caught attempting to find numerical convergence with increasingly smaller iteration steps over increasingly larger radii, and crash (fail to converge within allowable iterations). KEPLER's solution to this is a parameter (p69) that adds a small amount of pressure where $\rho = 0$, and in essence create a little surface tension, to keep the very outer regions of the star bound. One must be careful, however, as cranking this parameter too high will do PdV work on the star, possibly even causing it to collapse; while having it to low may cause KEPLER to crash.

As a result of the much larger stellar radius in KEPLER, $\frac{2M}{R} \longrightarrow 0$, and the criteria for the GRI found in chapt. 3 is not met until well after the collapse. This brought up the problem of determining the criteria for instability in KEPLER. Initially it was guessed that a better measure of instability was to look at the condition:

$$\gamma(r) = \widetilde{\Gamma}_1(r) - \frac{4}{3} - 1.124\left(\frac{2m(r)}{r}\right) <= 0 \tag{8.4}$$

It was guessed that the star would go unstable once $\gamma(r) <= 0$ anywhere in the star, rather than at the surface of the star. However, given that for a $n = 3$ polytrope profile the maximum metric deviation is always inside the star, i.e. $\left[\frac{2m(r)}{r}\right]_{max} \neq \frac{2M}{R}$ (see chapt. 3 and fig. 3.1), if the criteria for instability were in fact $\gamma(r) <= 0$, anywhere inside the star, rather than $\gamma(R) <= 0$, this would have been concluded via the theoretical derivation in the first place. Hence, this guess was made with some skepticism, and proved to not predict the instability point accurately. Instead, accounting for the relationship between the maximum metric deviation and the metric deviation at the surface of the star in the polytrope profile, $\left[\frac{2m(r)}{r}\right]_{max} = 1.935\left(\frac{2M}{R}\right)$ (see chapt. 3), it was found that in practice, a better method for determining the instability point was to use $\frac{1}{1.935} \cdot \left[\frac{2m(r)}{r}\right]_{max}$ instead of $\frac{2M}{R}$ in eq. 8.4, shown in the bottom row of fig. 8.1. This eliminated effects due to large deviations from the polytrope profile in the outer regions of the star. However, it also ignored effects due to changes in mean particle mass in the outer regions of the star. Consequentially, small differences between the predicted critical density, temperature, and energy

using $x_{crit} = \left(\widetilde{\frac{1}{\mu}}\right)$ and $\varepsilon_{crit} = -\left(\widetilde{\frac{1}{\mu}}\right)^2$, respectively (see chapt. 5) were still expected, as the value of $\left(\widetilde{\frac{1}{\mu}}\right)$ was only integrated to the point of maximum metric deviation. This is a small effect, as the outer regions carry progressively lower weights.

8.4 Simulation Results

Various KEPLER simulations were run for masses of M_4 =1.0, 1.5, 2.0, 3.0, 4.0, 5.0, 5.55, 6.0, 7.0, and 10.0. The results, overlaid on the theoretical dimensionless energy (ε vs. x) curves from fig. 5.1 are seen in are seen in figs. 8.3, 8.4, and 8.5. Initially, all masses were given the same start file (A.9), with the initial mass being the only difference. In all cases the star collapsed to a black hole upon going unstable (KEPLER cannot actually track a star down to a blackhole, as it is not a relativistic code, but the result is inferred as infall velocities reached the speed of light). This result disagrees with the findings of [44]. The conditions at the instability point for this set of simulations are summarized in the table in fig. 8.11. It should be noted, that the values in fig. 8.11 are taken from the first output file in which the star has passed the instability point. In actuality the star reached instability some time earlier, and hence the values in the table are likely a bit higher than they were at the true instability point. For masses of 2.0 M_4 and above, the effects of pair production were negligible, and only the GRI was important, which is in agreement with fig. 4.3. Figs. 8.6 - 8.10 show the elemental abundance profile at instability.

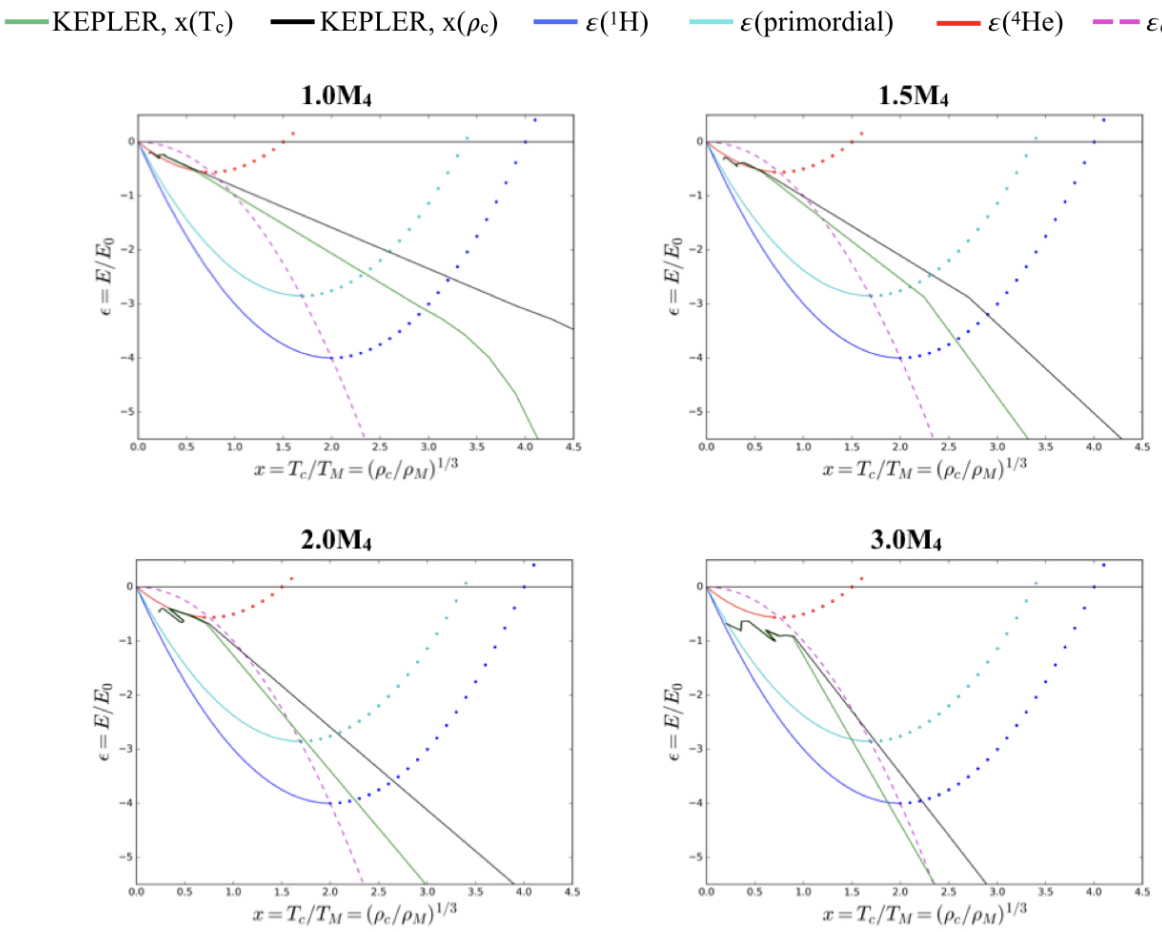

Figure 8.3: Results from KEPLER Simulations (1).
$M_4 = 1-3$. KEPLER simulation results overlaying the polytrope model dimensionless binding energy ($\varepsilon = E/E_0$) vs. dimensionless central temperature and density ($x = T_c/T_M = (\rho_c/\rho_M)^{1/3}$), as defined in chapt. 5. Simulations for all masses resulted in a collapse to a black hole. Despite the agreement of the density and temperature profiles of the polytrope model with KEPLER (fig. 8.1), the binding energies in KEPLER disagree with those predicted by the polytrope model, as all simulations should have started on the 'primordial abundances' curve (cyan). The location of the instability point is predicted by the polytrope model to lie along the dotted magenta line. The solid portions of the parabolic theoretical equilibrium ε curves are stable regimes, while the dotted portions are unstable. The green and black lines are $x(T_c)$ and $x(\rho_c)$ respectively for the KEPLER runs. Their divergence from one another indicates a departure from hydrostatic equilibrium.

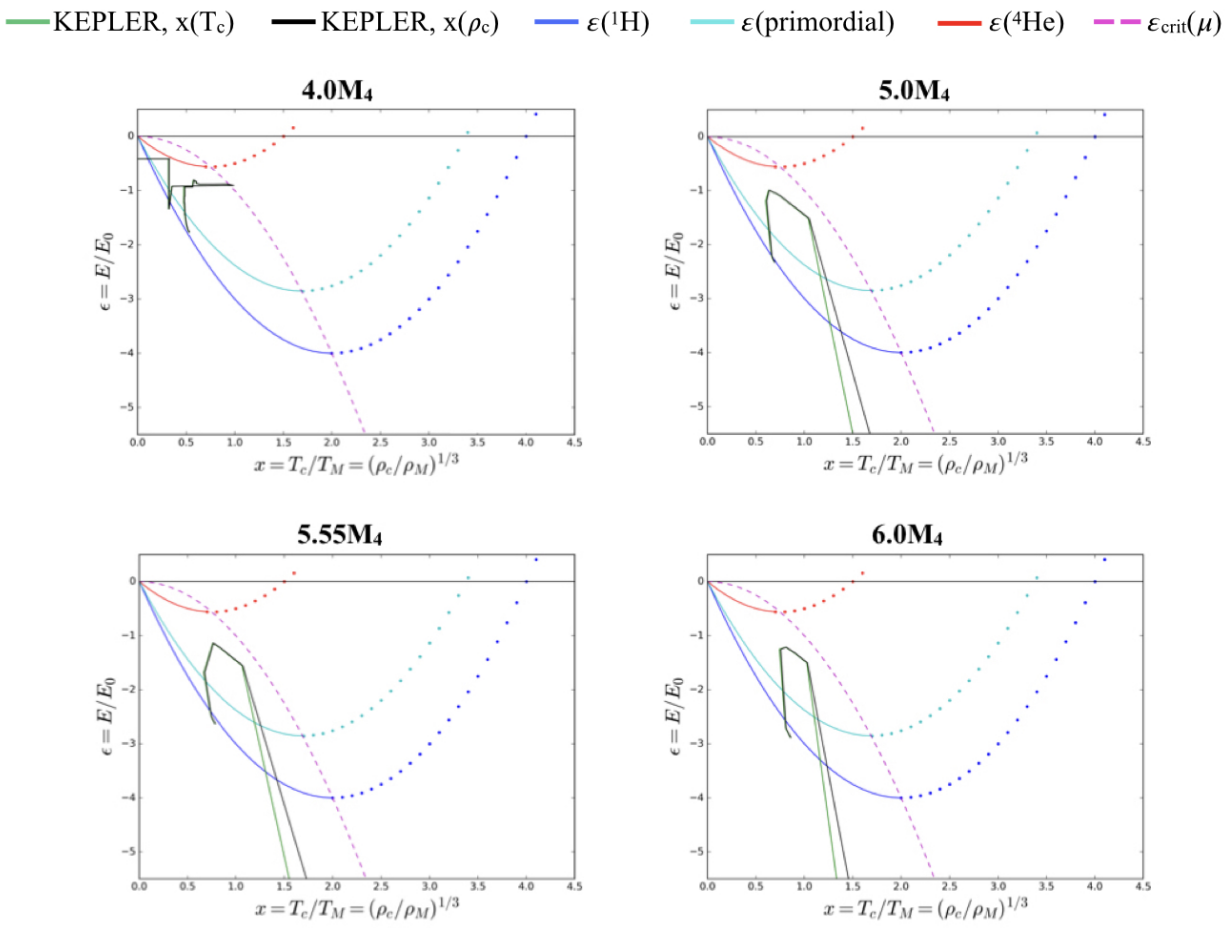

Figure 8.4: Results from KEPLER Simulations (2).
$M_4 = 4-6$. The $4M_4$ simulation (top left) had significant numerical convergence issues; requiring on average about 100 times as many iterations to find convergence as simulations for different stellar masses. After reaching the GRI, the simulation stalled, reducing to time steps of less than 1 second (the life time of the star is about $1M$ years). Despite not being evident in this figure, it nevertheless collapsed, as infall velocities reached of order 1% the speed of light. See fig. 8.3 for a full figure description.

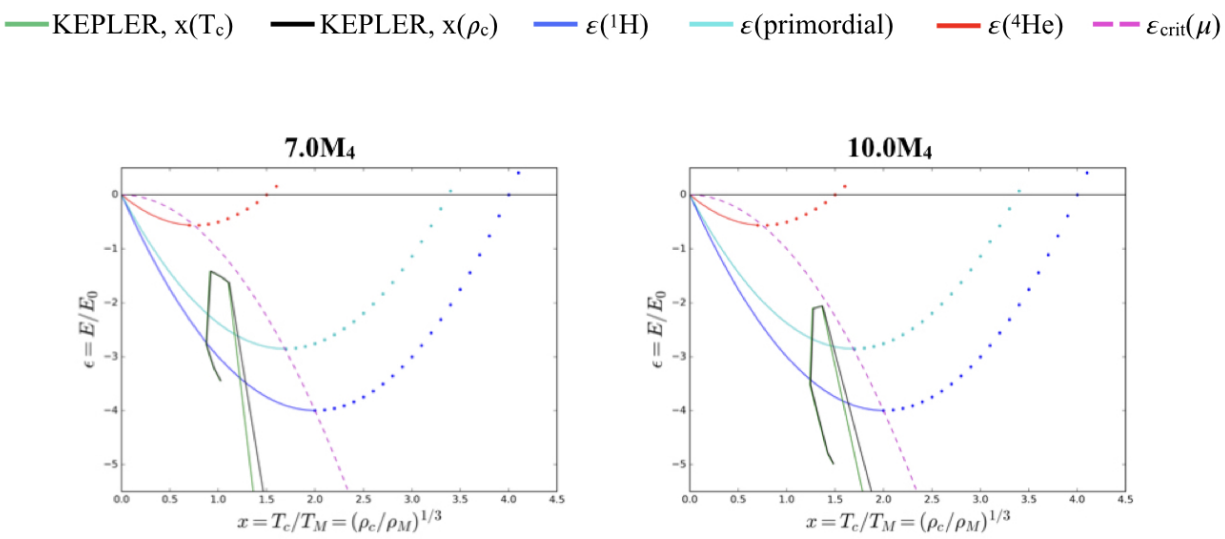

Figure 8.5: Results from KEPLER Simulations (3).
$M_4 = 7$ and 10. Expected binding energies for these larger mass stars differed significantly from the KEPLER results, as the started well below the primordial abundance equilibrium curve (cyan). See fig. 8.3 for a full figure description.

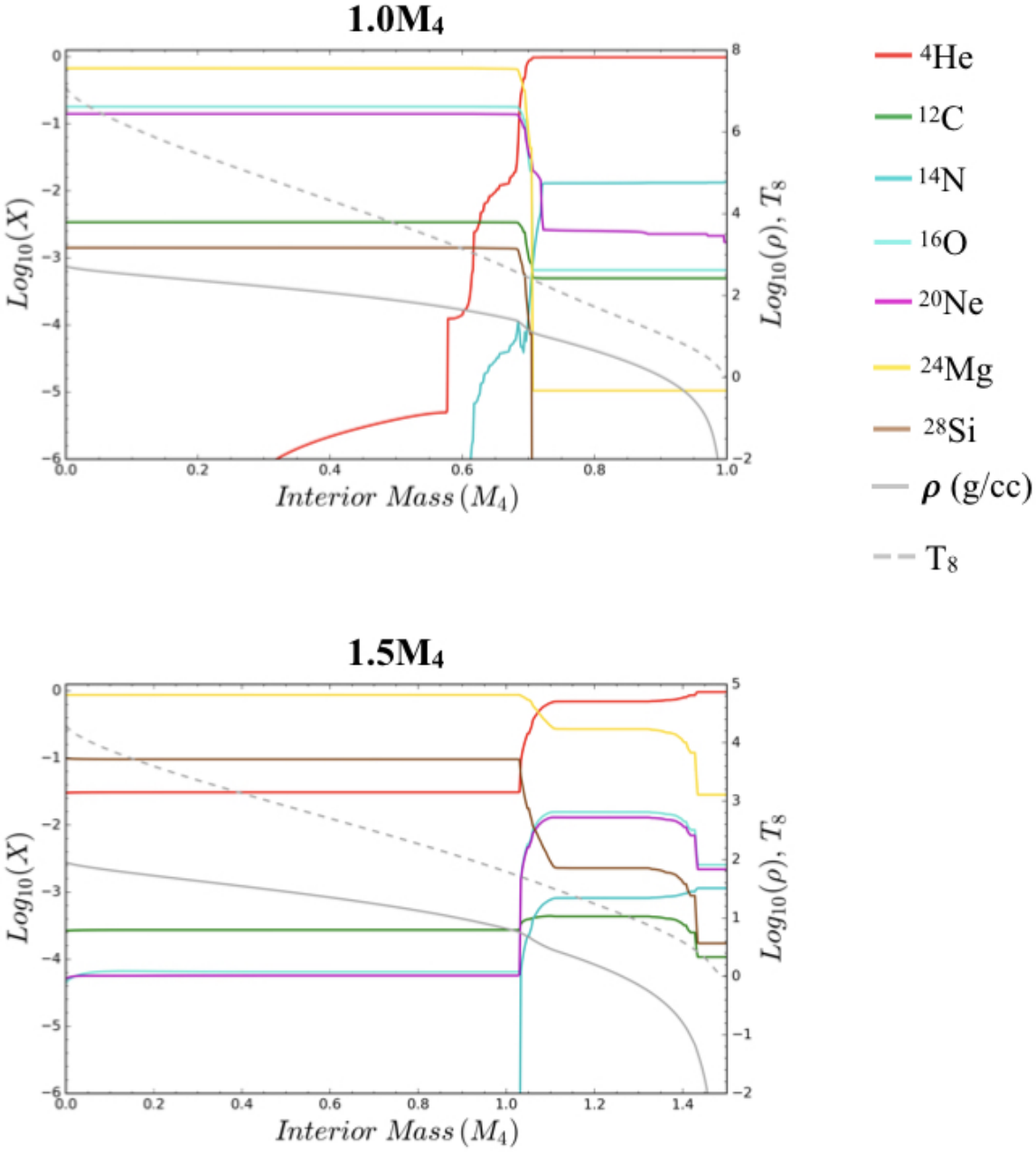

Figure 8.6: Elemental Abundances at Instability (1).
$M_4 = 1$ and 1.5. Elemental abundances by mass fraction, X, (left vertical axis) vs. enclosed mass at the instability point. Corresponding zone temperature and density profiles are plotted on the right vertical axis.

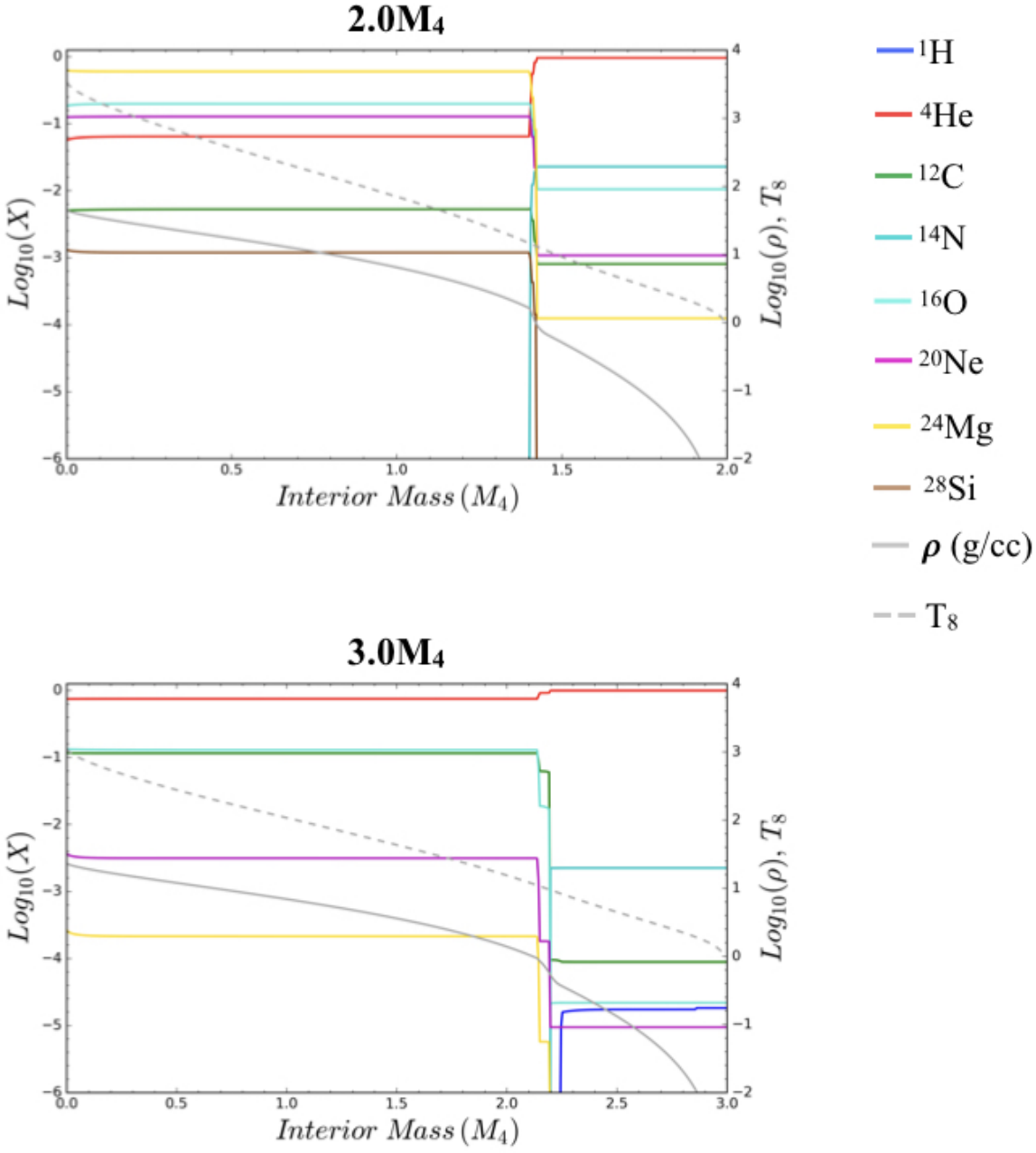

Figure 8.7: Elemental Abundances at Instability (2). $M_4 = 2$ and 3. See fig. 8.6 for a full figure description.

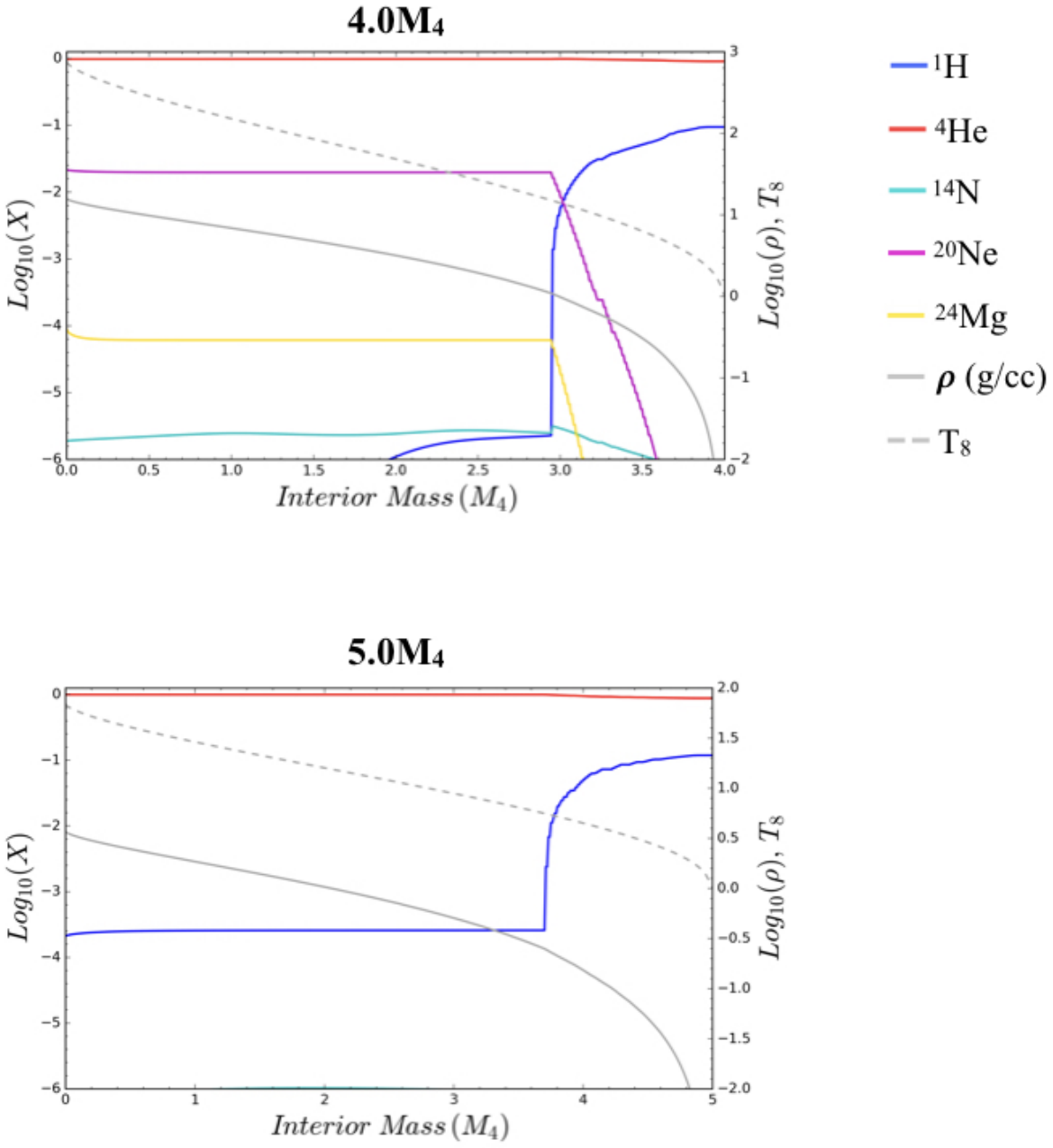

Figure 8.8: Elemental Abundances at Instability (3). $M_4 = 4$ and 5. See fig. 8.6 for a full figure description.

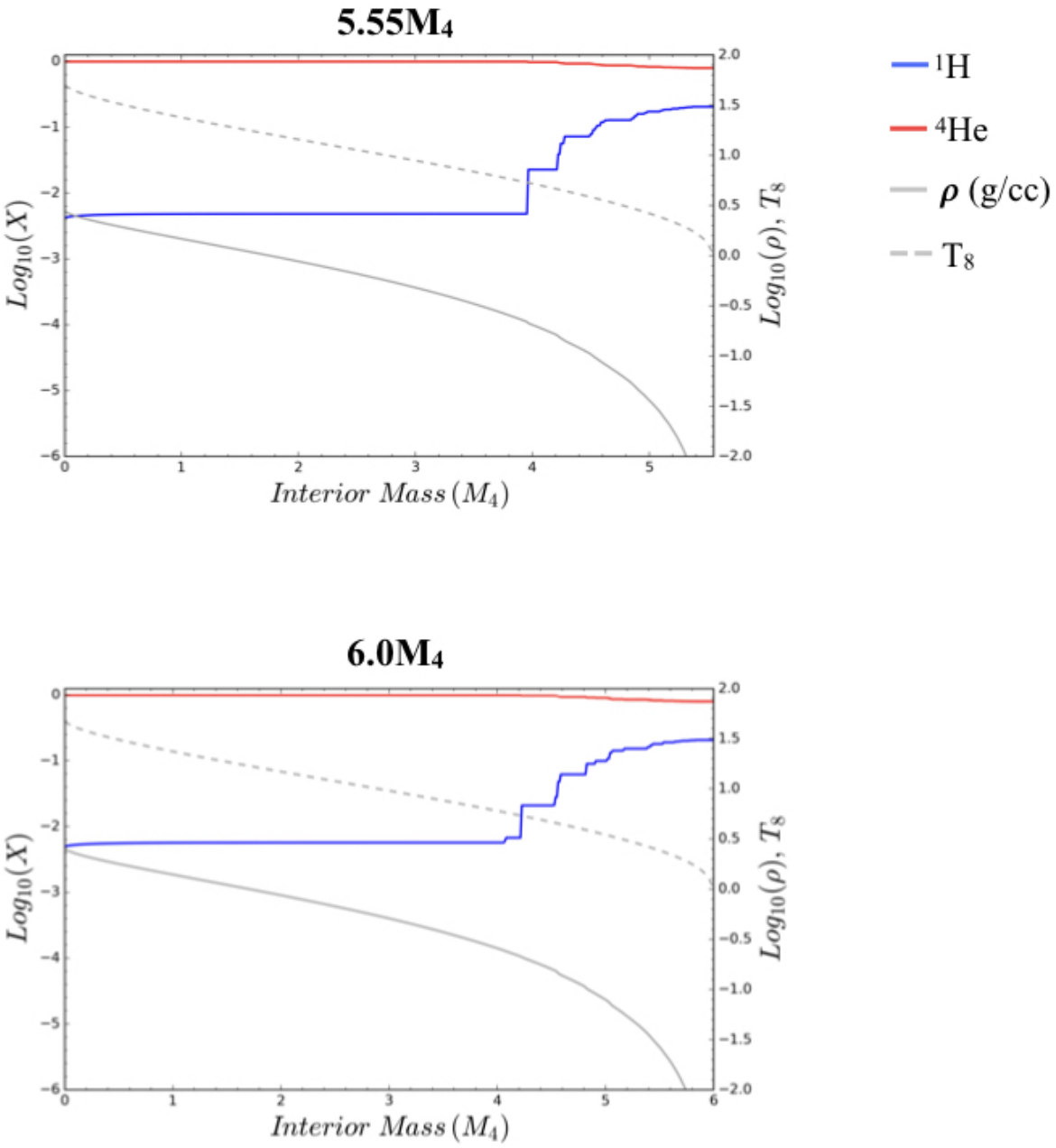

Figure 8.9: Elemental Abundances at Instability (4). $M_4 = 5.55$ and 6. See fig. 8.6 for a full figure description.

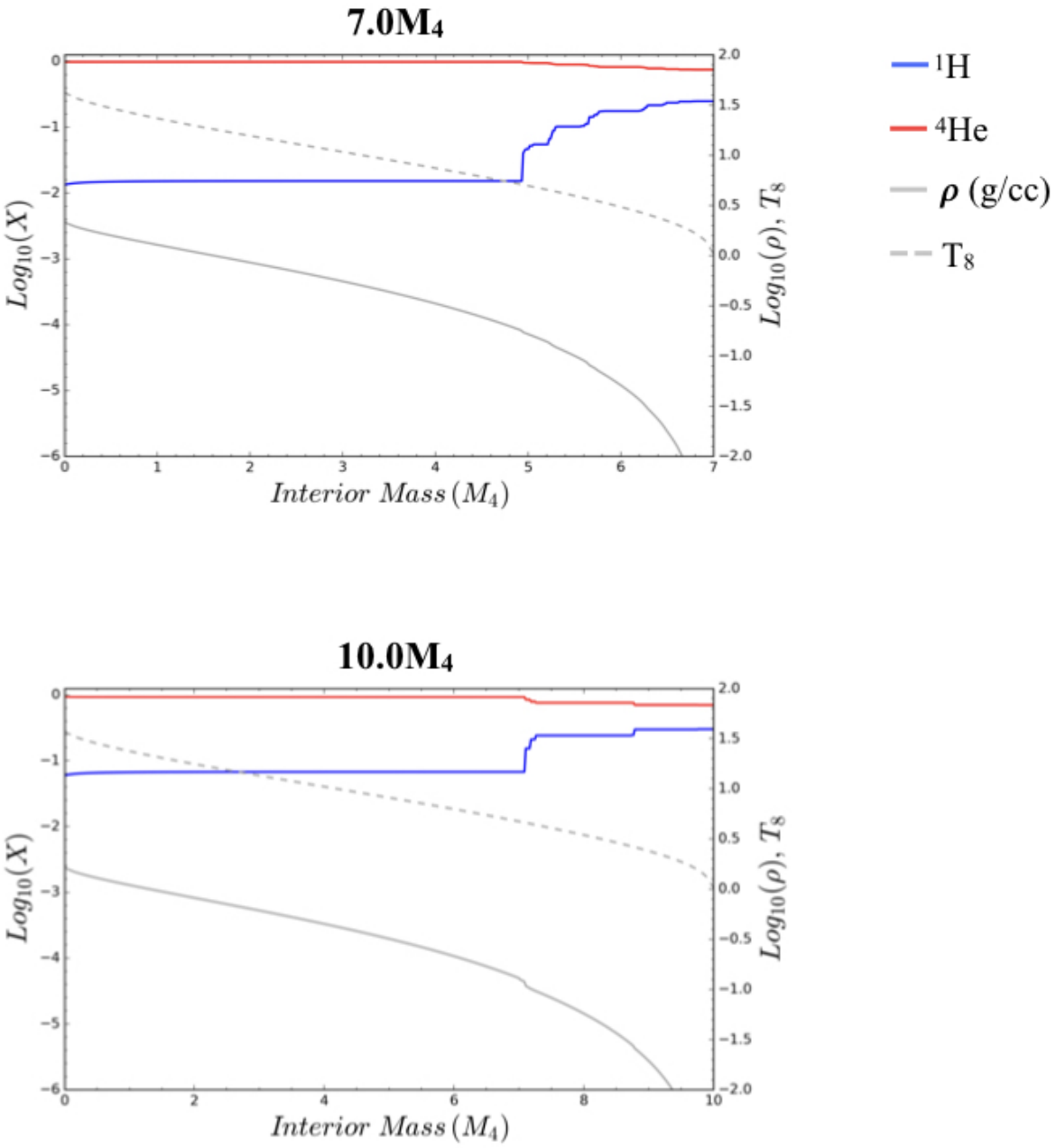

Figure 8.10: Elemental Abundances at Instability (5). $M_4 = 7$ and 10. See fig. 8.6 for a full figure description.

Mass [M_4]	1.0*	1.5	2.0	3.0	4.0**	5.0	5.55	6.0	7.0	10.0
Star's Fate	Black Hole	Black Hole	Black Hole	Black Hole	Black Hole	Black Hole	Black Hole	Black Hole	Black Hole	Black Hole
μ	1.8	1.8	1.8	1.4	1.3	1.3	1.3	1.3	1.3	1.2
$T_{8,\,crit}$ Expected	5.9	4.1	3.2	2.8	2.2	1.8	1.6	1.5	1.3	1.0
$T_{8,\,crit}$ KEPLER	7.1	4.3	3.5	3.0	2.9	1.8	1.7	1.7	1.6	1.6
ρ_{crit} [g/cc] Expected	250	71	30	16	7.1	3.4	2.5	1.9	1.2	0.4
ρ_{crit} [g/cc] KEPLER	520	91	45	23	16	3.7	2.8	2.5	2.2	1.7
γ	-5.6×10^{-5}	-2.8×10^{-5}	-3.4×10^{-5}	-7.2×10^{-5}	-7.3×10^{-4}	-7.0×10^{-6}	-3.1×10^{-5}	-1.6×10^{-4}	-4.1×10^{-4}	-9.3×10^{-4}
Dominant Instability Mechanism	EPPI & GRI	EPPI & GRI	GRI	GRI	GRI	GRI	GRI	GRI	GRI	GRI

Figure 8.11: Location of Instability in KEPLER Simulations.
Expected and observed quantities at the instability point for various stellar masses. Expected values are calculated using the, μ's (mean particle mass) found by KEPLER at the critical point. Effects of the EPPI are estimated using the low temperature electron-positron creation approximation (eq. 4.14). Observed (KEPLER) quantities are taken from the first output file with $\gamma < 0$ (see eq. 8.4 and sect. 8.3). Hence the observed values are slightly more elevated than right at the instability point, when $\gamma = 0$.
$*$The large discrepancies between expected and KEPLER values for the $1M_4$ case, are likely due to the low temperature pair creation approximation no longer being accurate.
$**$The $4M_4$ simulation had convergence issues, and is likely not reliable. This may explain the large discrepancy between expected and KEPLER results for ρ_{crit}.

As seen in fig. 8.11, that all masses collapsed to a black hole. As a result, various modifications to the $5.55M_4$ start file were made in an attempt to make the SMS explode. It was

found that a $5.55 M_4$ could be made to explode, but only if the number of zones was increased (form 1080 to 1200) and the convergence precisions were slightly lowered (fig. 8.12). The star did not explode if only one of these was changed. This suggested that the explosion was possibly not real, but rather due to numerical inaccuracies in energy conservation and zoning. Stars with artificial rotation were also simulated, but this did not result in any significant differences in the outcome, and all simulations resulted in collapse rather than explosion. This was true even when the rotation was set high enough so that centrifugal forces exceed gravitation, strongly suggesting that the 1-D rotational 'fudge' in KEPLER (parameter 'rigidl') is only reliable for low angular momentum ($\frac{L^2}{MR^2} << \frac{M^2}{R}$).

Despite the explosion being likely due to numerics, it does provide important information regarding the yield of heavy elements that would have been injected into a universe of primordial elemental abundance, were such explosion to have occurred. An explosion of this type would look considerably different from other forms of exploding stars/supernovae. Most notably, from the nucleosynthetic signature. Almost no elements above ^{28}Si were synthesized, as the nucleosynthesis was drastically halted at ^{28}Si. There were no Fe peak or r-process elements. Apart from $4He$ (the bulk of the material), the most abundant metal in the yield was ^{24}Mg. There was also no carbon burning, as temperatures never reached much higher than T_9 of 1. This is considerably different from the yields of, say, a type II supernova [72–74]or a pair instability supernovae [45, 46, 75, 76], which both have r-process elements as well as containing large amounts of first peak metals e.g. Fe, Co, Ni . Furthermore, these supernova contain little ^4He, as the progenitor cores are largely C and O [45, 46, 72–76]. The yield was consistent with the yield resulting from the exploding SMS in [44]. A table of the yield abundances is found in fig. 8.13.

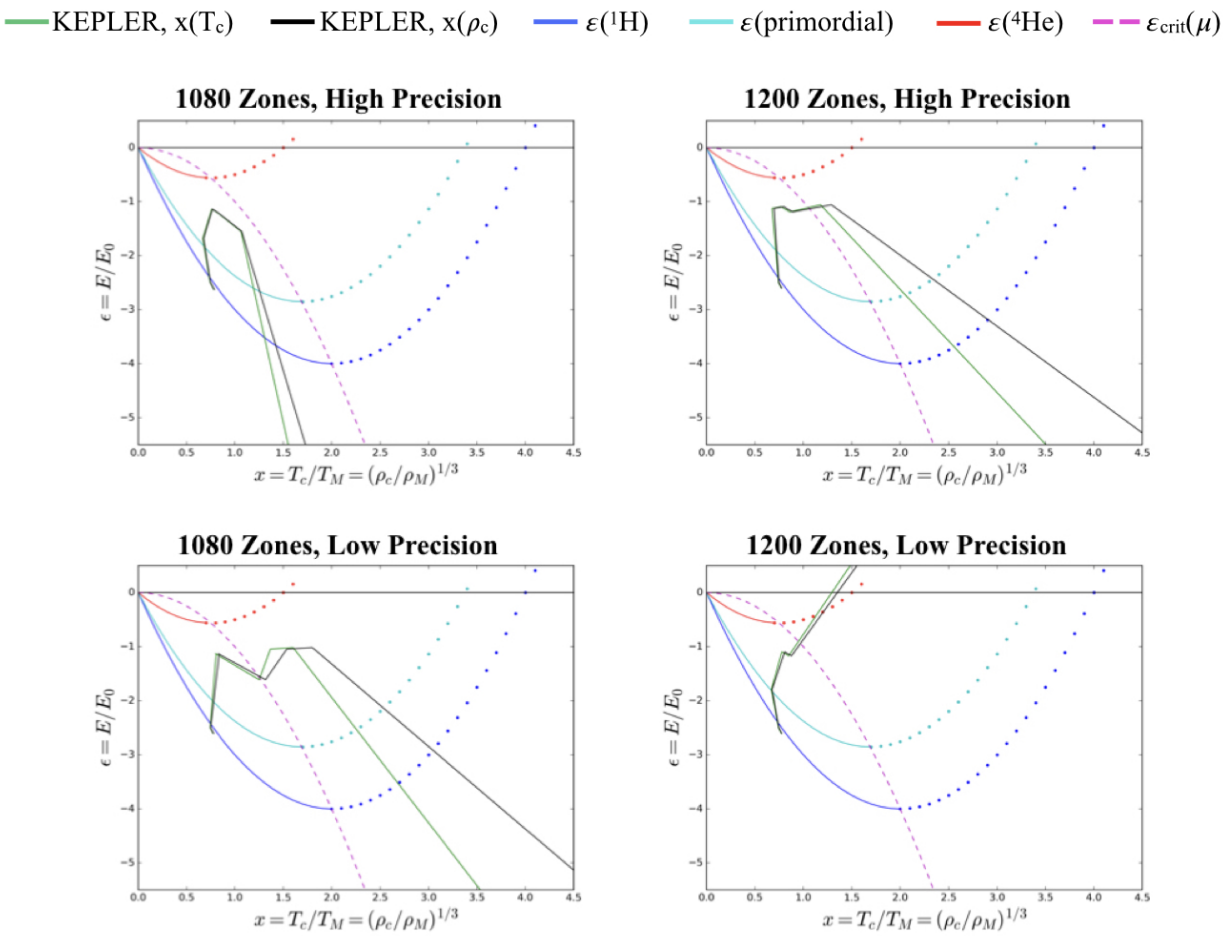

Figure 8.12: Numerical Effects in KEPLER.
KEPLER simulation results when adjusting numerical factors: number of zones and numerical convergence tolerance. Higher precision tolerance: $< 10^{-7}$. Low precision tolerance: $< 10^{-6}$. All four simulations are for a $5.55 M_4$ SMS. Explosion only occurred with both increased number of zones and reduced numerical precisions (bottom right).

Mass	^{1}H	^{4}He	^{12}C	^{16}O	^{20}Ne	^{24}Mg	^{28}Si	^{32}S
$M_\odot$	3,879	28,537	920	6,285	4,605	9,740	1,532	1
%	6.989	51.418	1.658	11.324	8.298	17.550	2.760	0.002

Figure 8.13: Elemental Yield form Exploding SMS
Elemental yield from a $5.55M_4$ exploding super-massive star, simulated in KEPLER

After numerous trials with varying parameters, it was not possible to reproduce the results found by [44]. That is, it was not possible to simulate a star of order $\sim 5M_4$ that resulted in an explosion after reaching the GRI, unless numerical tolerances in energy conservation were relaxed, combined with increasing the number of zones. This strongly suggest that an explosion is a result of numerical artifacts, rather than real physical processes. It also points to these stars being on a knife edge between collapsing and exploding, as small numerical inaccuracies can tip the scale from one outcome to the other. Furthermore, KEPLER struggled to find convergence near the instability point, and would often exceed the number of numerical iterations allowed in the setup, and terminate; further suggesting numerical difficulties around the GRI. It remains possible that there were relevant differences in parameters and processes used by [44], that were overlooked in the present simulations. Unfortunately, [44] did not give a start file or a sufficiently detailed description of their initial setup, to confidently compare to their simulations.

Nevertheless, having derived a possible theoretical mechanism for an explosion in the same mass range, as [44], it is at least possible to compare the physics in KEPLER to the theory. Investigating the energetics on KEPLER revealed a number of issues involving energy calcula-

tions, most notably in the calculation of the binding energy of the star.

8.5 Triple-α Networks in KEPLER

KEPLER has multiple methods for calculating triple-α rates [71]. The main subroutine is based on experimental rates from [66] (also used in this dissertation), plus updates from [77]. However, the subroutine combines the experimental rates with a number of possible theoretical rates and fits from various papers [71, 78–80], depending the value of the corresponding parameter set in the start file (p 484). This parameter can also be used to change the overall strengths of the rates by some factor in the default network. As a result, the explosion found by [44] may be due to them having used a different triple-α network, or modifying the default strengths. In this dissertation, only the default network was used.

8.6 Disagreement of the Total Binding Energy

When comparing the total binding energies calculated by KEPLER, it was found they that did not agree with the theoretical relationship between binding energy and central density or temperature predicted by the polytrope model in chapt. 3. In figs. 8.3 - 8.5, all SMS's should have started somewhere along the solid cyan curve ($\mu =$ primordial abundances). In some cases the binding energy was below the lowest allowed equilibrium binding energy of $-\frac{E_0}{\mu^2}$ (vertex of curve for a given μ). This is despite a good agreement with all other quantities at the GRI (μ, T_{crit}, ρ_{crit}), as well as with the polytrope profile throughout the star's evolution.

KEPLER computes the total energy in two different ways: by summing up the thermal, gravitational, and kinetic energy of each zone, and by adding/subtracting the energy created/lost

through thermonuclear and neutrino processes in each zone [11, 68, 71]. These two energies do not generally agree in KEPLER (although they should in theory), and also progressively diverge as time evolves. The magnitude of these differences are small (around a factor of 2-5), and in most circumstances are irrelevant to the results of the simulation. However, in this case, when dealing with a star that is not only teetering on instability, but who's energy generation rates are on a knife edge between being sufficient to cause an explosion versus collapse; even small inaccuracies in the energy budget are relevant to the fate of the star.

The simplest explanation for these discrepancies is that the star cannot in fact be modeled by a $n = 3$ polytrope. Comparing the density/temperature profiles of KEPLER runs to the polytrope model, however, reveals a very close match between the two (fig. 8.1). Only in the very outer regions of the star deviate from the model. This small amount of mass in the outer regions of the star is not important, as the bulk of the mass and important physics are concentrated in the core, as already discussed in sect. 8.3

8.7 Discrepancies in the General Relativistic Correction

As mentioned, KEPLER has a parameter that includes a general relativistic correction to the kinematics equations [11, 44, 68, 71]. The correction is adapted from the Tolman-Oppenheimer-Volkoff (TOV) equation (eq. 8.5) [81, 82], which is the general relativistic analog in a spherically symmetric geometry (while assuming a perfect fluid), to the Newtonian condition for hydrostatic equilibrium. While the modifications in KEPLER are simply first order correction to Newtonian gravity, the TOV equation (8.5) is fully general relativistic.

$$\frac{dP(r)}{dr} = -\frac{m(r)\rho(r)}{r^2} \longrightarrow \frac{dP(r)}{dr} = -\frac{m(r)\rho(r)}{r^2} \cdot \left[\frac{\left(1+\frac{P(r)}{\rho(r)}\right)\left(1+\frac{3P(r)}{\bar{\rho}(r)}\right)}{1-\frac{2m(r)}{r}} \right] \tag{8.5}$$

where ρ = the total energy density, excluding curvature, i.e $\rho = \rho_x(1+u)$. If this parameter is flagged, then the KEPLER multiplies the gravitational acceleration and gravitational potential energy by a simplified version of the factor in eq. 8.5:

$$\Delta v = -\frac{m(r)}{r^2}\Delta t \longrightarrow \Delta v = -\frac{m(r)}{r^2}\Delta t \cdot (\text{strength factor}) \cdot \left[\frac{\left(1+\frac{P(r)}{\rho_x(r)}+\frac{3P(r)}{\overline{\rho}_x(r)}\right)}{1-\frac{2m(r)}{r}}\right] \tag{8.6}$$

$$\Delta E_{grav} = -\frac{m(r)}{r}\Delta m \longrightarrow \Delta E_{grav} = \frac{m(r)}{r}\Delta m \cdot (\text{strength factor}) \cdot \left[\frac{\left(1+\frac{P(r)}{\rho_x(r)}+\frac{3P(r)}{\overline{\rho}_x(r)}\right)}{1-\frac{2m(r)}{r}}\right] \tag{8.7}$$

where the 'strength factor' is a float that can be adjusted to increase or decrease the magnitude of the gravitational force (default is 1).

For radiation dominated matter, the internal energy per gram is $u = \frac{3P}{\rho_x}$; which can be substituted into eq. 8.7 to get:

$$\Delta E_{KEPLER} = \sum\left\{\frac{m(r)}{r}\Delta m \cdot (\text{strength factor}) \cdot \left[\frac{\left(1+\frac{u}{r}+\frac{4\pi\rho_x u r^3}{3m(r)}\right)}{1-\frac{2m(r)}{r}}\right]\right\} \tag{8.8}$$

which, in the differential limit is not equal (but close) to ΔE_{GR} (eq. A.9).

It should also be noted that when considering relativistic effects, there is a distinction between rest mass and total mass energy that doesn't exist in a purely Newtonian regime. For the most part, KEPLER deals with this by treating all mass quantities as rest-mass. But not in all cases. The acceleration due to gravity (eq. 8.6), should depend on total mass energy, not just rest-mass. As a result the accelerations due to gravity computed by KEPLER when the general relativistic correction is flagged are slightly larger than they should be, by a factor of $\frac{m_x(r)}{m(r)} \approx 1 - \frac{E_{bind}(r)}{m_x(r)}$ (recall $E_{bind} < 0$). Again, these are small discrepancies which are not likely to be relevant in most cases, but may matter in special situations, where the fate of the star is sensitive to the precise value of the energy.

Finally, this discussion of discrepancies in energy calculations may in fact be a moot point. Before worrying about the proper post newtonian expansion, we must determine what is the correct definition of energy in GR (if there even exist such a thing). In GR, the definition of energy is not clear. Conserved quantities in GR require the existence of a symmetry, which may or may not have a Newtonian analog. Furthermore, Newtonian quantities may have multiple GR analogs, resulting in an ambiguity in how they are to be extended into GR. A deeper look into this subject is found in appendix A.2.

Chapter 9

A Final Look at In-Falling Energetics

Having failed to produce an exploding SMS around helium ignition, a final comparison of the in-falling energetics to the increased nuclear fusion as the temperature and density rise, can be done to get an idea if overcoming in-falling kinetic energy via increased triple-α is a possibility. To do so we can make a toy model of the collapse, by assuming that due to there being some pressure resisting the collapse, the star collapses at some fraction, f, of the free-fall rate, i.e. the net acceleration is: $a = -f \cdot \frac{M}{R^2}$, where f ranges from $0-1$. This yields:

$$E_{kin} \approx f \cdot \left(\frac{M^2}{R} - \frac{M^2}{R_{crit}} \right) \tag{9.1}$$

Using eqs. 2.8 and 2.20, and ignoring deviations from the polytrope profile during the collapse, we find:

$$E_{kin} \approx f \cdot 10^{54} M_4^{3/2} \cdot (T_8 - T_{8,crit}) \ ergs \tag{9.2}$$

Fig. 9.1 shows the ratio of the energy loss (in-falling kinetic energy + neutrino losses + change in binding energy) to the nuclear energy gain generated by triple-α + CNO. The star initially picks up a debt of in-falling kinetic energy; but as the temperature rises and the energy

produced ramps up, it rapidly catches up until the temperature has risen enough for pair-neutrino production to take over. At this point, a significant fraction the nuclear energy produced is dumped into the neutrinos and lost, and a black hole will eventually form. The ratio of the losses to the gains reaches a minimum somewhere around $T_9 \approx 1.5$, before neutrino losses take over. If the star collapses in complete free-fall, the net energy produced maxes out at about $\sim 1\%$ of the net energy loss. However, if the star collapses at less than $\sim 1\%$ the free-fall rate, there will be a point where the net energy of the star is positive, and it will unbind, likely via an explosion. It should be noted that there are other nuclear fusion channels, as the nuclear matter moves towards NSE, that will also dump energy into the star. They are not accounted for in this simplified calculation, as they are secondary energy sources, an would only be relevant to the energy budget if the star could approach sufficient energy levels to explode via triple-α alone.

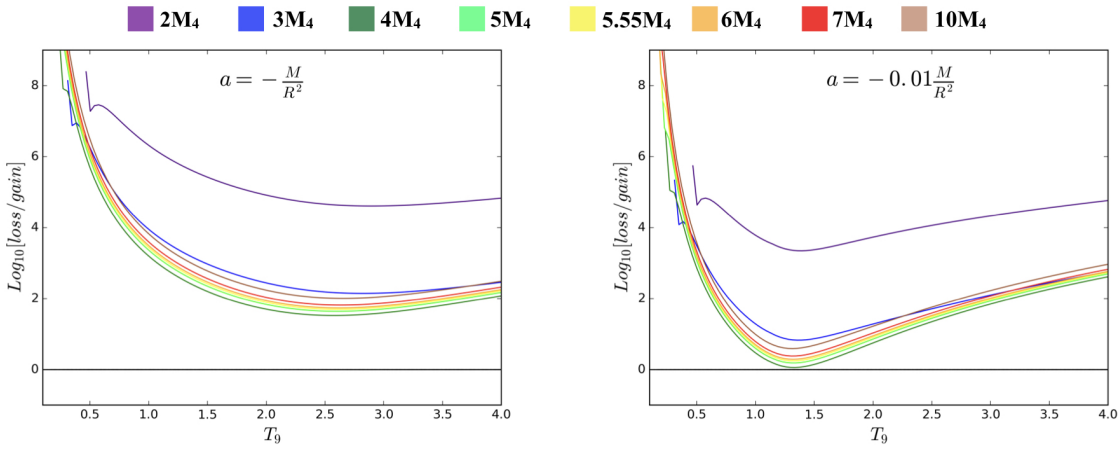

Figure 9.1: Energy Loss/Gain During Collapse.
Comparison of net energy lost and gained throughout the entire star for two cases: free-fall collapse (left) and 1% of free-fall collapse. For masses around $\sim 4M_4 - 7M_4$, if the net in-falling accelerations are less than 1% free-fall, the net energy gained through fusion may be enough to unbind the star, prior to neutrino losses taking over.

Fig. 9.1 should be interpreted as a coarse grained and qualitative result, as it only looks at the net energy produced/lost of the star as a whole, and does not consider regional effects inside

the star. In actuality, the nuclear energy produced would be concentrated at the star's center. If it were to rapidly expand, it would shock into in-falling material from the outer regions of the star. In order to truly get the energetics correct, a precise accounting of the energetics and kinematics must be done, as these stars are on a knife edge between exploding and collapsing. This would require using a stellar simulation code with a sophisticated nuclear network, such as KEPLER. A Newtonian code with and accurate post-Newtonian correction should be good enough to calculate the energies, as the kinematics are entirely Newtonian, with the exception of the location of the GRI. However, hydrodynamic calculations in 1-D, or even 2-D, do not necessarily translate to 3-D; and hence in order to have confidence in the results, a 3-D code is recommended.

Chapter 10

Conclusion

The objective of this dissertation was to investigate the effects of changes in the mean particle mass on the GRI, and determine if there is a theoretical basis for the existence of a narrow mass range of SMS's around $5M_4$ to explode as a result of reaching the GRI at the onset triple-α fusion. Additionally, it was a secondary objective to test, using the KEPLER stellar evolution code, if such an explosion, as found by [44], could be reproduced.

Along the way, arose the problem of defining the binding energy of a star in GR. It was found that the general relativistic definition of a star's binding energy is ambiguous. It was found that integrating the time-component of the 4-momentum of each differential rest-mass over the entire star, is the closest analog to the Newtonian energy. However, this approach failed when using the TOV equation, possibly due to the perfect fluid assumption of the stress-energy tensor not holding for stellar matter. The conventional definition of taking a time slice and integrating the rest-mass over a curved manifold is equivalent, but only for a spherically symmetric space-time geometry.

It was not possible to produce a SMS that resulted in an explosion, except when adjusting the number of mass zones and lowering the numerical precision. This strongly suggests that the results in [44] are due to numerical factors. However, it also points to the fact that these stars are

on a knife edge regime between exploding and collapsing, as small numerical changes can have significant effects on the outcome. It was also found that while the polytrope profile accurately matches the KEPLER results, the predicted corresponding binding energies of the stars do not. While unimportant in most cases, in a regime where outcomes are so sensitive to the energy, these discrepancies are relevant, and an accurate accounting of the energetics is paramount. It is also possible that differences between the current results and those of [44], may also have been due to relevant differences in the processes flagged in KEPLER.

Despite failing to reproduce the explosion in [44], it was found, on a theoretical basis, that the most likely regime for an explosion, was for a star to go unstable as it transitioned form CNO to -triple-α, i.e. while leaving the main sequence. In this regime the triple-α emissivity is highly temperature sensitive, but starts off relatively low. As a result, if the star goes unstable at too low a temperate (higher mass), even a very large increase in triple-α emissivity may not amount to large net amount of energy, and by the time the energy generation is significant, the debt of in-falling kinetic energy is large. The result is that it will take longer for the energy generated to turn the collapse around, and by that time the temperature will be sufficiently high for pair-neutrinos to take over, and the star will collapse to a black hole. On the other hand, if the initial temperature at the GRI is a bit higher (lower mass), the boost in energy may release enough nuclear energy, combined with remaining CNO burning, to unbind the star before it picks up too much in-falling kinetic energy, and before losses from pair-neutrinos kick in. At this point an explosion would be possible, but only if the net in-falling accelerations are less than about 1% free-fall. However, if the star reaches stable helium burning before the GRI, it will stop contracting until it starts running out helium fuel. In this case, there will be no ^1H left to help generate energy, and the increased triple-α rate as the temperatures rises will not only be suppressed by a factor of X_α^3, but the GRI will occur very close to the EPPI, and neutrino losses will take over very quickly, resulting in a collapse to a black hole. An (wide) estimate on the mass range for which an explosion may be possible is $3 \lesssim M_4 \lesssim 7$, corresponding to critical central

temperatures and densities of $1 \lesssim T_{8,crit} \lesssim 3$ and $1.0 \lesssim \rho_{crit} \lesssim 20$ g/cc.

In order to definitively determine if an explosion is possible, and for what mass range, it is recommended that high precision simulations be done using a hydrodynamic stellar evolution code containing the following: A) a 3-dimensional grid, B) a detailed nuclear fusion network (including neutrinos), and C) an accurate post-Newtonian correction. High precision is required as these stars are energetically on the edge between collapsing and unbinding. A 3-D code is recommended as 1-D and 2-D hydrodynamic results do not necessarily translate to 3-D. Furthermore, circulatory effects, such as turbulence, convection, torques, magnetic effects, etc. can be more reliably modeled in 3-D. In order to get the energetics right, a detailed accounting of nuclear processes is also needed, particularly prior to collapse, as this will determine the location of the GRI via the mean particle mass, the abundances of relevant nuclei, particularly ^{1}H, CNO catalysts, and ^{4}He. A fully general relativistic code is probably not necessary, as the structure and kinematics of SMS's are entirely Newtonian. Only the energy of the star and the location of the GRI require knowledge of general relativistic corrections, as the Newtonian energy is zero.

There are three possible observable signals resulting from an exploding SMS. In theory the photon luminosity could be observed, but at such high red shift it would be unlikely to be detected. If the star were to explode anisotropically, it may be accompanied by a large anisotropic neutrino burst, which could result in measurable gravitational wave signal. Finally, the explosion would results in an injection of heavy elements (mainly ^{4}He, ^{24}Mg, ^{16}O, ^{20}Ne, and ^{28}Si) into a background of primordial elemental abundances, during the epoch of early galaxy formation.

Chapter A

Appendix

A.1 General Relativistic Correction to the Binding Energy

This derivation is adapted from chapter 6.9 in [60]. The General Relativistic gravitational binding energy is defined as:

$$E = M - Nm_b = M - \int \frac{dm}{\sqrt{1-2m(r)/r}} \tag{A.1}$$

Where $N =$ the number of baryons. That is, $Nm_b = M_x =$ the baryonic rest-mass in flat (Minkowski) space at zero temperature. It is convenient to rewrite eq. A.1 in terms of the $m_b dN = \rho_x dV_x = \rho_x \frac{4\pi r^2 dr}{\sqrt{1-2m(r)/r}}$, since this quantity is an invariant. The x-subscripts indicate proper quantities. This gives:

$$E = \int_0^R \left[\rho \sqrt{1 - \frac{2m(r)}{r}} - \rho_x \right] dV_x \tag{A.2}$$

Here $\rho = \rho_x(1+u)$. Expanding to 2$^{\text{nd}}$ order in $\frac{m}{r}$ and u gives:

$$E = \int_0^R \rho_x \left[u - \frac{m}{r} - u\frac{m}{r} - \frac{1}{2}\left(\frac{m}{r}\right)^2 \right] dV_x \tag{A.3}$$

The Newtonian energy is: $E_{Newt} = \int_0^R \rho_x u dV_x - \int_0^M \frac{m_x}{r_x} dm_x$. We can now subtract E_{Newt} off of eq. A.3 to find the 1st order GR correction:

$$\Delta E_{GR} = \int_0^R \left[\frac{m_x}{r_x} - \frac{m}{r} - u\frac{m}{r} - \frac{1}{2}\left(\frac{m}{r}\right)^2 \right] dm_x \tag{A.4}$$

where we have used $dm_x = \rho_x dV_x$. We must now expand $\frac{m_x}{r_x}$.

$$V_x = \frac{4\pi}{3} r_x^3 = 4\pi \int \left(1 - \frac{2m}{r}\right)^{-1/2} r^2 dr \approx 4\pi \int \left(1 + \frac{m}{r}\right) r^2 dr \tag{A.5}$$

Solving for $r_x = \left(\frac{3V_x}{4\pi}\right)^{1/3}$ to first order we get:

$$r_x \approx r\left(1 + \frac{1}{r^3}\int_0^r m r dr\right) \tag{A.6}$$

Now we expand m_x:

$$m_x = \int \frac{dm}{(1+u)\sqrt{1-2m/r}} \approx m\left(1 - \frac{1}{m}\int_0^m u dm + \frac{1}{m}\int_0^m \frac{m}{r} dm\right) \tag{A.7}$$

Hence we get:

$$\frac{m_x}{r_x} \approx \frac{m}{r} - \frac{1}{r}\int_0^m u dm + \frac{1}{r}\int \frac{m}{r} dm - \frac{m}{r^4}\int_0^r m r dr \tag{A.8}$$

Plugging into eq. A.4 gives:

$$\Delta E_{GR} = \int_0^{M_x} \left[-u\frac{m}{r} - \frac{1}{2}\left(\frac{m}{r}\right)^2 - \frac{1}{r}\int_0^m u dm + \frac{1}{r}\int_0^m \frac{m}{r} dm - \frac{m}{r^4}\int_0^r m r dr \right] dm_x \tag{A.9}$$

Since every term in the brackets is already of second order in $\frac{m}{r}$ and u, we can evaluate the integrals over $dm_x \to dm$. Using an $n = 3$ polytrope to numerically integrate we get:

$$\Delta E_{GR} = -\alpha_3 M^{7/3} \rho_c^{2/3} \tag{A.10}$$

where α_3 is a constant of order 1 resulting form the integration. Hence the total binding energy is:

$$E = E_{Newt} + \Delta E_{GR} = \alpha_1 K M \rho_c^{\Gamma_1 - 1} - \alpha_2 M^{5/3} \rho_c^{1/3} - \alpha_3 M^{7/3} \rho_c^{2/3} \tag{A.11}$$

where similarly to α_3, α_1 and α_2 are constants of order 1.

A.2 Definition of Energy in General Relativity

A.2.1 General Definitions

Defining energy in GR is to some extent arbitrary. In order to have a conserved quantity in GR, there needs to be an associated symmetry. Furthermore, it is not guaranteed that that such a symmetry will have a unique Newtonian analog (or one at all); so one must be careful when attempting to connect the two.

We have used the fact that in GR, rest mass is not only a constant (assuming no mass accretion or ejection), but also invariant under coordinate transformations [82], to define the total binding energy as the mass defect between the total mass energy of the star, M, as measured via its gravitational field, and its rest mass, M_x. This definition is analogous to the definition of binding energy of nuclei bound by the strong nuclear force. It should be noted, however that unlike nuclear binding energy, there is no experiment that we know of that can measure the rest mass of star, as this would require the observer to first measure the mass of an unbound cloud, then wait around for millions of years until the cloud has collapsed into a star, and then remeasure its mass. Hence, the value of M_x, is purely theoretical.

The problem arises when deciding how to count up the rest mass. Thus far we have done so integrating the density over the proper volume, i.e. accounting for the fact that space is curved (see chapt. 3 and appendix A.1). This geometric interpretation of GR, in which the spacial components of the metric account for the curvature of space, is the conventional way of calculating the rest mass of a star, used throughout the literature and in text books.

However, when dealing with kinematics, the energy of a lump of rest-mass (or test particle), dm_x, in a gravitational field is conventionally defined as time component of the canonical 4-momentum. Starting from the principle of least action, $dm_x \Delta\tau$, where τ is the proper time, and using a $(+---)$ metric signature, we have:

$$dm_x \cdot \Delta\tau = dm_x \cdot \int d\tau = dm_x \cdot \int \sqrt{g_{\mu\nu} U^\mu U^\nu} d\tau \tag{A.12}$$

where U^μ is the 4-velocity. Minimizing proper time leads to the effective corresponding Lagrangian:

$$\mathcal{L} = dm_x \cdot g_{\mu\nu} U^\mu U^\nu = dm_x \tag{A.13}$$

If the 4-momentum is $P^\mu \equiv dm_x U^\mu$, then the corresponding canonical momentum $P_\mu = g_{\mu\nu} P^\nu$ is defined via the effective Lagrangian as:

$$P_\mu = \frac{1}{2} \frac{\mathcal{L}}{\partial U^\mu} \tag{A.14}$$

If $E_{GR} \equiv$ the time component of the 4-momentum, we have:

$$E_{GR} \equiv \frac{1}{2} \frac{\partial \mathcal{L}}{\partial U^t} = \frac{1}{2} \partial_{U^t} \left(g_{\mu\nu} U^\mu U^\nu \right) dm_x \tag{A.15}$$

If the mass has some temperature, then the internal energy is added to its rest-mass: $dm_x \longrightarrow dm_x(1+u)$.

In a static (no time-dependence in the metric) and spherically symmetric situation, the star will be Schwarzschild [81], i.e. the metric/spacetime interval will be of the form:

$$g_{tt}(r)dt^2 - \frac{dr^2}{1-\frac{2m(r)}{r}} - r^2 d\Omega^2 = d\tau^2 \tag{A.16}$$

Assuming a perfect fluid, the stress-energy tensor in a co-moving coordinate system [82] is:

$$T_t^{\ t} = \rho_x(1+u),\ T_i^{\ i} = P,\ T_{\mu\neq\nu}{}^{\nu} = 0 \tag{A.17}$$

Solving the Einstein Field Equations (EOF) with a perfect fluid, using eq. A.16, yields 8.5 and the condition:

$$\frac{d\ln(g_{tt})}{dr} = \frac{1}{r}\left(1-\frac{2m(r)}{r}\right)^{-1}\left(\frac{2m(r)}{r} + 8\pi P(r) r^2\right) \tag{A.18}$$

Using $d\left(\frac{2m}{r}\right) = \frac{dm}{r} - \frac{m}{r^2}dr$, and defining $w(r) \equiv 1 + u(r) + \frac{P(r)}{\rho_x(r)}$, eq. A.18 can be integrated to yield:

$$g_{tt}(r) = A \cdot \left(1 - \frac{2m(r)}{r}\right) \cdot e^{2f(r)} \tag{A.19}$$

where

$$f(r) = \int_0^r \frac{4\pi r' \rho_x(r') \cdot w(r')}{1-\frac{2m(r')}{r'}} dr' \tag{A.20}$$

and A is a constant of integration which can be set to 1 by demanding that $g_{tt}(0) = 1$. Combining eqs. A.15, A.16, and A.19, with velocities set to zero for hydrostatic equilibrium, and finally subtracting off the rest mass yields:

$$dE_{bind} = [(1+u)\sqrt{g_{tt}} - 1]\, dm_x = \left[(1+u)\sqrt{1 - \frac{2m(r)}{r} \cdot e^{f(r)}} - 1\right] dm_x \tag{A.21}$$

If $f(r) = 0$, at all radii, then we get back our original curved-space definition of binding energy (eq. 3.1). This would require $w = 1 + u + \frac{P}{\rho_x} = 0$ everywhere, implying $P = -\rho$. Not only is this condition not physical for stellar matter, but eq. A.21 does not reduce to the Newtonian binding energy in the weak field limit (for $w \neq 0$). So clearly, this definition cannot be the general relativistic extension to the Newtonian energy. But why not? The integration of eq. A.21 is simply adding up all the kinematic energy in the star, i.e. the summation of the time-component of the momentum four-vector over the entire star. Alternatively this is the kinetic energy lost when a mass element accretes onto the surface of the star, summed over the entire star, and therefore must be the total energy. Furthermore, KEPLER's GR correction is based on the TOV equation, and hence implicitly based on this definition of energy. Incidentally, it is interesting to note that $P = -\rho$ does hold for dark energy.

How to resolve this apparent disagreement in definitions of energy in GR? The most straight forward way would be to simply accept that the kinematic and geometric definitions of energy are measuring different quantities, and hence there is no reason to expect them to agree. In this case, since the kinematic definition does not reduce to the Newtonian energy in the weak field limit, it cannot be its analogue, and we must use the geometric definition. This is somewhat unsatisfactory, however, as it is difficult to get around the idea that simply adding up the total kinematic energy (which, for a test particle in a gravitational field, *does* reduce to the Newtonian definition) of the material in the star is somehow not equivalent to or measuring something different from the Newtonian energy in the weak field limit.

Let us conduct the following thought experiment: Imagine a spherically symmetric and static star with total mass-energy M and a shell of mass dM_x at infinity (see fig. A.1). Outside

of the star, space-time is Schwarzschild and static as there are no other fields. For the moment, we are not concerned with the geometry inside the star. Since the star is gravitationally bound, it has already lost its binding energy (whatever its value) to the universe. The total energy in the universe is then $M + dM_x - E_{bind}$ ($E_{bind} < 0$). Later on the shell has collapsed and is now sitting on the surface of the star in thermal equilibrium with the star. It is true that there is a time-changing field across the boundary of the shell as it falls in (an in-falling DC offset as the total mass enclosed changes when the shell pass by), but long after the shell has accreted onto the star, the field in the universe will once again be Schwarzschild. The total mass-energy of the shell is now its bare rest mass, plus its thermal energy, all sitting in the gravitational field of the star. In order to be at rest on its surface, the in-falling kinetic energy picked up must in part be transferred to internal energy, and the rest lost to the universe, e.g. as radiation, which we shall call the binding energy of that shell. The total energy of the universe must not change, and hence we have:

$$E_{universe} = M + dM_x - E_{bind} = M + dM_x(1+u)\sqrt{g_{tt}} - E_{bind} - dE_{bind} \tag{A.22}$$

Solving for the binding energy of the shell, dE_{bind}:

$$dE_{bind} = dM_x\left[(1+u)\sqrt{g_{tt}} - 1\right] \tag{A.23}$$

That is, the kinematics definition of binding energy. Since the shell at infinity and at the star's surface is in a Schwarzschild background, we have:

$$g_{tt} = 1 - \frac{2m}{r} = \frac{1}{g_{rr}} \tag{A.24}$$

and therefore, the geometric and kinematic definitions of binding energy are equivalent for the shell. By Birchoff's Theorem, the shell only knows about the interior mass. As more shells pile onto the star, the metric at the location of the first shell, as well as everywhere inside

the star, does not change, and therefore neither does the binding energy of the first shell.

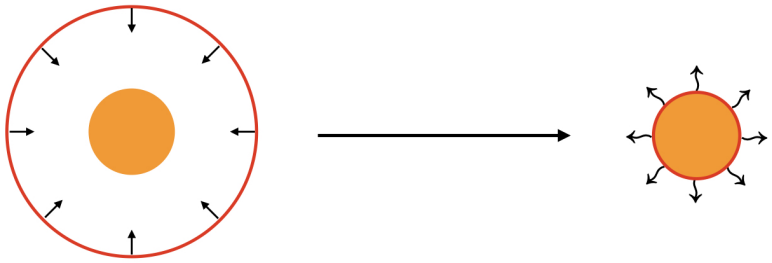

$$E_{universe} = dM_x + M - E_{bind} \qquad E_{universe} = dM_x(1+u)\sqrt{g_{tt}} + M - E_{bind} - dE_{bind}$$

$$d\tau^2 = \left(1 - \frac{2M}{r}\right) dt^2 - \left(1 - \frac{2M}{r}\right)^{-1} dr^2 - r^2 d\Omega^2$$

$$\longrightarrow dE_{bind} = dM_x \left[(1+u)\sqrt{g_{tt}} - 1\right] = dM_x \left[(1+u)\sqrt{1 - \frac{2M}{r}} - 1\right] = dM_x \left[(1+u)\frac{1}{\sqrt{g_{rr}}} - 1\right]$$

Figure A.1: Mass Accretion onto a Star and Binding Energy.
A spherical shell of rest mass dM_x accretes onto the surface of a spherically symmetric star with total mass-energy M and radius R. The in-falling kinetic energy of the shell is in part conserved in the shell as heat, with the rest being lost to the universe. This loss of kinetic energy is defined to be the binding energy of the shell.

Although this example does not imply that the geometric and kinematic definitions of energy are equivalent for a general metric, we have found them to equivalent in a spherically symmetric space-time geometry.

But this still disagrees with the results derived via the TOV equation (eq.A.21). Notice when the kinematics point of view was derived using the TOV equation, explicit use of the stress-energy tensor, $T_{\mu\nu}$, inside the star was needed, but no knowledge of $T_{\mu\nu}$ inside the star was necessary when using the geometric point of view, as $g_{rr}(r) = (1 - \frac{2m(r)}{r})^{-1}$, results from imposing rest-mass conservation [82]. Knowledge of $T_{\mu\nu}$ inside the star was also not necessary in the previous thought experiment, as the every subsequent shell always remains outside the star. It may therefore be the case that choice of $T_{\mu\nu}$ in deriving the TOV equation is not physically sound

for a star. That is, the perfect fluid assumption/approximation is not valid for normal matter.

A.3 Neutrino Processes

All neutrino emission rates are taken from [67], with $\mu_e = \frac{1}{Y_e} = \frac{A}{Z} = 2$ and number of neutrino species $= 2$.

A.3.1 $e^- + e^+ \rightleftharpoons \nu + \overline{\nu}$

The neutrino energy loss rate from electron positron pair annihilation is the only relevant neutrino process for the purposes of this dissertation. Although in this dissertation, the rate per unit volume, Q_{pair}, was computed using the fits from [67], it can be calculated analytically.

$$Q_{pair} = n_- n_+ \cdot (E_- + E_+) v \cdot \sigma \tag{A.25}$$

where $n_\pm$, $E_\pm$ are the electron/positron number densities and energies, v is the relative velocity, and σ is the cross section. If $\mu_\pm$ is the chemical potential, from the thermodynamic potential eq. A.55, we have:

$$n_\pm = -\frac{\partial \Omega_\pm}{\partial \mu_\pm} = \frac{2}{(2\pi)^3} \int \frac{d^3 p}{e^{(E-\mu_\pm)/T} + 1} \tag{A.26}$$

Since the electrons and positrons are in thermal equilibrium with the photons we have:

$$2\mu_\gamma = \mu_- + \mu_+ = 0 \longrightarrow \mu_- = -\mu_+ \tag{A.27}$$

where we have used $\mu_\gamma = 0$. Calling $\mu \equiv \mu_-$, we have:

$$Q_{pair} = \frac{4}{(2\pi)^6} \int \frac{d^3p_-}{e^{(E_- - \mu)/T} + 1} \cdot \frac{d^3p_+}{e^{(E_+ + \mu)/T} + 1} \cdot (E_- + E_+) v \cdot \sigma \tag{A.28}$$

The combination $v \cdot \sigma$ for this interaction works out to be [83]:

$$v \cdot \sigma = \frac{G_F^2}{12\pi E_- E_+} \cdot \Big\{ \left(C_V^2 + C_A^2\right) \left[m_e^4 + 3m_e^2 (\mathbf{p}_- \cdot \mathbf{p}_+) + 2 \left(\mathbf{p}_- \cdot \mathbf{p}_+\right)^2 \right] + 3 \left(C_V^2 - C_A^2\right) \left[m_e^4 + m_e^2 (\mathbf{p}_- \cdot \mathbf{p}_+) \right] \Big\} \tag{A.29}$$

where G_F id Fermi's constant. The $m_e^2(\mathbf{p}_- \cdot \mathbf{p}_+)$ terms are spherically odd, and with go to zero after integrating over the angular dimensions. Substituting the remaining terms into eq. A.28, and making the following variable changes: $x \equiv p/T$, $\varepsilon \equiv E/T$, and $\eta \equiv \mu/T$; the result of the angular integration is:

$$Q_{pair} = \frac{G_F^2 T^5 m_e^4}{6\pi^5} \left(2C_V^2 - C_A^2\right) \int \frac{x_-^2}{e^{(\varepsilon_- - \eta)} + 1} \cdot \frac{x_+^2}{e^{(\varepsilon_+ + \eta)} + 1} \cdot \frac{(\varepsilon_- + \varepsilon_+)}{\varepsilon_- \varepsilon_+} dx_- dx_+ + \frac{2G_F^2 T^9}{3\pi^5} \left(C_V^2 + C_A^2\right) \int \frac{x_-^4}{e^{(\varepsilon_- - \eta)} + 1} \cdot \frac{x_+^4}{e^{(\varepsilon_+ + \eta)} + 1} \cdot \frac{(\varepsilon_- + \varepsilon_+)}{\varepsilon_- \varepsilon_+} dx_- dx_+ \tag{A.30}$$

As the temperature approaches m_e, the pair-neutrino emissivity will go a T^9.

A.4 Polytrope Numerical Integration

The following details the procedure used to numerically integrate the Lane-Emden Equation with an $n = 3$ polytrope (eq. 2.4). A simple 2^{nd} order Taylor series was used to approximate $\theta(\xi)$ over k zones.

$$k \equiv \#\text{ of zones},\ \ d\xi \equiv \frac{\xi_1}{k-1} \tag{A.31}$$

where $\xi_1 = 6.95808863$ is defined such that $\theta(\xi_1) = 0$.

Start with initial conditions: $\xi_0 = 0,\ \theta_0 = 1,\ \theta_0' = 0$. We still need to find θ_0''. By eq. 2.4: $\theta_0'' + \frac{2\theta_0'}{\xi_0} + \theta_0^3 = 0 \longrightarrow \theta_0'' + 2\frac{0}{0} + 1 = 0$. Using L'Hopital's Rule we have: $\theta_0'' + \frac{2\theta_0''}{1} = -1 \longrightarrow \theta_0'' = -\frac{1}{3}$. From here we can use a recursive Taylor expansion to 2^{nd} order:

$$\xi_{i+1} = \xi_i + d\xi \tag{A.32}$$

$$\theta_{i+1} = \theta_i + \theta_i' \cdot d\xi + \frac{1}{2}\theta_i'' \cdot (d\xi)^2 \tag{A.33}$$

$$\theta_{i+1}' = \theta_i' + \theta_i'' \cdot d\xi \tag{A.34}$$

$$\theta_{i+1}'' = -\frac{2\theta_{i+1}'}{\xi_{i+1}} - \theta_{i+1}^3 \text{ (use eq. 2.4)} \tag{A.35}$$

A.5 Eddington Luminosity

The Eddington luminosity is the luminosity a star would have were it to be entirely supported by photon radiation pressure. The radiation momentum flux through a spherical surface, p_γ, is:

$$p_\gamma = \frac{L_\gamma}{4\pi r^2} \tag{A.36}$$

The photons will primarily scatter off of electrons and positrons, consequently dragging positively charged nuclei with them. Balancing the gravitational force with the radiation force on

a single nucleus (A,Z), with N_e electrons/positrons per baryon, we have:

$$N_e p_\gamma \sigma_{Thom} = \frac{N_e L_\gamma \sigma_{Thom}}{4\pi r^2} = \frac{m(r) m_b}{r^2} \tag{A.37}$$

where σ_{Thom} is the Thomson cross section. In a regime where electrons-positron pairs are negligible, $N_e = \frac{Z}{A} = Y_e$. Solving for the luminosity at the surface of the star, we get:

$$L_{Edd} = \frac{4\pi M m_b}{\sigma_{Thom}} \frac{A}{Z} = \frac{4\pi M m_b}{\sigma_{Thom} Y_e} \tag{A.38}$$

A.6 Mean Free Path Calculations

A.6.1 Derivation

To determine the mean free path, λ, of a particle we start with a single particle streaming through a medium with a number density of targets, n_T. In a time dt, the particle will travel a distance dx, through the medium. The probability that it will scatter, p_s, in a differential volume with cross section σ and length, dx, containing N_T targets is:

$$p_s = f \cdot n_T \sigma dx \tag{A.39}$$

where f is some factor that can be absorbed into σ. For numerous particles we simply multiply p_s by the number of particles, N, with $p_s N = dN$, the number of scattered particles:

$$dN = N n_T \sigma dx \tag{A.40}$$

Now imagine a source emits N_0 particles. After traveling dx, the number of remaining

particles (those that haven't scattered) will be:

$$N(dx) = N_0 - dN_0 = N_0(1 - n_T \sigma dx) \tag{A.41}$$

After another distance of dx, the number of particles remaining will be:

$$N(2dx) = N(dx) - dN(dx) = N(dx)(1 - n_T \sigma dx) = N_0(1 - n_T \sigma dx)^2 \tag{A.42}$$

Repeating the process k times we have:

$$N(kdx) = N_0(1 - n_T \sigma dx)^k \tag{A.43}$$

The total distance travelled, r, will be kdx. Now we define $z \equiv n_T \sigma dx$, and take the limit as $(dx, z) \longrightarrow 0$. eq. A.43 becomes:

$$N(r) = \lim_{z \to 0} \left[N_0(1-z)^{\frac{rn_T\sigma}{z}} \right] = N_0 \left[\lim_{z \to 0} (1-z)^{\frac{1}{z}} \right]^{rn_T\sigma} = N_0 e^{-rn_T\sigma} \equiv N_0 e^{-\frac{r}{\lambda}} \tag{A.44}$$

Hence the mean free path is:

$$\lambda = (n_T \sigma)^{-1} \tag{A.45}$$

A.6.2 Photons

The primary targets for photons scattering are electrons. Their number density in a gas of average atomic nuclei $(\overline{A}, \overline{Z})$, if electron-positron pairs are negligible is $\frac{\overline{Z}\rho}{\overline{A}m_b}$. While the scattering cross section is simply the Thomson cross section. Hence from eq. A.45 we have that the photon mean free path is:

$$\lambda_\gamma = \frac{\overline{A} m_b}{\overline{Z} \rho \sigma_{Thom}} = \frac{m_b}{Y_e \rho \sigma_{Thom}} \tag{A.46}$$

The average photon mean free path at the GRI is $\approx 3 \cdot M_4^{7/2}\ mm$.

A.6.3 Neutrinos

The mean free path of a particle is $(\sigma n_{targets})^{-1}$. The neutrino scattering cross section is approximately $G_F^2 E_\nu E_e$. In a regime where electron-positron pairs are rare, and electrons are non-relativistic, most of the electrons and positrons will have energies close to their rest mass. For neutrinos created by electron-positron annihilation, the typical energy will therefore be about one electron mass. The number of targets (electrons) will be approximately the number of protons, as electron-positron pairs will be negligible in comparison. Hence we have:

$$n_e \approx \frac{\overline{Z} \rho_{crit}}{\overline{A} m_b} = \frac{Y_e \rho_{crit}}{m_b} \tag{A.47}$$

$$\sigma_\nu \approx (G_F m_e)^2 \longrightarrow \lambda_\nu \approx \frac{m_b}{Y_e G_F^2 m_e^2 \rho_{crit}} \longrightarrow \lambda_\nu \approx 10^4 M_4^{7/2}\ AU \tag{A.48}$$

A.7 Thermodynamic Calculations

A.7.1 Thermodynamic Potential

The general thermodynamic potential, Ω, for a given species with rest mass, m, is given as:

$$\Omega = -\frac{gV}{6\pi^2}\int_0^\infty \frac{p^4 dp}{E(p)\cdot\left[e^{\left(\frac{E(p)}{T}-\eta\right)}\pm 1\right]} \tag{A.49}$$

where g is the particle degeneracy, V = volume, T = temperature, p = the momentum states, $E(p) = \sqrt{m^2+p^2}$ is the associated energy, η is the degeneracy parameter (chemical potential divided by temperature), and the $\pm$ is for fermions/bosons. Defining $x \equiv p/T$ and $\varepsilon(x) \equiv E(p)/T$, yields:

$$\Omega(T,V,\eta) = -\frac{gVT^4}{6\pi^2}\int_0^\infty \frac{x^4 dx}{\varepsilon(x)\cdot\left[e^{(\varepsilon(x)-\eta)}\pm 1\right]} \tag{A.50}$$

The following thermodynamic quantities are given via Ω:

$$\text{Pressure: } P = -\frac{\partial\Omega}{\partial V} \tag{A.51}$$

$$\text{Entropy: } s = -\frac{\partial\Omega}{\partial T} \tag{A.52}$$

$$\text{Number: } N = -\frac{1}{T}\frac{\partial\Omega}{\partial\eta} \tag{A.53}$$

$$\text{Energy: } E = -PV + Ts + T\eta N = \Omega - T\cdot\frac{\partial\Omega}{\partial T} - \eta\cdot\frac{\partial\Omega}{\partial\eta} \tag{A.54}$$

A.7.2 Entropy in a SMS

For a a given particle species, the general thermodynamic potential (see eq. A.50) for a volume, V, at temperature, T, is:

$$\Omega = -\frac{gVT^4}{6\pi^2}\int_0^\infty \frac{x^4 dx}{\varepsilon(x)\cdot\left(e^{\varepsilon(x)-\eta}\pm 1\right)} \tag{A.55}$$

For radiation dominated matter ($\varepsilon = x$), we can calculate $S \approx S_{rad}$. Starting from the thermodynamic potential for a relativistic species in a volume, V,is:

$$\Omega = -\frac{gVT^4}{6\pi^2}\int_0^\infty \frac{x^3 dx}{e^{x-\eta}\pm 1} \tag{A.56}$$

The total entropy, s, for a given radiation species is given by:

$$s = -\frac{\partial\Omega}{\partial T} = \frac{2gVT^3}{3\pi^2}\int_0^\infty \frac{x^3 - \frac{4}{3}\eta x^2}{e^{x-\eta}\pm 1}dx \tag{A.57}$$

For the purposes of this dissertation, the only radiative species are photons, which have $g = 2$ and $\eta = 0$. If temperatures were to approach the electron mass, then relativistic electrons would also be included in the radiation. The number of baryons in a volume with mass, m, will be $\frac{m}{m_b}$. Using $V = \frac{m}{\rho}$, the entropy per baryon, S, for a given volume of material is:

$$S \approx S_\gamma = \frac{m_p}{\rho}\cdot\frac{4T^3}{3\pi^2}\int_0^\infty \frac{x^3 dx}{e^x - 1} \tag{A.58}$$

The integral evaluates to $\frac{\pi^4}{15}$. Using the relation $T^3 \propto \rho$ (eq. 2.20) we find:

$$S \approx 94\sqrt{M_4} \tag{A.59}$$

Hence the entropy per baryon is constant everywhere in the star. This results in the star being convectively unstable. Note that this result holds under the assumption that the ratio of the gas pressure to the total pressure, β, is also constant throughout the star. As this assumption does not hold in the outer regions (envelope) of the star, the convective currents do not penetrate the envelope, eventually resulting in the envelope being shed.

A.7.3 Number Density of Electrons

The number density for electrons/poistron, $n_\mp$, is given from general thermodynamic potential for fermions (eqs. A.50, A.51):

$$n_{\mp} = -\frac{1}{T}\frac{\partial\Omega}{\partial\eta_{\mp}} = \frac{T^3}{\pi^2}\int_0^{\infty}\frac{x^2dx}{e^{(\varepsilon\pm\eta)}+1} = \frac{T^3}{\pi^2}\int_{\mu}^{\infty}\frac{\sqrt{\varepsilon^2-\mu^2}\cdot\varepsilon d\varepsilon}{e^{(\varepsilon\pm\eta)}+1} \tag{A.60}$$

where we have used $g = 2$, $\eta \equiv \eta_- = -\eta_+$ (Saha relation), and $\varepsilon = \sqrt{x^2+\mu^2}$, with $\mu \equiv m_e/T$. Now using:

$$\frac{1}{e^{(\varepsilon\mp\eta)}+1} = \frac{e^{-(\varepsilon\mp\eta)}}{1+e^{-(\varepsilon\mp\eta)}} = e^{-(\varepsilon\mp\eta)}\cdot\sum_{n=0}^{\infty}(-1)^n\cdot e^{-n(\varepsilon\mp\eta)} \tag{A.61}$$

to find:

$$n_{\mp} = \frac{T^3}{\pi^2}\sum_{n=1}^{\infty}(-1)^{n+1}e^{\pm n\cdot\eta}\int_{\mu}^{\infty}\sqrt{\varepsilon^2-\mu^2}\cdot\varepsilon\cdot e^{-n\cdot\varepsilon}d\varepsilon \tag{A.62}$$

Note that the series only converges if $e^{-(\varepsilon-\eta)} < 1 \longrightarrow |\eta| < \mu$. Integrating be parts gives:

$$n_{\mp} = \frac{T^3}{3\pi^2}\sum_{n=1}^{\infty}(-1)^{n+1}\cdot n\cdot e^{\pm n\cdot\eta}\int_{\mu}^{\infty}\left(\varepsilon^2-\mu^2\right)^{3/2}e^{-n\cdot\varepsilon}d\varepsilon \tag{A.63}$$

We can now solve the integral with the use of modified Bessel functions of the second kind, $K_\nu(x)$:

$$K_\nu(n\cdot\mu) = \frac{\sqrt{\pi}\cdot n^\nu}{(2\mu)^\nu\cdot\Gamma(\nu+1/2)}\int_{\mu}^{\infty}\left(\varepsilon^2-\mu^2\right)^{\nu-1/2}e^{-n\cdot\varepsilon}d\varepsilon \tag{A.64}$$

Substituting $K_2(n\cdot\mu)$ into $n_{\mp}$ yields:

$$n_{\mp}(T,\eta) = \frac{m_e^3}{\pi^2}\cdot\left(\frac{T}{m_e}\right)\sum_{n=1}^{\infty}\frac{(-1)^{n+1}}{n}e^{\pm n\cdot\eta}\cdot K_2\left(n\cdot\frac{m_e}{T}\right) \tag{A.65}$$

If $m_e > T$ the first term in eq. A.65 will dominate, and $n_{\mp}$ can approximated as:

$$n_{\mp}(T,\eta) \approx \frac{m_e^3}{\pi^2}\cdot\left(\frac{T}{m_e}\right)e^{\pm\eta}\cdot K_2\left(\frac{m_e}{T}\right) \tag{A.66}$$

A.7.4 Number Density and Chemical Potential in Maxwell-Boltzmann Regime

For a Maxwell-Boltzmann gas we have the conditions: $m >> T$ and $\eta < \frac{m}{T}$. From eqs. A.51, number density of a given species is:

$$n = \frac{gT^3}{2\pi^2} \int_0^\infty \frac{x^2}{e^{\varepsilon(x)-\eta} \pm 1} dx \tag{A.67}$$

Using $\mu \equiv \frac{m}{T} >> 1$ and $\varepsilon = \sqrt{x^2+\mu^2} \approx \mu + \frac{x^2}{2\mu}$. Since $\eta > \frac{m}{T}$, the integral can be rewritten in terms of $\overline{\varepsilon} \equiv \varepsilon - \mu$ and $\overline{\eta} \equiv \eta - \mu$ to give:

$$n \approx \frac{gT^3}{\pi^2} \sqrt{\frac{\mu^3}{2}} e^{\overline{\eta}} \int_0^\infty e^{-\overline{\varepsilon}} \cdot \overline{\varepsilon}^{1/2} d\varepsilon \tag{A.68}$$

The integral is simply $\Gamma(3/2)$, giving:

$$n \approx g \left(\frac{m \cdot T}{2\pi} \right)^{3/2} e^{\overline{\eta}} \tag{A.69}$$

Or solving for $\overline{\eta}$ in terms of the number density:

$$\overline{\eta} = \eta - \frac{m}{T} = \ln \left[\left(\frac{2\pi}{m \cdot T} \right)^{3/2} \cdot \frac{n}{g} \right] \tag{A.70}$$

A.8 Nuclear Abundance in NSE

For matter in NSE, the details of individual reaction rates need not be considered. Instead the net reaction sequence can be summarized by the disintegration rate of nuclei into bare protons and neutrons, being in equilibrium with the binding of bare neutrons and protons into nuclei:

$$Z_p + N_n \rightleftharpoons A(Z,N) + \gamma \tag{A.71}$$

The corresponding Saha equation for the chemical potentials, μ_i, [55] is:

$$Z \cdot \mu_p + N \cdot \mu_n = \mu_A \tag{A.72}$$

The chemical potentials can be rewritten in terms of a kinetic contribution, $\overline{\mu}$, plus the rest mass: $\mu_i = m_i + \overline{\mu}_i$, to give:

$$Z \cdot \overline{\mu}_p + N \cdot \overline{\mu}_n = \overline{\mu}_A - Q(Z,N) \tag{A.73}$$

where $-Q(Z,N) \equiv -Z \cdot m_p - N \cdot m_n + m_A$ is the binding energy of a given nucleus. Treating the baryons as a Maxwell-Boltzmann gas, the chemical potentials can be written in terms of the species' corresponding number density (eq. A.70). Plugging eq. A.70 into eq. A.73 we get:

$$\ln\left[\left(\frac{2\pi}{T \cdot m_p^Z}\right)^{3/2}\left(\frac{n_p}{2}\right)^Z\right] + \ln\left[\left(\frac{2\pi}{T \cdot m_n^N}\right)^{3/2}\left(\frac{n_n}{2}\right)^N\right] = \ln\left[\left(\frac{2\pi}{T \cdot m_A}\right)^{3/2}\left(\frac{n_p}{G(Z,A)}\right)\right] - \frac{Q}{T} \tag{A.74}$$

where $G(Z,A) = \sum_i (2J_i + 1)e^{-E_i/T}$ is the statistical weight of a nucleus with energy levels E_i and spin J_i [55]. Rearranging, and using $m_p \approx m_n \approx m_A/A \equiv m_b$ gives:

$$n_A \approx G(Z,A)\left[A\left(\frac{2\pi}{T \cdot m_b}\right)^{A-1}\right]^{3/2} \frac{n_p^Z \cdot n_n^N}{2^A} e^{\frac{Q_A}{T}} \tag{A.75}$$

Converting the number densities to mass fractions using: $n_i = X_i \frac{\rho}{m_i}$, eq. A.75 becomes:

$$X_A \approx G(Z,A) \cdot \frac{A^{5/2}}{2^A}\left[\left(\frac{2\pi}{T}\right)^{3/2}\frac{\rho}{m_b^{5/2}}\right]^{A-1} \cdot X_p^Z \cdot X_n^N \cdot e^{\frac{Q_A}{T}} \tag{A.76}$$

Now using eq. 2.20 to replace ρ yields:

$$X_A \propto \frac{1}{2} \cdot G(Z,A) \cdot A^{5/2} \left[4 \cdot 10^{-18} \cdot \frac{T_8^3}{M_4} \right]^{\frac{(A-1)}{2}} \cdot X_p^Z \cdot X_n^N \cdot e^{\frac{Q_A}{T}} \tag{A.77}$$

A.9 Start File Example

```
c zero composition
c
c box and id information:
box q85
c
c input for approx network (network #1):
net 1 h1 he3 he4 n14 c12 o16 ne20 mg24 si28 s32
net 1 ar36 ca40 ti44 cr48 fe52 ni56 fe54 pn1 nt1
c
c include ise and nse networks (networks #2 and #3)
isenet
c
c zero metallicity abundances (weight %):
c data from B Fields, p.c. 2002
c mapping H1+H2–¿h2
c mapping H3+Li6...B11–¿he3
c mapping C12+C13+N15–¿c12
c mapping O16+O17+O18–¿o16
m zero 0.751276498 h1
m zero 6.450198e-5 he3
m zero 0.248659 he4
m zero 0.0 o16
m zero 0.0 c12
m zero 0.0 ne20
m zero 0.0 fe56
m zero 0.0 n14
m zero 0.0 si28
m zero 0.0 mg24
m zero 0.0 s32
m zero 0.0 ne22
m zero 0.0 mg26
```

```
m zero 0.0 ar36
m zero 0.0 fe54
m zero 0.0 mg25
m zero 0.0 ca40
m zero 0.0 al27
m zero 0.0 ni58
m zero 0.0 c13
c This abundance set should also be used for BURN
c mass units 1E4 Msolar
p 273 1.9892E+37
c initial grid (zone #, exterior mass(g), network #,...
c ... temp(K), rho(g/cc), [omega(1/s)[, u(cm/s)]])
g 0 -1.50000E+02 1 zero 5.000E+07 6.000E-02 0.000E+00
g 1 -1.49998E+02 1 zero 4.000E+07 4.800E-02
g 2 -1.49995E+02 1 zero 4.000E+07 4.000E-02
g 3 -1.49990E+02 1 zero 4.000E+07 4.000E-02
g 4 -1.49985E+02 1 zero 4.000E+07 4.000E-02
g 5 -1.49980E+02 1 zero 4.000E+07 4.000E-02
g 6 -1.49975E+02 1 zero 4.000E+07 4.000E-02
g 7 -1.49970E+02 1 zero 4.000E+07 4.000E-02
g 8 -1.49963E+02 1 zero 4.000E+07 4.000E-02
g 9 -1.49955E+02 1 zero 4.000E+07 4.000E-02
g 10 -1.49948E+02 1 zero 4.000E+07 4.000E-02
g 11 -1.49940E+02 1 zero 4.000E+07 4.000E-02
g 12 -1.49880E+02 1 zero 4.000E+07 4.000E-02
g 13 -1.49820E+02 1 zero 4.000E+07 4.000E-02
g 276 -1.34040E+02 1 zero 8.000E+06 3.300E-02
g 277 -1.33980E+02 1 zero 8.000E+06 3.300E-02
g 386 -1.23100E+02 1 zero 8.000E+06 3.000E-02
g 387 -1.22960E+02 1 zero 8.000E+06 3.000E-02
g 696 -7.96400E+01 1 zero 8.000E+06 3.000E-02
g 697 -7.95000E+01 1 zero 8.000E+06 3.000E-02
g 717 -7.66000E+01 1 zero 8.000E+06 3.000E-02
g 718 -7.64550E+01 1 zero 8.000E+06 3.000E-02
g 796 -6.51450E+01 1 zero 8.000E+06 3.000E-02
g 797 -6.50000E+01 1 zero 8.000E+06 3.000E-02
g 855 -5.21000E+01 1 zero 8.000E+06 2.100E-02
g 856 -5.18000E+01 1 zero 8.000E+06 2.100E-02
g 898 -3.92000E+01 1 zero 8.000E+06 2.100E-02
g 941 -2.63000E+01 1 zero 8.000E+06 1.920E-02
g 984 -1.34000E+01 1 zero 8.000E+06 1.800E-02
g 985 -1.31000E+01 1 zero 8.000E+06 1.800E-02
g 1036 -5.00000E-01 1 zero 8.000E+06 1.200E-02
```

```
g 1046 -5.00000E-02 1 zero 8.000E+06 6.000E-03
g 1056 -5.00000E-03 1 zero 8.000E+06 3.600E-03
g 1066 -5.00000E-04 1 zero 8.000E+06 2.400E-03
g 1076 -5.00000E-05 1 zero 8.000E+06 1.800E-03
g 1080 0.000000E+00 1 zero 1.000E+06 1.500E-03
c scale mass
rescalem 150. div
rescalem 4.d4 mult
c specify burn-generator-file name to turn on isotopic co-processing
c genburn ¡to be specified¿
c
c adjust initial temperature to yield hydrostatic equilibrium
hstat
c
c rotation c rigidl 5.00e+60
c reset default parameter values:
c
c time-step and back-up controls (changed 6,7,8,9,55)
c p 6 .05
p 6 .1
c p 7 .035
p 7 .07
c p 8 .1
p 8 .2
c p 9 .05
p 9 .1
p 25 1.00000E+11
p 46 .15
p 47 .001
c p 55 2.00000E+00
p 55 4.0
p 205 .3
p 206 .001
c
c turn off postprocessor edits
p 299 1000000
c
c convergence control parameters
p 11 1.e-7
p 12 1.e-7
c
c problem termination criteria
p 158 9999999
```

```
p 306 1.e+11
c
c turn on sparse matrix inverter
p 258 1
c
c special command execution
p 331 1.2e+9
p 332 .05
c
c linear artificial viscosity coefficient (reset to 0.1 at zero-age ms)
p 13 1000.
c
c edit and dump controls
p 16 1000000
p 18 100
p 156 50
p 197 1000
p 268 53
c
c equation of state parameters
p 92 1.e-8
c
c semiconvection and overshoot mixing coefficients
p 24 0.1
p 148 0.01
p 324 4.
p 325 0.1
p 326 0.01
c
c graphics parameters
p 42 10240750
p 64 50
p 113 2713
c
c rezoning criteria (changed 78,79,80,81,83,84)
c p 78 .2
p 78 .4
c p 79 .08
p 79 .16
c p 80 .2
p 80 .4
c p 81 .08
p 81 .16
```

```
c p 83 1.e+4
p 83 1.e+5
c p 84 1.e-8
p 84 1.e-7
p 86 0
p 87 1
p 138 4.70000E-01
p 139 5.66667E-01
p 150 2.24000E-03
p 151 2.32000E-03
p 152 4.80000E-03
p 193 1.06667E-01
p 195 9.60000E-04
p 216 3
c
c ise control parameters
p 185 -1.0
p 203 1.e+5
c
c c12(a,g) rate multipliers
c (obsolete)
p 227 1.7
p 228 1.7
c
c post-processor-dump control parameters
p 44 6000000
c p 300 8192
p 303 0.5
c
c set the time at which to make zero-age-main-sequence parameter changes
p 308 5.e+10
c
c turn on rezoner at the zero-age main sequence by reseting p 86
c to the value of p 309
p 309 1
c
c turn down the linear artificial viscosity at the zero-age main
c sequence by reseting p 13 to the value of p 310
p 310 .1
c
c set the core temperature at which to make pre-carbon-burning
c parameter changes
p 311 1.e99
```

```
c
c raise floor on abundances considered in calculating the time-step
c just before carbon ignition by reseting p47 to the value of p312
p 312 .003
c
c finely zone zone #2 just before carbon ignition
c by reseting p195 to the value of p313 and p150 to the value of p314
c (currently not used)
p 313 9.60000E-04
p 314 2.24000E-03
c
c ——————————————————————————
c [ALIASES]
c ——————————————————————————
c
c Definitions of aliased commands...
c The tnchar command is executed when the central temperature
c exceeds tempchar (p333) degK.
c The cdep command is executed when the central temperature
c exceeds tempcdep (p331) degK.
c The odep command is executed when the oxygen abundance drops below
c o16odep (p332) in weight
c exceeds tqselim (p184) degK.
c The presn command is executed when the infall velocity exceeds
c vinfall (p306) cm/sec.
c
alias tnchar "p 87 1"
alias cdep "p 206 .003, p 331 1.e+99"
alias odep1 "p 6 .02, p 7 .02, p 8 .02, p 11 1.e-8"
alias odep2 "p 12 1.e-8, p 54 10., p 55 10., p 70 1.e+99"
alias odep3 "p 73 1.e+99, p 206 3.e-3, p 332 -1.e+99, zerotime"
alias odep "odep1, odep2, odep3"
c
c for our convenience (...)
alias t1 "tq,1,1 i"
c
c ——————————————————————————
c EXTENSIONS beyond WW95
c ——————————————————————————
c
c write out convection data file
p 376 1
c
```

```
c write out wind data file
p 390 1
c
c no convective surface layers
p 408 0.666d0
c
c turn off Niewenhuijzen & de Jager mass loss
p 363 0.0d0
c
c maximum APPROX network number for BURN coprocessing
p 240 2
c
c surface boundary pressure
p 69 1.0e5
c
c under-relaxation for Newton-Raphson solver
p 375 0.333
c
c turn on burn co-processing down to T= 0.0010000000
p 233 1.00E-03
p 235 -1.D99
c
c 1.2 times Buchmann et al. (2000, priv. com) C12(a,g) rate
p 208 1.2
c
c use Jaeger et al. Ne22(a,g) rate
p 421 6
c
c switch on adaptive network
p 137 1
c
c undo mixing in case of backup
p 433 2
c
c resolve fine abundances in Z=0 stars
p 246 1.d-10
p 206 1.d-4
p 47 1.d-4
c
c mass conservation
p 204 -1.d-6
c
c do not trace Al26 in Z=0 stars
```

```
c p 266 1.d0 (originally on)
c
c allow more backups
p 52 50
c
datapath ../../../../../source/data/
c mass and radius rezoning restrictions
p 336 2.e30
p 88 5.e13
c red giant mass loss off
p 363 0.
p 387 0.
c magnetic torques off
p 423 0
c abar and zbar rezoning restrictions
p 426 4.
p 427 2.
c hstat
c p 386 1.e35
c swich on rotational mixing processes (nangmix)
p 364 1
p 365 5.00D-2
p 366 3.33D-2
p 367 1.0
p 368 2.5D+3
p 369 0.25
p 370 1.0
p 371 1.0
p 372 0.9
p 373 0.9
p 374 0.9
c smoothing of gradients and time derivative
p 380 0.2
p 381 2
p 382 1.0D-3
p 383 1.0D-3
p 14 30000
c turn on postnewtonian gravity
p 358 1.0
c turn on magnetic torques
c p 423 2
c p 65 1.e7
```

Bibliography

[1] Hideyuki Umeda and Ken'ichi Nomoto. First-generation black-hole-forming supernovae and the metal abundance pattern of a very iron-poor star. *Nature*, 422(6934):871–873, 2003. doi: 10.1038/nature01571. URL https://doi.org/10.1038/nature01571.

[2] Tom Abel, Greg L. Bryan, and Michael L. Norman. The formation of the first star in the universe. *Science*, 295(5552):93–98, 2002. ISSN 0036-8075. doi: 10.1126/science.1063991. URL https://science.sciencemag.org/content/295/5552/93.

[3] Volker Bromm, Paolo S Coppi, and Richard B Larson. The formation of the first stars. i. the primordial star-forming cloud. *The Astrophysical Journal*, 564(1):23, 2002.

[4] Hajime Susa, Kenji Hasegawa, and Nozomu Tominaga. THE MASS SPECTRUM OF THE FIRST STARS. *The Astrophysical Journal*, 792(1):32, aug 2014. doi: 10.1088/0004-637x/792/1/32. URL https://doi.org/10.1088%2F0004-637x%2F792%2F1%2F32.

[5] F. Hoyle and William A. Fowler. On the Nature of Strong Radio Sources. *Monthly Notices of the Royal Astronomical Society*, 125(2):169–176, 08 1962. ISSN 0035-8711. doi: 10.1093/mnras/125.2.169. URL https://doi.org/10.1093/mnras/125.2.169.

[6] F. HOYLE and WILLIAM A. FOWLER. Nature of strong radio sources. *Nature*, 197(4867): 533–535, 1963. doi: 10.1038/197533a0. URL https://doi.org/10.1038/197533a0.

[7] Ya B Zel'dovich. Gravitational instability: An approximate theory for large density perturbations. *Astronomy and astrophysics*, 5:84–89, 1970.

[8] M. J. Kashlinsky, A. & Ress. Formation of population iii stars and pregalactic evolution. *Royal Astronomy Society*, 205:955–971, 1983.

[9] Jr. Iben, Icko. Massive Stars in Quasi-Static Equlibrium. *Apj*, 138:1090, Nov 1963. doi: 10.1086/147708.

[10] WILLIAM A. Fowler. Massive stars, relativistic polytropes, and gravitational radiation. *Rev. Mod. Phys.*, 36:545–555, Apr 1964. doi: 10.1103/RevModPhys.36.545. URL https://link.aps.org/doi/10.1103/RevModPhys.36.545.

[11] G. M. Fuller, S. E. Woosley, and T. A. Weaver. The Evolution of Radiation-dominated Stars. I. Nonrotating Supermassive Stars. *Apj*, 307:675, Aug 1986. doi: 10.1086/164452.

[12] R. A. E. Fosbury, M. Villar-Martín, A. Humphrey, M. Lombardi, P. Rosati, D. Stern, R. N. Hook, B. P. Holden, S. A. Stanford, G. K. Squires, M. Rauch, and W. L. W. Sargent. Massive Star Formation in a Gravitationally Lensed H II Galaxy at z = 3.357. *Apj*, 596:797–809, October 2003. doi: 10.1086/378228.

[13] Eduardo Bañados, Bram P. Venemans, Chiara Mazzucchelli, Emanuele P. Farina, Fabian Walter, Feige Wang, Roberto Decarli, Daniel Stern, Xiaohui Fan, Frederick B. Davies, Joseph F. Hennawi, Robert A. Simcoe, Monica L. Turner, Hans-Walter Rix, Jinyi Yang, Daniel D. Kelson, Gwen C. Rudie, and Jan Martin Winters. An 800-million-solar-mass black hole in a significantly neutral universe at a redshift of 7.5. *Nature*, 553:473 EP –, 12 2017. URL https://doi.org/10.1038/nature25180.

[14] B. P. Venemans, J. R. Findlay, W. J. Sutherland, G. De Rosa, R. G. McMahon, R. Simcoe, E. A. González-Solares, K. Kuijken, and J. R. Lewis. DISCOVERY OF THREEz> 6.5 QUASARS IN THE VISTA KILO-DEGREE INFRARED GALAXY (VIKING) SURVEY. *The Astrophysical Journal*, 779(1):24, nov 2013. doi: 10.1088/0004-637x/779/1/24. URL https://doi.org/10.1088%2F0004-637x%2F779%2F1%2F24.

[15] Daniel J. Mortlock, Stephen J. Warren, Bram P. Venemans, Mitesh Patel, Paul C. Hewett, Richard G. McMahon, Chris Simpson, Tom Theuns, Eduardo A. Gonzáles-Solares, Andy Adamson, Simon Dye, Nigel C. Hambly, Paul Hirst, Mike J. Irwin, Ernst Kuiper, Andy Lawrence, and Huub J. A. Röttgering. A luminous quasar at a redshift of z = 7.085. *Nature*, 474(7353):616–619, 2011. doi: 10.1038/nature10159. URL https://doi.org/10.1038/nature10159.

[16] Xue-Bing Wu, Feige Wang, Xiaohui Fan, Weimin Yi, Wenwen Zuo, Fuyan Bian, Linhua Jiang, Ian D. McGreer, Ran Wang, Jinyi Yang, Qian Yang, David Thompson, and Yuri Beletsky. An ultraluminous quasar with a twelve-billion-solar-mass black hole at redshift 6.30. *Nature*, 518:512 EP –, 02 2015. URL https://doi.org/10.1038/nature14241.

[17] Bram P. Venemans, Fabian Walter, Roberto Decarli, Eduardo Bañados, Chris Carilli, Jan Martin Winters, Karl Schuster, Elisabete da Cunha, Xiaohui Fan, Emanuele Paolo Farina, Chiara Mazzucchelli, Hans-Walter Rix, and Axel Weiss. Copious amounts of dust and gas in az= 7.5 quasar host galaxy. *The Astrophysical Journal*, 851(1):L8, dec 2017. doi: 10.3847/2041-8213/aa943a. URL https://doi.org/10.3847%2F2041-8213%2Faa943a.

[18] Rachel Bean and João Magueijo. Could supermassive black holes be quintessential primordial black holes? *Phys. Rev. D*, 66:063505, Sep 2002. doi: 10.1103/PhysRevD.66.063505. URL https://link.aps.org/doi/10.1103/PhysRevD.66.063505.

[19] Joseph Silk and Martin J Rees. Quasars and galaxy formation. *arXiv preprint astro-ph/9801013*, 1998.

[20] Marta Volonteri. Formation of supermassive black holes. *The Astronomy and Astrophysics Review*, 18(3):279–315, 2010.

[21] Martin G Haehnelt and Martin J Rees. The formation of nuclei in newly formed galaxies and the evolution of the quasar population. *Monthly Notices of the Royal Astronomical Society*, 263(1):168–178, 1993.

[22] Abraham Loeb and Frederic A. Rasio. Collapse of Primordial Gas Clouds and the Formation of Quasar Black Holes. *Apj*, 432:52, Sep 1994. doi: 10.1086/174548.

[23] Daniel J. Eisenstein and A. Loeb. Origin of Quasar Progenitors from the Collapse of Low-Spin Cosmological Perturbations. *Apj*, 443:11, Apr 1995. doi: 10.1086/175498.

[24] S. Peng Oh and Zoltan Haiman. Second-generation objects in the universe: Radiative cooling and collapse of halos with virial temperatures above 104k. *The Astrophysical Journal*, 569(2): 558–572, apr 2002. doi: 10.1086/339393. URL https://doi.org/10.1086%2F339393.

[25] Savvas M Koushiappas, James S Bullock, and Avishai Dekel. Massive black hole seeds from low angular momentum material. *Monthly Notices of the Royal Astronomical Society*, 354(1):292–304, 2004.

[26] Giuseppe Lodato and Priyamvada Natarajan. Supermassive black hole formation during the assembly of pre-galactic discs. *Monthly Notices of the Royal Astronomical Society*, 371(4): 1813–1823, 2006.

[27] S. L. Shapiro and S. A. Teukolsky. The collapse of dense star clusters to supermassive black holes : theorigin of quasars and AGNs. *Apjl*, 292:L41–L44, May 1985. doi: 10.1086/184469.

[28] Gerald D. Quinlan and Stuart L. Shapiro. The Collapse of Dense Star Clusters to Supermassive Black Holes: Binaries and Gravitational Radiation. *Apj*, 321:199, Oct 1987. doi: 10.1086/165624.

[29] Gerald D. Quinlan and Stuart L. Shapiro. Dynamical Evolution of Dense Clusters of Compact Stars. *Apj*, 343:725, Aug 1989. doi: 10.1086/167745.

[30] Simon F. Portegies Zwart, Holger Baumgardt, Piet Hut, Junichiro Makino, and Stephen L. W. McMillan. Formation of massive black holes through runaway collisions in dense young star clusters. *Nature*, 428(6984):724–726, 2004. doi: 10.1038/nature02448. URL https://doi.org/10.1038/nature02448.

[31] Mitchell C. Begelman and Martin J. Rees. The fate of dense stellar systems. *Monthly Notices of the Royal Astronomical Society*, 185(4):847–860, 12 1978. ISSN 0035-8711. doi: 10.1093/mnras/185.4.847. URL https://doi.org/10.1093/mnras/185.4.847.

[32] Martin J. Rees. Black hole models for active galactic nuclei. *Annual Review of Astronomy and Astrophysics*, 22(1):471–506, 1984. doi: 10.1146/annurev.aa.22.090184.002351. URL https://doi.org/10.1146/annurev.aa.22.090184.002351.

[33] Mitchell C Begelman, Marta Volonteri, and Martin J Rees. Formation of supermassive black

holes by direct collapse in pre-galactic haloes. *Monthly Notices of the Royal Astronomical Society*, 370(1):289–298, 2006.

[34] Mitchell C Begelman. Evolution of supermassive stars as a pathway to black hole formation. *Monthly Notices of the Royal Astronomical Society*, 402(1):673–681, 2010.

[35] Masaru Shibata, Yuichiro Sekiguchi, Haruki Uchida, and Hideyuki Umeda. Gravitational waves from supermassive stars collapsing to a supermassive black hole. *Phys. Rev. D*, 94: 021501, Jul 2016. doi: 10.1103/PhysRevD.94.021501. URL https://link.aps.org/doi/10.1103/PhysRevD.94.021501.

[36] Jung-Tsung Li, George M. Fuller, and Chad T. Kishimoto. Neutrino burst-generated gravitational radiation from collapsing supermassive stars. *Phys. Rev. D*, 98:023002, Jul 2018. doi: 10.1103/PhysRevD.98.023002. URL https://link.aps.org/doi/10.1103/PhysRevD.98.023002.

[37] G.M. Shi, X. & Fuller. Neutrinos and supermassive stars: Prospects for neutrino emission and detection. *The Astronomical Journal*, 503:307–313, August 10 1998.

[38] Xiangdong Shi, George M. Fuller, and Francis Halzen. Observing the birth of supermassive black holes with the planned icecube neutrino detector. *Phys. Rev. Lett.*, 81:5722–5725, Dec 1998. doi: 10.1103/PhysRevLett.81.5722. URL https://link.aps.org/doi/10.1103/PhysRevLett.81.5722.

[39] Felix Linke, José A Font, H-T Janka, Ewald Müller, and Philippos Papadopoulos. Spherical collapse of supermassive stars: Neutrino emission and gamma-ray bursts. *Astronomy & Astrophysics*, 376(2):568–579, 2001.

[40] K. J. Fricke. Dynamical Phases of Supermassive Stars. *Apj*, 183:941–958, August 1973. doi: 10.1086/152280.

[41] A. Heger, C. L. Fryer, S. E. Woosley, N. Langer, and D. H. Hartmann. How massive single stars end their life. *The Astrophysical Journal*, 591(1):288–300, jul 2003. doi: 10.1086/375341. URL https://doi.org/10.1086%2F375341.

[42] S. Chandrasekhar. The Dynamical Instability of Gaseous Masses Approaching the Schwarzschild Limit in General Relativity. *Apj*, 140:417, Aug 1964. doi: 10.1086/147938.

[43] RP Feynman. Feynman lectures on gravitation, edited by fb morinigo, wg wagner, and b, 1996.

[44] K. Chen, A. Heger, Woosley, S., A. Almgren, D.J. Whalen, and J.L Johnson. The general relativistic instability of a supermassive population iii star. *The Astronomical Journal*, 790 (162), August 1 2014.

[45] A. Heger and S. E. Woosley. The Nucleosynthetic Signature of Population III. *Apj*, 567:

532–543, March 2002. doi: 10.1086/338487.

[46] Ke-Jung Chen, Alexander Heger, Stan Woosley, Ann Almgren, and Daniel J Whalen. Pair instability supernovae of very massive population iii stars. *The Astrophysical Journal*, 792 (1):44, 2014.

[47] Daniel J Whalen. The first stars. *arXiv preprint arXiv:1209.4688*, 2012.

[48] Adam Burrows and John Hayes. Pulsar recoil and gravitational radiation due to asymmetrical stellar collapse and explosion. *Phys. Rev. Lett.*, 76:352–355, Jan 1996. doi: 10.1103/PhysRevLett.76.352. URL https://link.aps.org/doi/10.1103/PhysRevLett.76.352.

[49] Ewald Müller and H-T Janka. Gravitational radiation from convective instabilities in type ii supernova explosions. *Astronomy and Astrophysics*, 317:140–163, 1997.

[50] Chris L. Fryer, Daniel E. Holz, and Scott A. Hughes. Gravitational waves from stellar collapse: Correlations to explosion asymmetries. *The Astrophysical Journal*, 609(1):288–300, jul 2004. doi: 10.1086/421040. URL https://doi.org/10.1086%2F421040.

[51] Christian D. Ott, Adam Burrows, Luc Dessart, and Eli Livne. A new mechanism for gravitational-wave emission in core-collapse supernovae. *Phys. Rev. Lett.*, 96:201102, May 2006. doi: 10.1103/PhysRevLett.96.201102. URL https://link.aps.org/doi/10.1103/PhysRevLett.96.201102.

[52] L. Dessart, A. Burrows, C. D. Ott, E. Livne, S.-Y. Yoon, and N. Langer. Multidimensional simulations of the accretion-induced collapse of white dwarfs to neutron stars. *The Astrophysical Journal*, 644(2):1063–1084, jun 2006. doi: 10.1086/503626. URL https://doi.org/10.1086%2F503626.

[53] Kei Kotake, Naofumi Ohnishi, and Shoichi Yamada. Gravitational radiation from standing accretion shock instability in core-collapse supernovae. *The Astrophysical Journal*, 655(1):406–415, jan 2007. doi: 10.1086/509320. URL https://doi.org/10.1086%2F509320.

[54] Subrahmanyan Chandrasekhar and Subrahmanyan Chandrasekhar. *An introduction to the study of stellar structure*, volume 2. Courier Corporation, 1957.

[55] Donald D Clayton. *Principles of stellar evolution and nucleosynthesis*. University of Chicago press, 1983.

[56] Jorick S. Vink, A. de Koter, and H. J. G. L. M. Lamers. Mass-loss predictions for O and B stars as a function of metallicity. *aap*, 369:574–588, Apr 2001. doi: 10.1051/0004-6361:20010127.

[57] I. Baraffe, A. Heger, and S. E. Woosley. On the Stability of Very Massive Primordial Stars. *apj*, 550(2):890–896, Apr 2001. doi: 10.1086/319808.

[58] S. Ekström, G. Meynet, C. Chiappini, R. Hirschi, and A. Maeder. Effects of rotation on the evolution of primordial stars. *aap*, 489(2):685–698, Oct 2008. doi: 10.1051/0004-6361:200809633.

[59] R Kudritzki. The first stars, ed. a. weiss, tg abel, & v. hill, 2000.

[60] S.A. Shapiro, S.L. & Teukolsky. *Black Holes, White Dwarves, and Neutron Stars*. Wiley-Interscience, 1983.

[61] Humitaka Satō. General Relativistic Instability of Supermassive Stars. *Progress of Theoretical Physics*, 35(2):241–260, 02 1966. ISSN 0033-068X. doi: 10.1143/PTP.35.241. URL https://doi.org/10.1143/PTP.35.241.

[62] William A Fowler and Fred Hoyle. Neutrino processes and pair formation in massive stars and supernovae. *The Astrophysical Journal Supplement Series*, 9:201, 1964.

[63] G. Audi, F. G. Kondev, Meng Wang, W. J. Huang, and S. Naimi. The NUBASE2016 evaluation of nuclear properties. *Chinese Physics C*, 41(3):030001, Mar 2017. doi: 10.1088/1674-1137/41/3/030001.

[64] Fred Hoyle. On nuclear reactions occuring in very hot stars. i. the synthesis of elements from carbon to nickel. *The Astrophysical Journal Supplement Series*, 1:121, 1954.

[65] C. W. Cook, W. A. Fowler, C. C. Lauritsen, and T. Lauritsen. b^{12}, c^{12}, and the red giants. *Phys. Rev.*, 107:508–515, Jul 1957. doi: 10.1103/PhysRev.107.508. URL https://link.aps.org/doi/10.1103/PhysRev.107.508.

[66] G. R. Caughlan, W. A. Fowler, M. J. Harris, and B. A. Zimmerman. Tables of thermonuclear reaction rates for low-mass nuclei $(1 \leq z \leq 14)$. *Atomic Data and Nuclear Data Tables*, 32:197–233, 1985.

[67] Itoh, H. N., Hayashi, A. Nishikawa, and Y. Kohyama. Neutrino energy loss in stellar interiors. vii. pair, photo-, plasma, bremsstrahlung, and recombination neutrino process. *The Astronomical Journal Supplement Series*, 102:411–424, February 1996.

[68] T. A. Weaver, G. B. Zimmerman, and S. E. Woosley. Presupernova evolution of massive stars. *The Astrophysical Journal*, 225:1021–1029, 1978.

[69] F. X. Timmes. Integration of Nuclear Reaction Networks for Stellar Hydrodynamics. *apjs*, 124(1):241–263, Sep 1999. doi: 10.1086/313257.

[70] F. X. Timmes and F. Douglas Swesty. The Accuracy, Consistency, and Speed of an Electron-Positron Equation of State Based on Table Interpolation of the Helmholtz Free Energy. *apjs*, 126(2):501–516, Feb 2000. doi: 10.1086/313304.

[71] Alex Heger. Kepler documentation. *https://2sn.org/kepler/doc/*, 2019.

[72] F. X. Timmes, S. E. Woosley, D. H. Hartmann, and R. D. Hoffman. The Production of 44Ti and 60Co in Supernovae. *apj*, 464:332, Jun 1996. doi: 10.1086/177323.

[73] F. X. Timmes, S. E. Woosley, D. H. Hartmann, R. D. Hoffman, T. A. Weaver, and F. Matteucci. 26Al and 60Fe from Supernova Explosions. *apj*, 449:204, Aug 1995. doi: 10.1086/176046.

[74] Takayoshi Nakamura, Hideyuki Umeda, Ken'ichi Nomoto, Friedrich-Karl Thielemann, and Adam Burrows. Nucleosynthesis in type II supernovae and the abundances in metal-poor stars. *The Astrophysical Journal*, 517(1):193–208, may 1999. doi: 10.1086/307167. URL https://doi.org/10.1086%2F307167.

[75] Alexandra Kozyreva, S-C Yoon, and Norbert Langer. Explosion and nucleosynthesis of low-redshift pair-instability supernovae. *Astronomy & Astrophysics*, 566:A146, 2014.

[76] Alexander Heger, Stan Woosley, Isabelle Baraffe, and Tom Abel. Evolution and explosion of very massive primordial stars. In Marat Gilfanov, Rashid Sunyeav, and Eugene Churazov, editors, *Lighthouses of the Universe: The Most Luminous Celestial Objects and Their Use for Cosmology*, pages 369–375, Berlin, Heidelberg, 2002. Springer Berlin Heidelberg. ISBN 978-3-540-48014-3.

[77] Carmen Angulo. Nacre: A european compilation of reaction rates for astrophysics. *AIP Conference Proceedings*, 495(1):365–366, 1999. doi: 10.1063/1.1301821. URL https://aip.scitation.org/doi/abs/10.1063/1.1301821.

[78] N. B. Nguyen, F. M. Nunes, I. J. Thompson, and E. F. Brown. Low-temperature triple-alpha rate in a full three-body nuclear model. *Phys. Rev. Lett.*, 109:141101, Oct 2012. doi: 10.1103/PhysRevLett.109.141101. URL https://link.aps.org/doi/10.1103/PhysRevLett.109.141101.

[79] Hans OU Fynbo, Christian Aa Diget, Uffe C Bergmann, Maria JG Borge, Joakim Cederkäll, Peter Dendooven, Luis M Fraile, Serge Franchoo, Valentin N Fedosseev, Brian R Fulton, et al. Revised rates for the stellar triple-α process from measurement of 12 c nuclear resonances. *Nature*, 433(7022):136, 2005.

[80] Kazuyuki Ogata, Masataka Kan, and Masayasu Kamimura. Quantum three-body calculation of the nonresonant triple-α reaction rate at low temperatures. *Progress of theoretical physics*, 122(4):1055–1064, 2009.

[81] J. R. Oppenheimer and G. M. Volkoff. On massive neutron cores. *Phys. Rev.*, 55:374–381, Feb 1939. doi: 10.1103/PhysRev.55.374. URL https://link.aps.org/doi/10.1103/PhysRev.55.374.

[82] Michael M. May and Richard H. White. Hydrodynamic calculations of general-relativistic collapse. *Phys. Rev.*, 141:1232–1241, Jan 1966. doi: 10.1103/PhysRev.141.1232. URL https://link.aps.org/doi/10.1103/PhysRev.141.1232.

[83] Duane A. Dicus. Stellar energy-loss rates in a convergent theory of weak and electromagnetic interactions. *Phys. Rev. D*, 6:941–949, Aug 1972. doi: 10.1103/PhysRevD.6.941. URL https://link.aps.org/doi/10.1103/PhysRevD.6.941.